NFPA 285 Screening Rig Evaluation

A Major Qualifying Project Report

Submitted to the Faculty of

WORCESTER POLYTECHNIC INSTITUTE

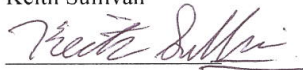In partial fulfillment of the requirement for the
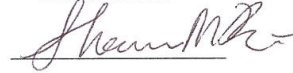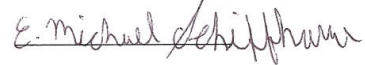
Degree of Bachelor of Science

By

Jiawen Michelle Dong

Keith Sullivan

Shannon Rice

Michael Schiffhauer

April 28th, 2016

Approved by

Professor Nicholas Dembsey

_____

1

Abstract

Composite building materials, such as Fiber Reinforced Polymers (FRP) are widely used in the exterior cladding systems of modern buildings. Its characteristic of light-weight, fast, and easily customizable design has appealed to both architects and engineers. However, FRP's classification as a combustible material presents concerns with respect to external fire spread. Combustible exterior cladding assemblies are required to pass the NFPA 285 multi-story building test. The full-scale NFPA 285 test is expensive to run, and it is challenging to repeatedly test the exterior cladding specimen when considering potential alterations to the assembly. This project focuses on utilizing a cost-effective intermediate-scale screening rig in the WPI Fire Laboratory to provide results, which are indicative of the full-scale NFPA 285 test. An instrumented assembly specimen is tested in the intermediate-scale test, and results are compared to previous tests, and the NFPA 285 standardized test.

Acknowledgements

MQP Report Organization

This MQP report is a 20-pages conference paper, which contains the comparison between NFPA 285, southwest test and past MQP test, construction of the rig, mobile base, instrumentation details and the

design of our practice wall platform. The supplemental information includes calculation for wall design,

calibration process and results, and relevant in-depth information are included in the appendix.

Table of Contents

Table of figures:

Table of tables

Authorship

Section	Author
Abstract	Keith
Acknowledgements	Michelle
Introduction	Michelle
Background	Shannon
Intermediate Scale Rig	Michael
Instrumentation Details	Michelle
Practice Wall Design	Keith & Shannon
Conclusion	Michelle
Recommendation	Michael & Michelle
Appendix A	Michael
Appendix B	Michelle & Michael
Appendix C	Michelle
Appendix D	Shannon
Appendix E	Keith
Appendix F	Shannon
Appendix G	Shannon & Keith
Formatting	Michael, Michelle, Shannon

Introduction

 The external wall containing combustible materials need to meet certain regulation from NFPA 285 testing for building construction. Fiber reinforced polymer is a widely used composite building materials. However, its combustible property has concerned our sponsor Kreysler and Associates to determine if this material can be used and pass the NFPA 285 test. NFPA 285 is a test that studies the potential for vertical and horizontal fire spread on the exterior of buildings however it is also a relatively expensive and large test to run. Therefore, the MQP group decide to build an intermediate scale rig to closely replicate the full-scale NFPA 285 test.

In order to evaluate if the intermediate scale rig would be a good representation for the full-scale NFPA 285 Test, we will first design and calibrate all instrumentations to closely simulate NFPA 285 test then design and optimized our practice wall based on the design from past MQP team.

Background

Exterior Cladding – FRP

Exterior Wall

Exterior walls are a protective assembly layer of materials that separate a building's structure and interior, from exterior conditions. The exterior wall system is commonly comprised of a layer of interior sheathing or drywall, framing, a water penetration layer, insulation, exterior sheathing, drainage segment, and a base coat, and a finish coat. The outermost layer of an exterior wall is known as the exterior cladding. Exterior cladding includes poured concrete, stucco, masonry (brick or stone), vinyl, wood shingles (cedar), fiber-cement siding w/ plywood sheathing on vertical furring strips, tile siding with horizontal furring strips, clay tiles, and aluminum. For this project, our exterior cladding will be comprised of a fiber reinforced polymer rainscreen.
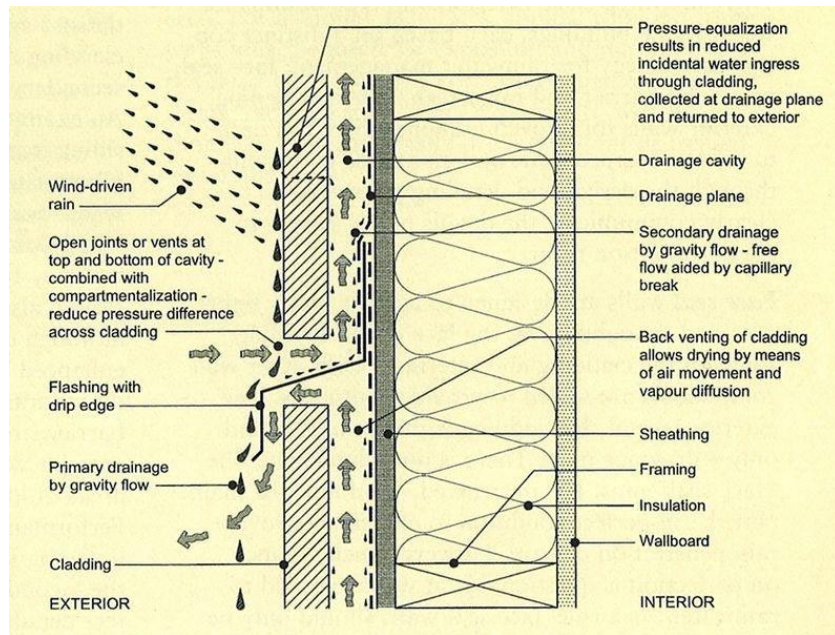
Figure 1: Rainscreen Example

A rainscreen is a form of exterior cladding, where the cladding is separated from the remainder of the exterior wall system, as shown in Figure 1, creating a capillary break to allow for drainage and evaporation. The rainscreen also adds strength to the building's structure. When a rainscreen is used, the layer beneath the exterior cladding must consider exterior conditions. Rainscreens also provide the structure with an additional layer of thermal insulation.

Fiber Reinforced Polymer

Fiber reinforced polymer is a composite material composed of a polymer matrix of resins reinforced with fibers. Polyester, epoxy, vinyl ester, and urethane are materials used in the resin matrix to protect and transfer stress between the reinforcing fibers. Thermoset resins are typically used, which begin as liquid polymers and are curing to solid form during the molding process. This process is called crosslinking, and is irreversible. Thermoset resins may not be melted or reshaped. Thermoplastics, on the other hand, will melt at a given temperature and can be solidified into new shapes by cooling to ambient temperatures. Carbon, glass, basalt and aramid are used as reinforcing fibers to provide strength and stiffness. Glass accounts for over 90% of the reinforcements in use. These reinforcements are arranged to provide support in the direction of loading (uni-directional orientation), if there are multidirectional

forces, the fiber shall be arranged in either bi-directional or multi-directional orientation. Additives to fiber reinforced polymers may present fire retardant properties.

Additives are typically used to modify the properties of the material, and tailor its performance, to its desired use. For polyester FRP a type of peroxide or benzoyl peroxide is added to induce the curing process, and crosslinking. Tertiary butyl catechol may be used to slow the process, while dimethyl aniline may be used as an accelerator. Fillers are used in composite design to reduce costs, and the organic content, in addition to tailoring the performance of the material. Fillers also improve dimensional stability of the FRP for thermoplastic resins, as fillers will deform less. Alumina trihydrate and calcium sulfate are commonly used fillers. Alumina trihydrate will give off water when exposed to high temperature, which helps reduce smoke and fire from propagating. Calcium sulfate is a lower cost alternative that works on a similar concept, but with less water released, and at a lower temperature. Panels of fiber reinforced polymers are used in a sandwich construction, commonly with a foam material, to reduce weight, and increase durability and stability in construction. Surface finishes on the FRP provide corrosion resistance to exterior conditions. Alternatives to foam include waffle patterned, or honeycomb designed cores, or balsa wood cores.

Figure 2: Fiber Reinforced Panel in Sandwiched Construction

FRP possesses linear elastic behavior until failure, with no yielding, and its design shall account for this. FRP therefore has a higher ultimate strength, and presents a lower strain at failure. FRP is incorporated in designs for weight saving for building loading design, and can also be easier and faster to

operate during construction. Architects are fond of FRP's easily formable properties, as it may take a multitude of creatively designed shapes.

Kreysler and Associates erected an FRP rainscreen for the San Francisco, California Museum of Modern Art, as shown in Figure 3. The panels used for this design are approximately 1 meter x 10 meters. The average weight of the panels, including the integral frame is approximately 8 pounds per foot.
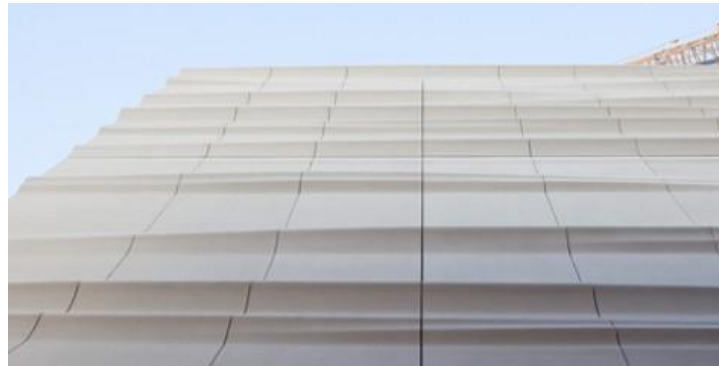
Figure 3: FRP panels on the San Francisco MoMA building

FRP panels were chosen for this design because of their ability to be easily formed into complex shapes, as well as FRP's high strength and lightweight characteristics. The material's light weight allowed for fewer, and smaller, connections.

Since there are many different options for the creation of FRP, from the choice of resin, reinforcements, additives, fillers, and tailoring the FRP to its designed use, it is not an exact science to quantify the material properties of all FRP. However, a general comparison to steel, aluminum, and wood may be considered based off tested materials. FRP weighs 75% less than steel and 30% less than aluminum, yet presents a similar strength when in the lengthwise direction. (Steel: 36ksi, Aluminum: 25ksi, FRP: 30ksi, Wood: 12ksi). FRP is also corrosion resistant, non-conductive, and a good thermal insulator, which are beneficial qualities for exterior cladding.

International Building Code

The International Building Code (IBC) is a regulated code adapted on a federal level and amended on a state level. We have considered the federal level regulations in regards to FRP and exterior

wall systems. Chapter 26 of the most recent IBC (2015) focuses on Plastics, which covers Fiber Reinforced Polymers in section 2613. Exterior cladding is covered by chapter 14.

FRP may not exceed 20 percent of a wall covering, or may not exceed 10 percent of an architectural element. When using FRP on an exterior system, the flame spread index shall not exceed 25. Fire blocking must also be used with FRP. When installing FRP on a building exterior, the layer the FRP is attached to must be of noncombustible material substrate, or separated from the exterior wall by corrosion-resistant steel with a minimum base thickness of 0.016 inches, or aluminum with a minimum base thickness of 0.019 inches. When the building is less than 40 feet above grade, and the fire separation distance is no greater than 5 feet, FRP may not cover more than 10 percent of an exterior wall. When the building is less than 40 feet above grade, and the fire separation distance is more than 5 feet, there shall be no restriction on the percent covering of FRP on exterior walls. On buildings less than 40 feet above grade, the flame spread index shall not exceed 200; unless the thickness of paint or coatings applied directly to FRP does not exceed 0.036 inches, in which case there will be not flame spread index requirement.

Requirements for the foam plastic insulation in panels are to follow test methods as outlined in NFPA 259, "Standard Test Method for Potential Heat of Building Materials." The vertical and lateral flame propagation of the exterior wall shall be in accordance with NFPA 285, "Standard Fire Test Method for Evaluation of Fire Propagation Characteristics of Exterior Non-Load-Bearing Wall Assemblies Containing Combustible Components." In addition, the exterior wall may not display sustained flaming when tested in accordance with NFPA 268, "Standard Test Method for Determining Ignitability of Exterior Wall Assemblies Using a Radiant Heat Energy Source." Fireblocking shall also be used in the exterior wall system, to separate combustible construction and break up flaming regions.

Requirements in the International Building Code for exterior cladding revolve around general requirements that encompass the main concerns for fire safety, and the tests referenced to be passed for appropriate material behavior in fire conditions. In addition to these general requirements, there are

additional modified requirements for Exterior Insulation and Finish Systems (EIFS), High-Pressure Decorative Exterior-Grade Laminate (HPL), and Metal Composite Material (MCM).

Exterior cladding may be constructed of combustible material. However, non-plastic material may not exceed 10 percent of an exterior wall surface when the fire separation distance is less than 5 feet, and may not be more than 40 feet in height above the plane. The ignition resistance of the cladding shall be tested in accordance with NFPA 268, "Standard Test Method for Determining Ignitability of Exterior Wall Assemblies Using a Radiant Heat Energy Source" unless the material is wood, or meets a minimum thickness requirement. For results from the NFPA 268 test, sustained flaming shall not be present. Refer to the table 1406.2.1.1.2 in the IBC for allowable fire separation distance based on the incident radiant heat flux experienced in accordance with NFPA 268. The exterior cladding must be separated from the exterior wall shall not exceed 1 5/8 inches when fireblocked.

Exterior Insulation and Finish Systems (EIFS), are non-structural, non-load bearing, exterior wall cladding systems that consist of an insulation board attached either adhesively or mechanically, or both, to the substrate, with an integrally reinforced base coat and a textured protective finish coat. This is required to comply with all general specifications with the addition of meeting the performance standards of ASTM E 2568, "Standard Specification for PB Exterior Insulation and Finish Systems."

High-Pressure Decorative Exterior-Grade Laminate (HPL), are panels consisting of layers of cellulose fibrous material impregnated with thermosetting resins and bonded together by a high-pressure process to form a homogeneous non porous core suitable for exterior use. Specifications are in line with general requirements with some additions and modifications. The flame spread index is specified at 75 or less and smoke-development index of 450 or less, in accordance with ASTM E 84, "Test Method for Surface Burning Characteristics of Building Materials." HPL shall be separated from the building by an approved thermal barrier of ½ inch material tested by NFPA 275, "Temperature Transmission Fire Test and the Integrity Fire Test." The HPL system must also be tested with minimum and maximum thicknesses and pass the full-scale NFPA 285, "Standard Test Method for Evaluating the Fire Propagation Characteristics of Exterior Non-Load-Bearing Wall Assemblies Containing Combustible Components." If

none of the above mentioned requirements are met for HPL systems, there are requirements based on height and fire separation distance to determine the percentage covering the HPL system may present on the building.

Metal Composite Material (MCM) is a factory manufactured panel consisting of metal skins bonded to both faces of solid plastic. The requirements for MCM are the same as HPL, with added requirements if the NFPA 285 test is not passed. Since there are different combustibility classes of MCM, the fire separation distances and max allowable percentage coverings vary slightly.

NFPA 285

The National Fire Protection Association (NFPA) developed fire test 285 to study the potential for vertical and horizontal fire spread on the exterior of buildings. In the 1970s foam plastic was a proposed material for exterior wall insulating. This material did not meet the requirements for the building codes at the time and was rejected as an idea. The Society of the Plastics Industry (SPI) was tasked with developing a test to prove that a wall with foam plastic insulation that was on fire would not spread to far horizontally or vertically. The test standard was created and has gone through a couple of adaptations. The most recent version of NFPA was created in 2012. NFPA 285 is used to test four abilities of the exterior wall assemble that is to be tested. These abilities include the wall assembly's ability to resist flame over the exterior face of the wall assembly, resist vertical fame propagation within the combustible components from one story to the next, to resist vertical flame propagation over the interior surface of the wall assembly from one story to the next, and the ability to resist lateral flame propagation from the compartment of fire origin to adjacent compartments or spaces.

The setup of the most recent 285 test is relatively simple. The test involves a two story concrete structure with the exterior wall assembly attached to its front face. The structure has two vertically stacked rooms. The lower room has a single window in the test specimen where a burner is placed to replicate the fire spilling out of the window. Also inside the lower room there is a burner which replicates a fire burning inside of the room. For an apparatus that is being tested using NFPA 285 there are some criteria that the test must meet. This criteria includes no vertical and horizontal spread outside of the

impingement zone in the exterior face, no vertical and horizontal spread in the components or insulation, the maximum temperature in the second story test room cannot exceed 500 degrees Fahrenheit, there are no flames present in the second story test room, and there is no flame spread to the side walls of the assembly.

2.1.4.1 Problems with current test

The NFPA 285 test poses multiple complications for companies or individuals who would like to run the test:

1. Size- The dimensions of the 285 rig is 14'X18'. These dimensions can be too large for an average test facility to accommodate.

2. Price- The current test is expensive and for an assembly to fail is also inherently expensive. The price of the test can range from $15,000 to $50,000.

3. Walls must be built on site- The exterior wall need to be attached to the testing rig. This increases the time, cost, and manpower necessary to run the test.

4. Portability- The 285 rig is made of concrete and brick walls. This means that it is a stationary rig that will permanently occupy the space it will be built in.

5. Test time- The current test takes a long time to occur. This limits the amount of tests that can be performed in one day.

Intermediate Scale Rig

Comparison Chapter

The intermediate scale rig we are using is meant to replicate, to the best of its ability, the results that would be expected from an NFPA 285 test. To corroborate that our scale rig does provide data that matches with data from NFPA 285 we compared our scale rig data with NFPA 285 test calibration data and two NFPA 285 tests performed by the Southwest Company.

One area of comparison for these four sets of test data is the average temperature in Celsius of the thermocouples spaced out at one foot intervals up the wall at the six designated time steps. This data can

be observed on table 1 through table 4 in Appendix A. From this data you can observe that the scale rig

data provides similar temperature readings to the NFPA 285 calibration data and the Southwest tests

when you compare the temperature readings above the three foot mark for each test. The scale rig data

shows a higher temperature at the bottom of the wall during the entire duration of the test. An explanation

for this is that the NFPA 285 test is run with a larger wall face without side walls and there is an internal

combustion chamber below the window in addition to the line burner. The internal chamber creates a

flame plume outside of the window and that is why the temperatures lower on the wall are lower in

comparison to the scale rig.

The charts displayed in Appendix A show the temperature differences between the four tests as well at

each Heat Release Rate Step. Please note that all data points are up to six feet above the "top of the

window", because after that point, we do not have data from all four sources. Also note, that we do not

have comparative data for the critical ten foot point either, with the reason of having the NFPA flame

temperature line for each graph is for a means of giving an update of where the test temperatures are

3/5ths of the way up the face of the wall.

 A second means of comparison can be derived from the average temperature readings of the four tests.

The flame height cannot exceed ten feet from the top of the window opening for the NFPA 285 test,

otherwise that constitutes as a failure of the material meeting the minimum requirements. Flame height

can be determined based on temperature readings. When a temperature of 538^0C is detected by a

thermocouple at a determined height that indicates that flames are present at that height. The following

bar chart shows a comparison of the four tests where a flame temperature of $538\,^0C$ have been reached at

various heights during the time steps. From this chart, it can be observed that the screening rig has similar

flame heights to the other three tests.
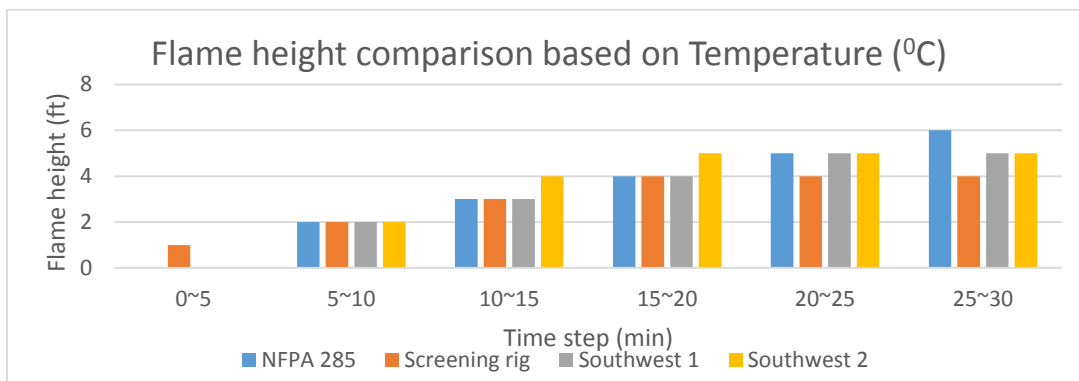
Figure 4: Flame height comparison based on Temperature

Besides determining flame heights based on temperature readings visual observations can be used to make comparisons. The flame heights based on visual observations of the screening rig test from last year, Southwest test one, and Southwest test two can all be compared. The screening rig test from last year flames reached the 2 foot mark after about 1.5 minutes. Southwest test 1 flames took 12 minutes to reach the 2 foot mark and Southwest test 2 flames took 8 minutes to reach the 2 foot mark. The second point of comparison is the flame heights of the tests after 15 minutes of burner exposure. The screening rig test from last year flame height at this time are reaching the 6 foot mark. For Southwest test 1 the flame height at this time is at the 11 foot mark which is located 6 feet above the top of the window. For Southwest test 2 the flame height at this time is at the 9.5 foot mark which is located 4.5 feet above the top of the window. The maximum flame height of the screening rig test from last year is about 6.5 feet. For Southwest test 1 the max flame height is about 6.5 feet and for Southwest test 2 the max flame height is about 5.5 feet.

The chart below shows the comparison of the internal air cavity temperatures of each of the screening rig test data from last year and both of the Southwest tests. Last year's data and the first Southwest test have the most comparable data. The rate at which the temperature increased in last year's test is at a rate that was in between the rates of the Southwest tests. Southwest 2 ends at a temperature around 212.8 ^{0}C and the test last year ended at a value closer to 67.7 ^{0}C. The reason for a discrepancy in the data collected can be attributed to the differences in materials tested and the differences in how the screening rig is run in comparison to the NFPA 285 test.
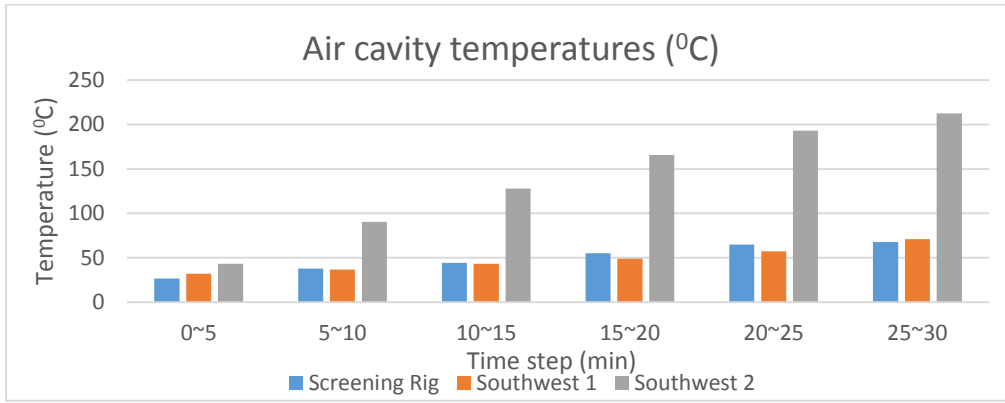
Figure 5: Air cavity temperature comparisons

The burn pattern of the screening rig test and both Southwest tests are represented below. Each burn pattern is observed to have a wider char pattern at the base and the pattern becomes thinner to form a parabolic point. The char pattern tips are at similar locations for all three tests. The char patterns at the base for both Southwest tests are just a bit thinner than the width of the pipe burner. The entire wall face of last year's rig test is charred. For last year's test the tip is just getting to the 7 foot mark, for Southwest test 1 it was at 9 feet above the burner, and Southwest 2 was just at 8 feet above the burner.

There are some differences in the shape of the char pattern of the rig test last year and both Southwest tests. This is attributed to the fact that our rig has sidewalls that are attached to the vertical wall face we are burning. Where as in the Southwest test they are burning a wall with a larger width and no sidewalls.

Figure 6: Left to Right, Final burn pattern of last year's experiment. The white line is drawn to distinctly show the char pattern, Final burn pattern of Southwest 1, Final burn pattern of Southwest 2

Instrumentation Details

Two primary instruments for temperature measurement in this project are thermocouples and thin skin calorimeters.

Thermocouples

Thermocouples were built by the MQP team to measure temperature for this project. Thermocouple wires were stripped on both ends, one end is twisted and welded together for a contact point. The other end of the thermocouple is attached to the type K thermocouple plug. The welded point produce and pass temperature reading for data collection. Detail information for thermocouple are listed in Appendix B.

Thin skin calorimeters

The thin skin calorimeter is used to measure an incident heat flux. Incident heat flux is the sum of the incoming radiation and convection. This instrument is created by welding a thermocouple to the back of a thin metal plate, two layers of ceramic fiber board and gypsum wall board. The face of the plate is painted black to minimize radiation heat loss. Thin skin calorimeters can be calibrated under a known heat flux generated by a cone calorimeter. With known thermal properties of each layer of material, temperature distribution throughout the thin skin calorimeter can be determined. The thin skin calorimeters are then calibrated under three different incident heat flux 25kw/m2, 50 kw/m2 and 75 kw/m2. Following equation was used to backtrack the incident heat flux and evaluate the accuracy of our calibration process

$$\rho Cp\delta \frac{dT_{PL}}{dt} = \varepsilon q_i'' - \varepsilon\sigma(T_{PL}^4 - T_0^4) - h_{cov}\,(T_{PL} - T_\infty) - hcc(T_{PL} - T_0^i)$$

Where left-hand side of the equation is the change of energy stored in the plate of the thin skin calorimeter. The first term on the right-hand side is the radiative energy absorbed by the plate. The second term is the radiative energy emitted by the plate. The third term is the conductive heat loss. The last term is calculating the heat loss into the ceramic fiberboard which requires using a contact conductance factor (h_{cc}). T_{pL} is the temperature of the thin skin calorimeter, T_∞ is the ambient temperature, and T_0 is the temperature of the first node using finite difference method.

By creating and using the explicit finite difference method, two calibration process were conducted to better determine if the thin skin is calibrated correctly. Following graph provides results from two calibration method (dynamic and constant contact conductance) for thin skin calorimeter under 25kw/m2 incident heat flux.
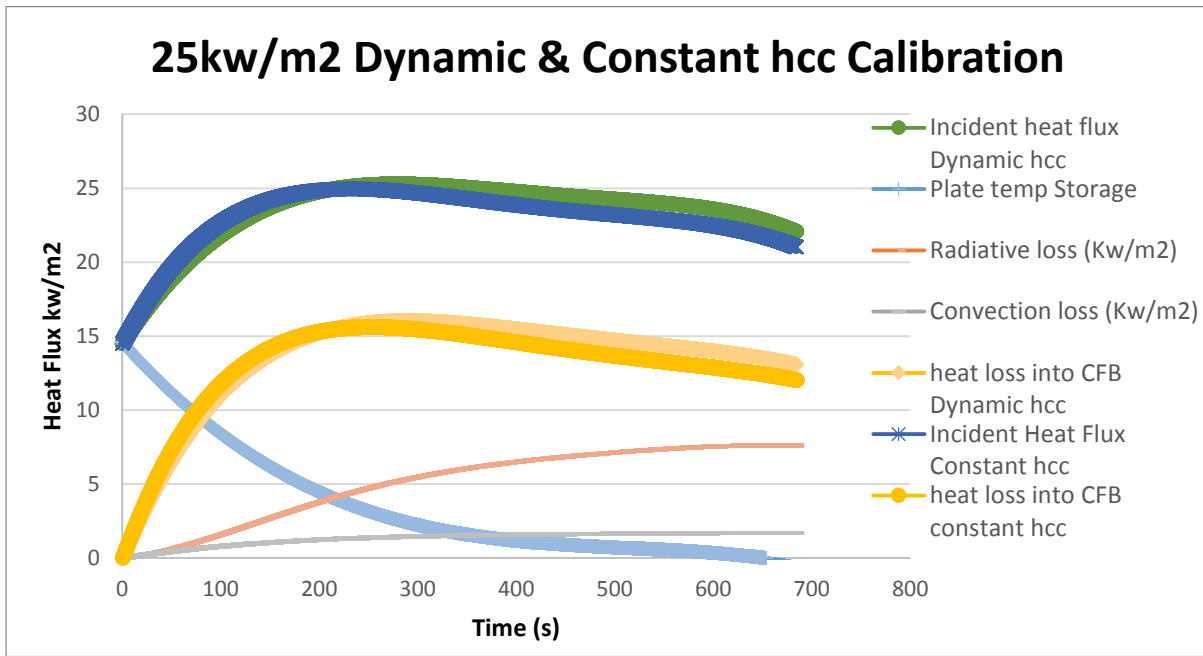
Figure 7: Calibration Comparison between constant and dynamic hcc

The overall incident heat flux from finite difference model for both methods contains some errors. Two calibration process provides an error of ±10kw/m2 in compared to the known incident heat flux 25kw/m2. One reason why there are errors occurred is delayed response from thermocouples and varying h_{cc} value only gives a minor affect to the calibration results. The fluctuation of the heat loss into ceramic fiberboard affects the heat flux after 200s, which tells us this model will not work for a time base of seconds. However, as we will be working on the time base of a minute for this project, we can conclude that the thin skin calorimeter has been calibrated successfully.

 Detail thin skin calorimeter design and calibration calculation can be found in Appendix B.

Practice Wall Design

The practice wall was designed with durability and efficiency in mind. In accordance with appendix D, the practice wall composition was adjusted so that none of the materials would reach critical temperatures apart from the front face of sheetrock, from which the instrumentation is mounted.

21
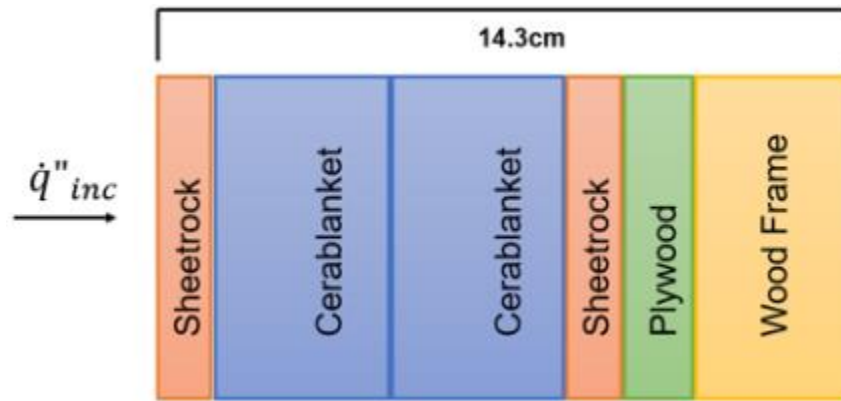
Figure 8: Schematic showing the construction of the practice wall

Two layers of cerablanket will prevent the second layer of sheetrock from critical dehydration. The wood frame is only in discrete locations, therefore considerations for backface temperature will be considered to the plywood backface. Figure 8 above is a schematic displaying the construction of the practice wall.

The aluminum rig temperature is of concern as well, as the temperature shall not cause structural of strength concerns, as well as maintaining a safe temperature if a human were to come in contact with it. Analysis of semi-infinite behavior, and finite difference method were used and outlined in Appendix C to come to the conclusion of two layers of cerablanket being required to maintain temperatures under the critical limits.

Mobile Base Construction

In order to make our intermediate-scale test rig easier to transport, we created a mobile platform on four 6-inch diameter wheels. The platform itself, we made a frame of two 2X6s 72 inches long on their side (on the 6 inch side), and two 2X6s 58 inches long on their side as well. Two interior 58 inch 2X6s were added to support the interior of the platform as well, which was topped with a sheet of plywood. In order to make sure that we had a robust and satisfactory platform, we calculated the clamp force of the top layer of the platform, the rolling and sliding force required to push the rig and platform assembly, the rig's center of gravity, the tipping force required to tip the rig over, and the bending stress acting upon the platform itself.
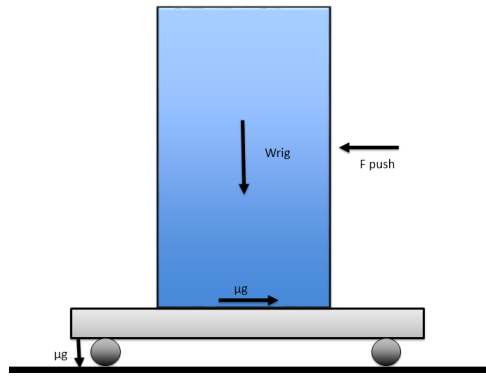
Figure 9: Schematic of the forces in play with the rig and platform assembly

The first factor we looked into with the platform was the clamp force of the platform top, which measures how secure the top of the platform is put together. This was determined based on the diameter of the screws we used to fasten the platform top along with the amount of screws used. Fortunately for us, it was determined that a monumental and unrealistic force of 48,000 LBS would be required to unfasten the top of the platform from the rest of the structure.

We calculated the force required to move the rig by itself if it were on a stationary plywood platform (I.e. no wheels) versus the force required to move the rig on the mobile platform. We found that in order to move the mobile base with the rig, one needs to exert 18.4 LBS of force vs. 161 LBS of force for pushing the rig off of a stationary platform.

The next factor we determined was the center of gravity of the rig and platform assembly. This was done by using the dimensions of the rig and platform and their respective weights, or weight of each part in the case of the rig, and then determining the overall center of gravity from there. We ended up with a final center of gravity of (28.5, 41.1, 37.2) inches in the (x, y, z) direction.

The force required tipping the rig and platform over was determined if somehow the platform were to somehow get stuck while being rolled. We determined that in order to tip the 850 pound rig and base over, we would have to exert a force of 305 LBs at a height of 80 inches, which was our assumed maximum push height. For lower heights, the required force would only be larger due to the decreased area between the "stuck wheel" and the push.

We also looked into doing a worst-case scenario analysis for the strength of the supporting 2X6s. In order to do this, we calculated the bending stress of a 72 inch 2X6 which was acted upon by a 2400 LB force at the center (weight used based on the max capacity of the wheels). Using a beam supported by a pin and roller as a model, we determined that the bending stress exerted on the beam equals 3600 PSI, which is well under the 5100 PSI rupture modulus for the wood we used (pine). We then assumed that the other supporting members would check out too, since their length only 58 inches as opposed to 72, which would lead to a lesser bending stress if acted upon at the center.

Design Factor	Equation	Value for Platform
Rolling Force	$\mu k * \left(\dfrac{W}{R}\right) * n$	18.4 LBS
Sliding Force	$\mu s * W$	161.3 LBS
Platform Top Clamp Force	$\left(\dfrac{T}{Dbolt * \mu}\right) * n$	48,000 LBS
Center of Gravity	$\sqrt{(x^2 + y^2 + z^2)}$	(28.5, 41.1, 37.2) inches for (x, y, z) direction
Tipping Force	$(W * Cx)/h$	305.0 Lbs
Maximum Bending Stress	$\dfrac{3 * W * L}{2 * w * d^2}$	3600 PSI, 1500 PSI less than our material rupture modulus of 5,100 PSI.

Figure 10: Equation used in the construction of the platform

Conclusion

The project successfully established an intermediate practice rig with all instruments constructed and calibrated successfully. Based on the comparison results between NFPA 285 test, southwest and test from past MQP we are able to conclude that our intermediate rig can closely replicate the full-scale NFPA 285 test. Through this project, improvement and adjustments were done to the intermediate scale rig to improve the efficiency for further experiment process. With the mobile base, the mobility of the rig is greatly improved. By adding additional insulation layer, the test wall is able to operate under multiple practice runs which will also allow for the FRP panels provided by Kreysler and Associates to be suitably tested and analyzed when the time comes. Through the simulation results, the intermediate scale rig is safe to operate and is an indication of the full scale NFPA rig test, however, improvements should be considered with future experiment results.

Recommendations

Through this project, following recommendations are established by the MQP team,

1. Total weight for practice wall and rig should stay below the weight limit and placed on the mobile base properly.

2. When performing practice calculations in regards to an exterior cladding test it is recommended to perform more than one test. To perform two tests it is recommended to construct a practice wall that can be used for more than one burn test. A way of doing this is to construct a practice wall in the form of a sandwich with one piece of test wall at the back face, insulating material, and then a front piece of test wall, as shown in Figure 8.

3. When constructing the practice wall in sandwich orientation it is recommended to experiment with different insulation material to study the potential of extending the multi-usage feature.

4. In order to receive more accurate data from the experiment based on our 2-D plume theory design, we recommend using line burner instead of pool fire, as included in Appendix F.

5. Additional fire modeling tools are recommended to add into this project to improve the accuracy of this intermediate-scale rig in compare to the full scale NFPA 285 test.

Reference

Past MQPs:

Ciampa, C., Forbes, E., & Kawalya, D. (2014). Design of an Intermediate Scale Fire Test Rig for Exterior Wall Assemblies.

Cornachini, B., Foley, M., Knight, S., & Ritchey, T. (2015). Calibration of an Intermediate Scale Fire Test Rig for Exterior Wall Assemblies: Source Fire.

Gillis, S., Houghton, N., Scott, D., & Weiler, J. (2015). CALIBRATION OF AN INTERMEDIATE SCALE FIRE TEST RIG FOR EXTERIOR WALL ASSEMBLIES: INSTRUMENTATION AND INSULATION.

Other References:

ASTM International. (n.d.). *Standard Test Method for Measuring Heat Transfer Rate Using a Thin-Skin Calorimeter*. Retrieved from ASTM website: http://www.astm.org/Standards/E459.htm

Cécilia, F. (2008). *Characteristics of a flame spreading on a corrugated cardboard*. Worcester, MA: WPI.

Drysdale, D. (2011). *An Introduction to Fire Dynamics: 3rd ed.* Chichester, West Sussex: Wiley.

Engineering Toolbox. (n.d.). Thermal Conductivity of Materials and Gases. Retrieved from http://www.engineeringtoolbox.com/thermal-conductivity-d_429.html

Gardon, R. *An Instrument for the Direct Measurement of Intense Thermal Radiation, Review of Scientific Instruments, Vol. 24, No. 5.* Retrieved from the database of WPI's Gordon Library. 1953. 21 Sept. 2015.

Heskestad, G. and McCaffrey, B. *A Robust Bidirectional Low-Velocity Probe for Flame and Fire Application.* Retrieved from the internet. February 1976. 8 Sept. 2015.

International Code Council. "2015 International Building Code." *ICC*. ICC, 2015. Web. 15 Oct. 2015. <http://codes.iccsafe.org/app/book/toc/2015/I-Codes/2015%20IBC%20HTML/index.html

Molded Fiber Glass Companies. "Technical Design Guide for FRP Composite Products and Parts."*Techniques and Technologies for Cost Effectiveness.* Molded Fiber Glass Companies, 2014. Web. 15 Oct. 2015. <http://www.moldedfiberglass.com/sites/default/files/docs/MFG_Technical_Design_Guide_FRP_Composite_0.pdf>.

National Fire Protection Agency, comp. *NFPA 285 Standard Method of Test for the Evaluation of Flammability Characteristics of Exterior Non-Load-Bearing Wall Assemblies Containing Combustible Components Using the Intermediate-Scale, Multistory Test Apparatus*. Tech. 2012 ed. Quincy: National Fire Protection Agency Association, n.d. Print.

Talukdar, P., & IIT Dehli. (2010). Transient Heat Conduction. Retrieved from http://web.iitd.ac.in/~prabal/MEL242/ (9-10)-Transient-heat-conduction.pdf

Understanding and choosing thermocouples. (2013, January 29). Retrieved October 19, 2015, from https://www.google.com/url?sa=t&rct=j&q=&esrc=s&source=web&cd=1&ved=0CB0QFjAAahUK EwiQ94XTxs3IAhVL3mMKHbWTBFQ&url=http://www.ni.com/white-paper/4218/en/pdf usg=AFQjCNF4OKsKJgSQBozkC09p8fSEOeoQHA&bvm=bv.105454873,d.cGc&cad=rja

"Use of the Thermogage Circular Foil Heat Flux Gage". Vatell Corporation. Web. 5 Sept. 2015. http://vatell.com/vatellwebfiles/Use%20of%20Thermogage%20v2.pdf.

"Use of the Vatell Schmidt-Boelter Heat Flux Sensor". Vatell Corporation. Web. 5 Sept. 2015. http://vatell.com/vatellwebfiles/Use%20of%20SchmidtBoelter%20v2.pdf.

Appendix A: Test comparison information

	Time interval(min)					
Thermocouple height (ft.)	0-5	5-10	10-15	15-20	20-25	25-30
Interior wall surface	573.8	703.3	778.3	858.9	857.8	901.7
1 ft. above window	316.7	465.6	511.1	533.3	563.3	581.1
2ft	359.4	546.1	605	639.4	673.9	702.2
3ft	341.1	521.7	591.1	634.4	673.9	712.2
4ft	302.8	458.9	527.8	572.8	612.8	662.2
5ft	271.7	407.2	468.3	509.4	541.7	596.6
6ft	244.4	365.6	419.4	457.8	489.4	543.3

Table 1: NFPA 285 Calibration Temperatures

	Time interval (min)					
Thermocouple height (ft.)	0-5	5-10	10-15	15-20	20-25	25-30
0	665.3	729.2	774.5	784.3	767.6	732.5
1	602.5	682.1	723	780	800.1	763.7
2	483.5	597.9	635.8	727.5	767.8	758.7
3	342	484.7	541.2	682.1	725.6	703.4
4	234.7	341.7	384.3	552.6	593.7	598.9
5	185.4	262.3	297.8	449.8	497.5	505
6	147.5	204.3	230.2	337.1	383.	389.2
7	124.3	167.5	185.6	260.2	293.9	298.6
8	106.2	141.9	155.7	211.2	236.2	242.2
9	90	118.8	129	167.7	186.6	192.3
10	81.2	107	124.4	170.6	186.4	213.4
11	83.7	111	116.4	154.1	167.7	163.2

Table 2: Temperature Table for last year's MQP Test.

	Time interval(min)					
Thermocouple height (ft.)	0-5	5-10	10-15	15-20	20-25	25-30
Interior wall surface	632.1	750.8	787.2	852.7	890.6	929
1	332.3	524.8	546.7	582.9	597.8	608.3
2	358.3	572.3	604.3	646.7	675	691.1
3	318.2	516.1	565.7	618.6	651.7	667.8
4	272.7	446.3	499.8	557.4	628.3	640
5	243.1	384.9	441.2	498.1	562.8	573.9
6	217.1	331.5	383.1	436.1	525.6	537.2

Table 3: Temperature Table for the first Southwest Research Test

	Time interval(min)					
Thermocouple height (ft.)	0-5	5-10	10-15	15-20	20-25	25-30
Interior wall surface	638.3	720	792.8	865	890.6	907.2
1	328.3	476.1	541.7	588.9	597.8	608.3
2	328.3	540	611.1	667.8	675	691.1
3	318.3	503.3	587.2	645.6	651.7	667.8
4	296.7	472.2	561.1	620	628.3	640
5	247.2	402.2	496.1	548.9	562.8	573.9
6	229.4	366.1	456.1	508.3	525.6	537.2

Table 4: Temperature Table for the second Southwest Research Test.

The four above tables show the average temperature readings at determined heights of the four

tests. The orange highlighted cells indicate where temperatures are high enough for flames to be present.

The following charts display the temperature differences between the four tests as well at each Heat Release Rate Step.
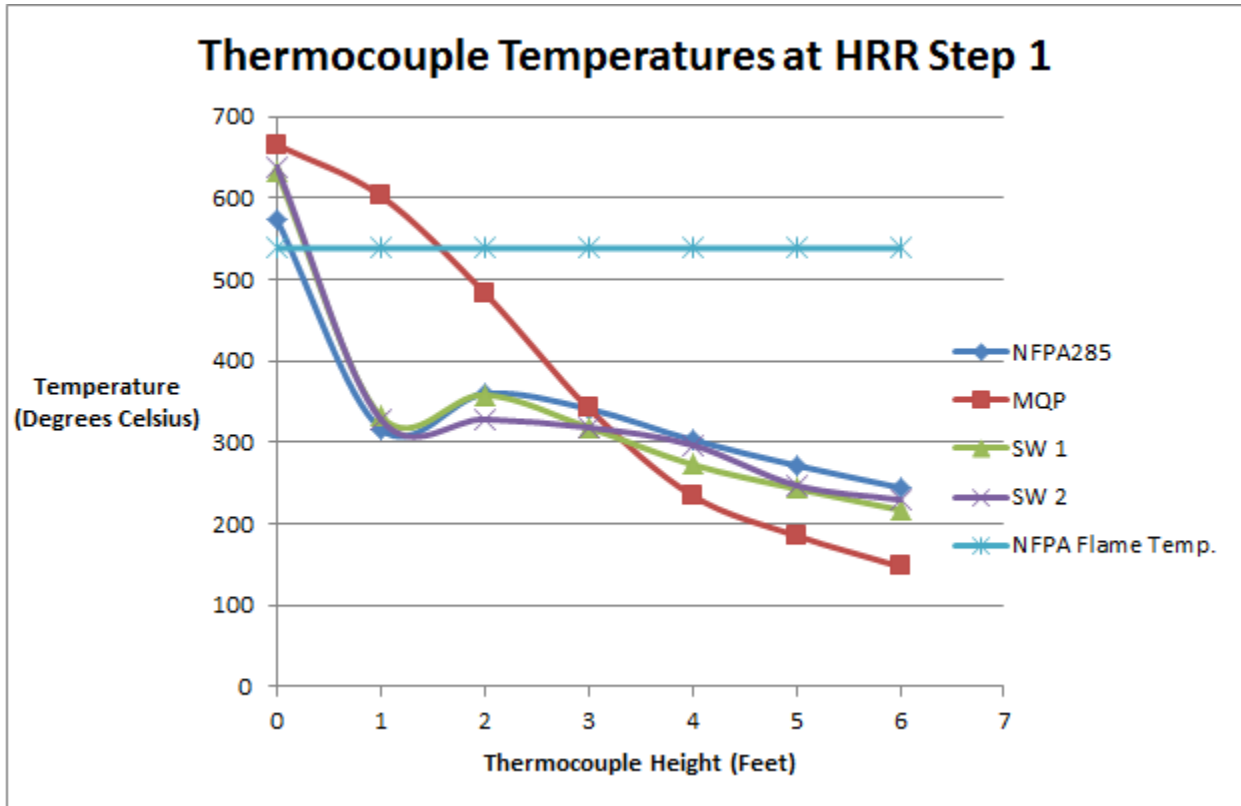
Figure 11: Thermocouple Temperatures at HRR Step 1
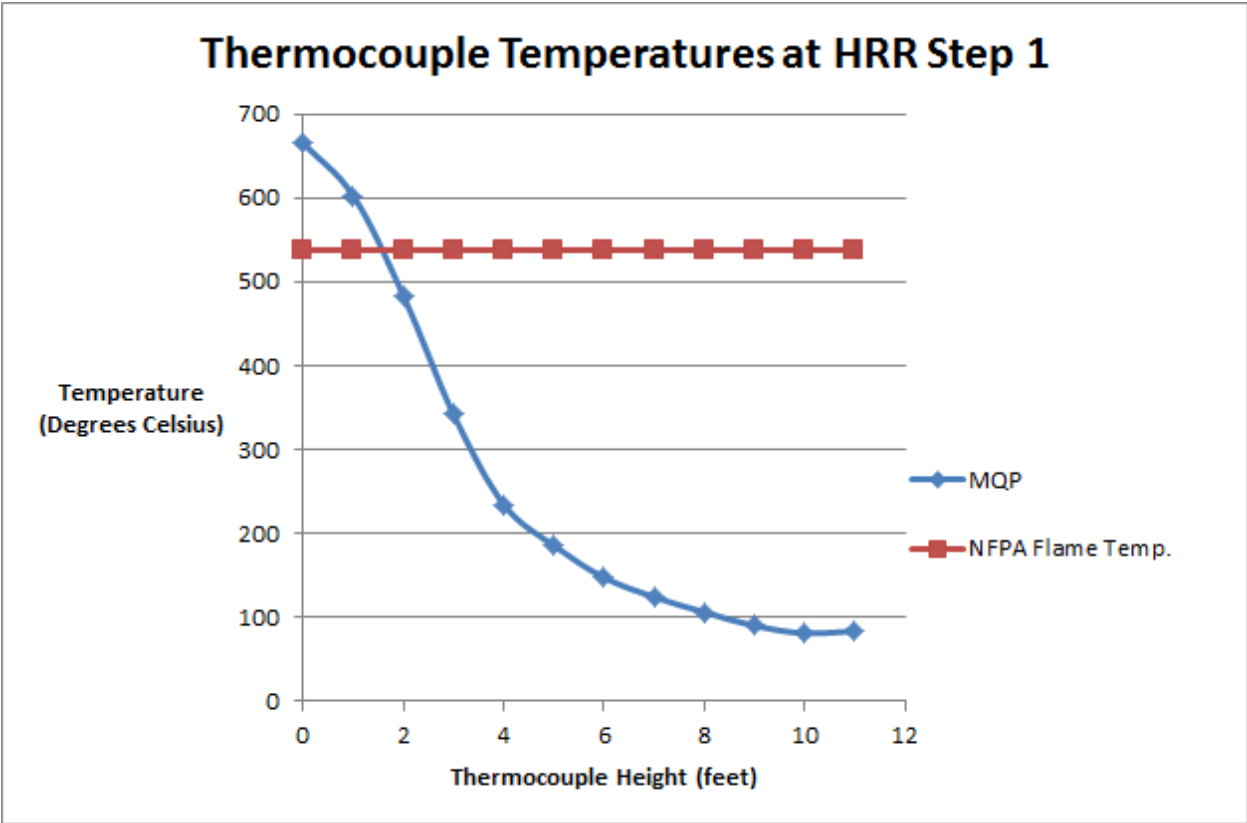
Figure 12: Thermocouple Temperatures at HRR Step 1 MQP and NFPA 285
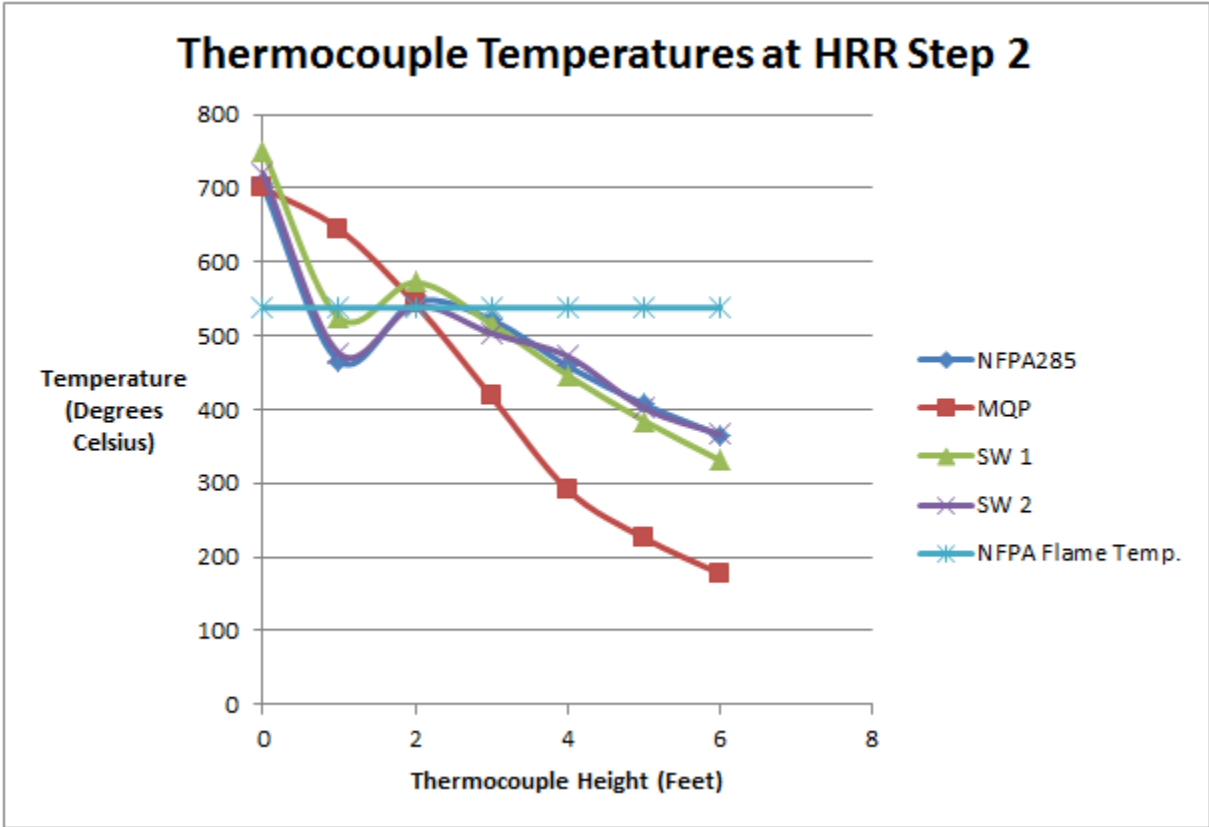
Figure 13: Thermocouple Temperatures at HRR Step 2
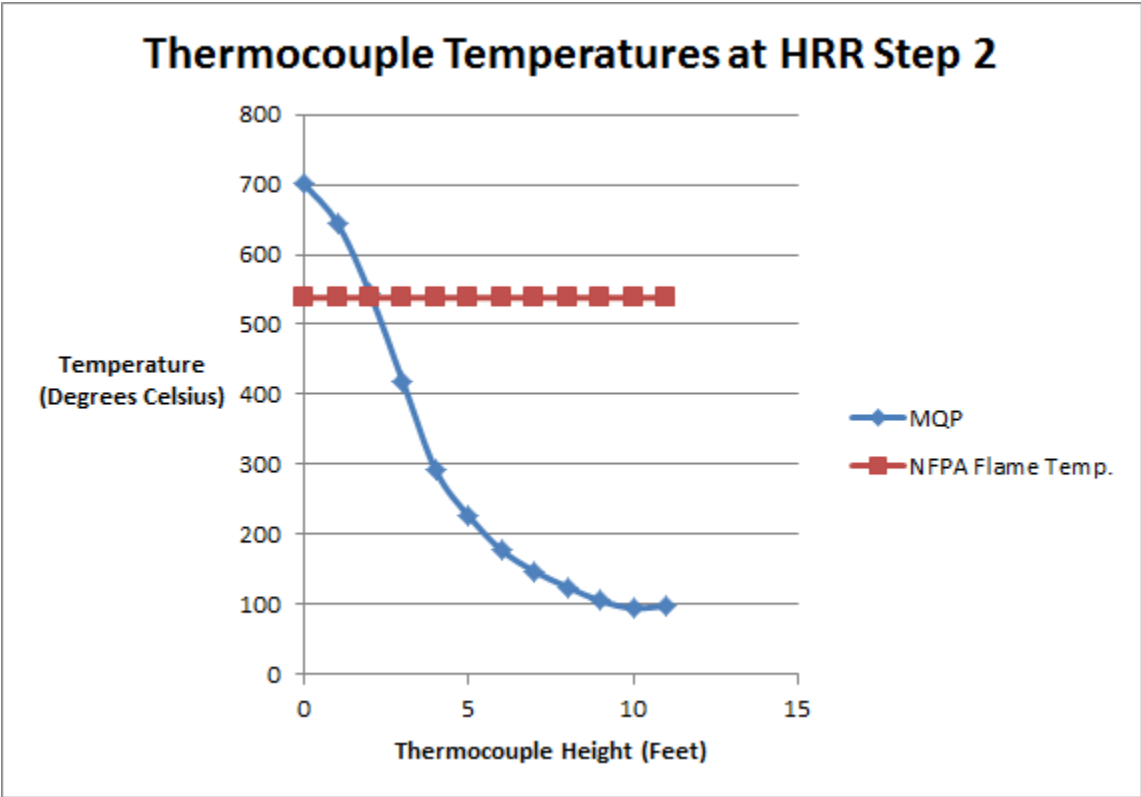
Figure 14: Thermocouple Temperatures at HRR Step 2 MQP and NFPA 285
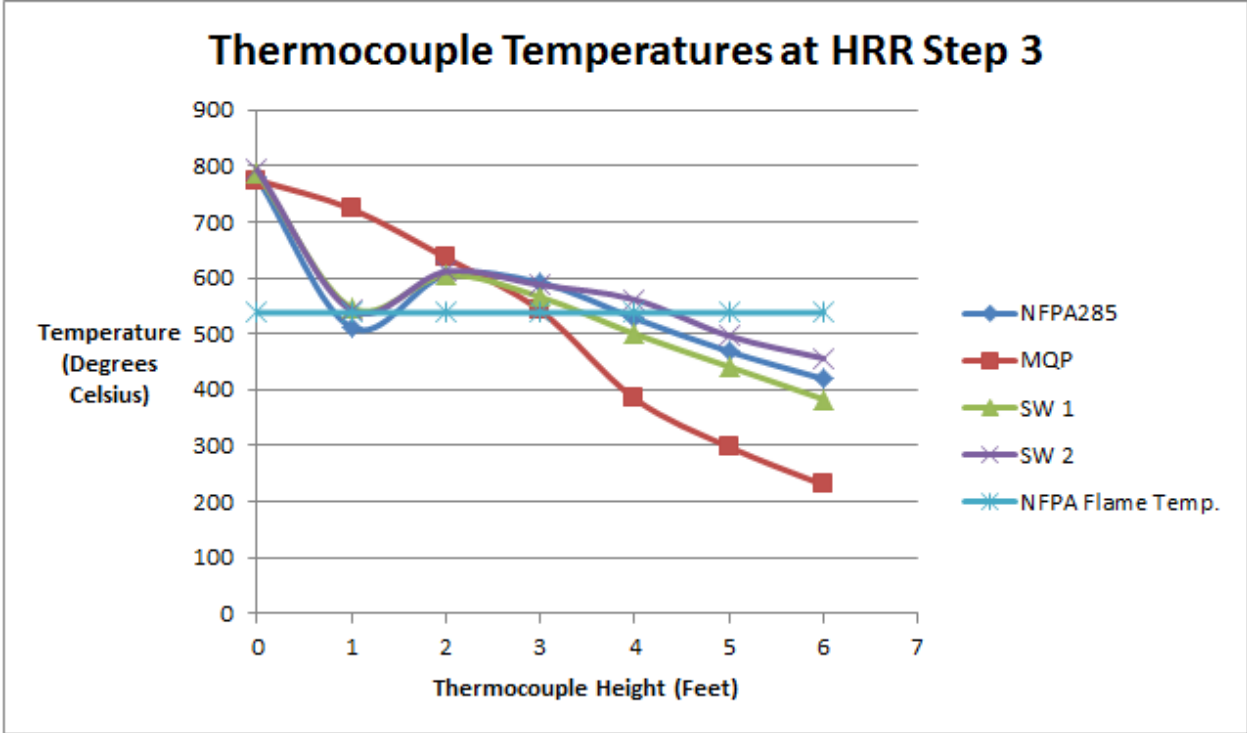
Figure 15: Thermocouple Temperatures at HRR Step 3
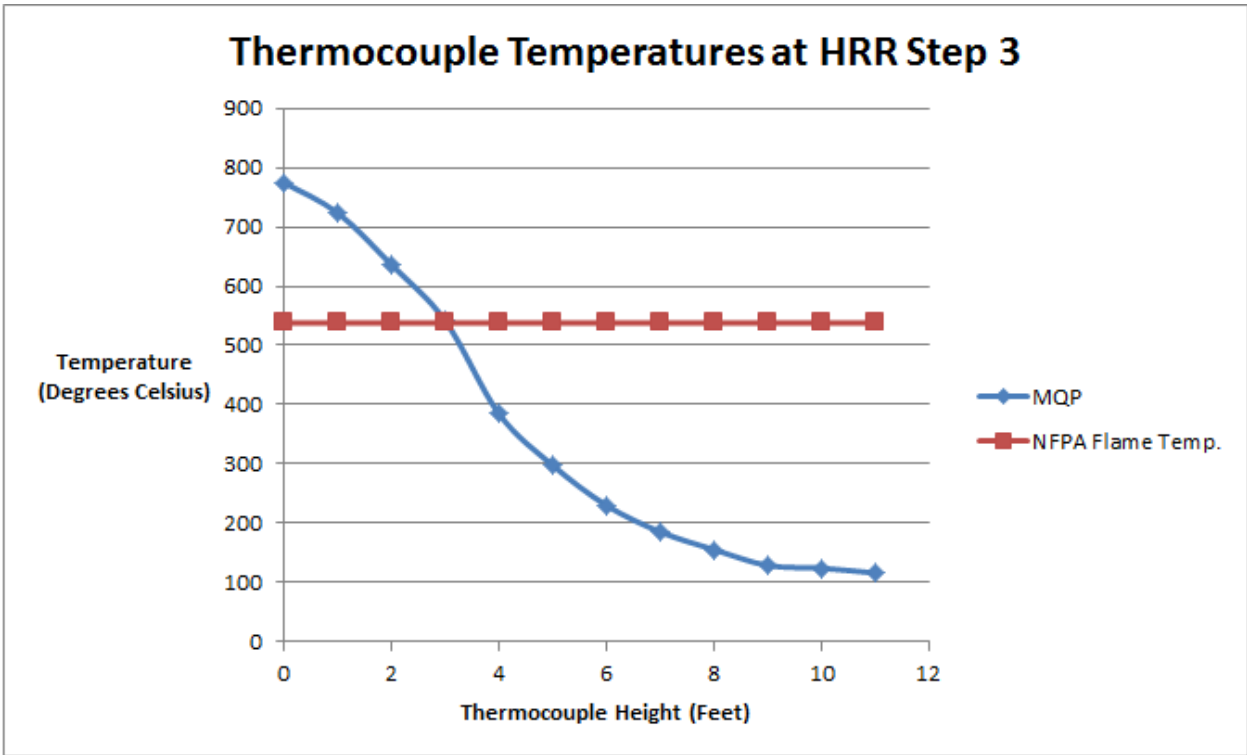
Figure 16: Thermocouple Temperatures at HRR Step 3 MQP and NFPA 285
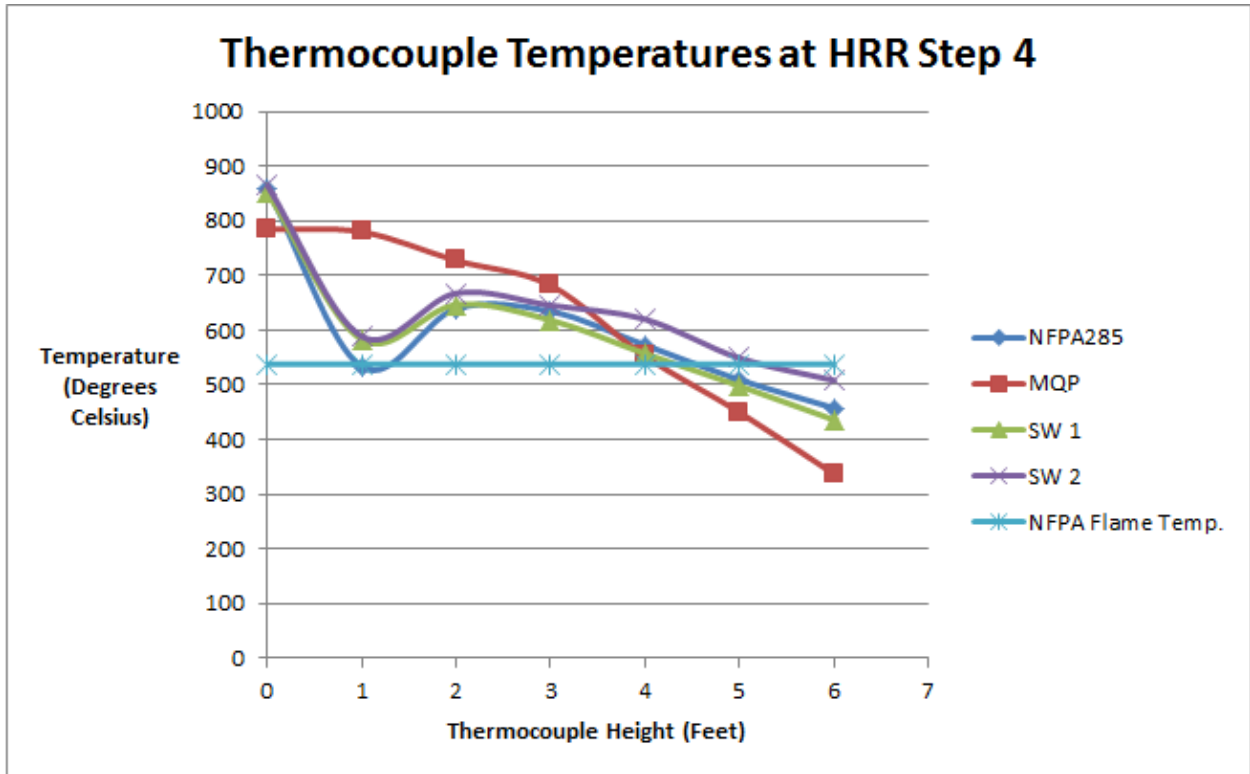
Figure 17: Thermocouple Temperatures at HRR Step 4
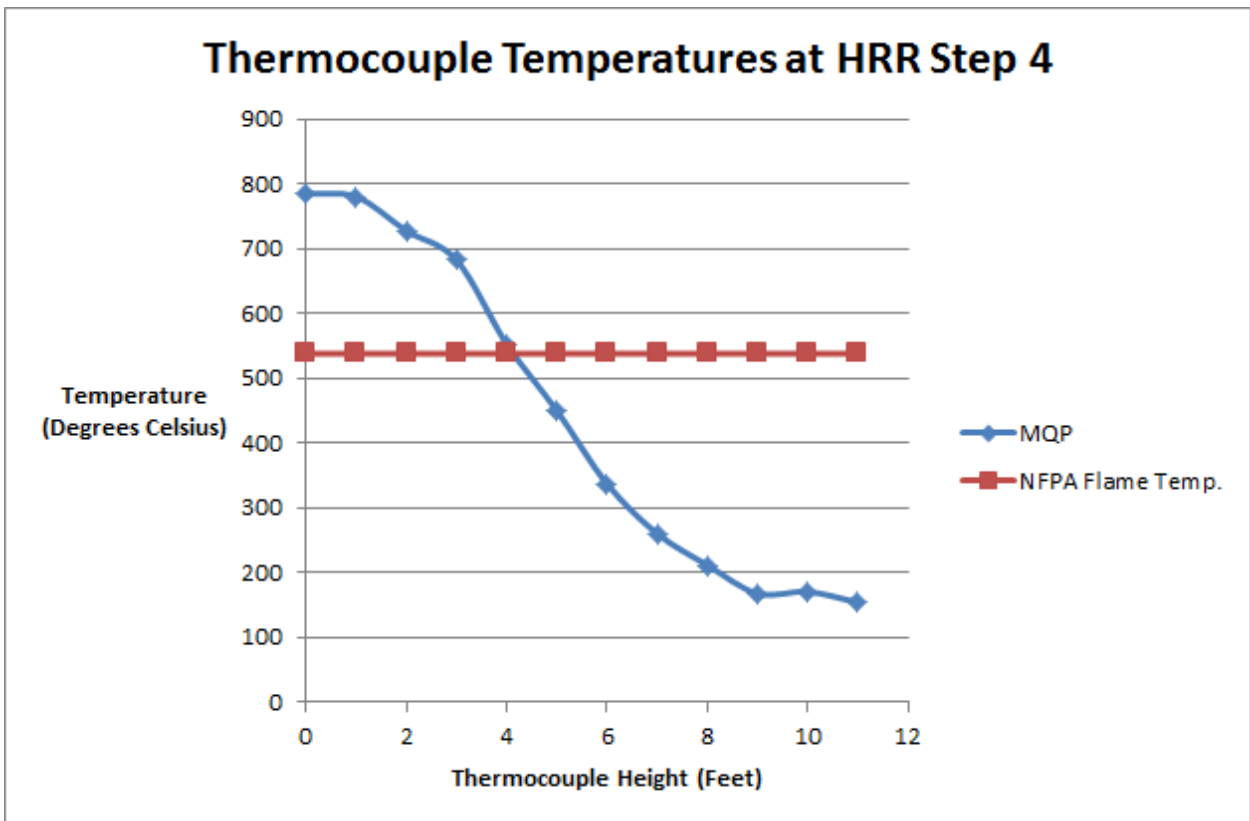
Figure 18: Thermocouple Temperatures at HRR Step 4 MQP and NFPA 285
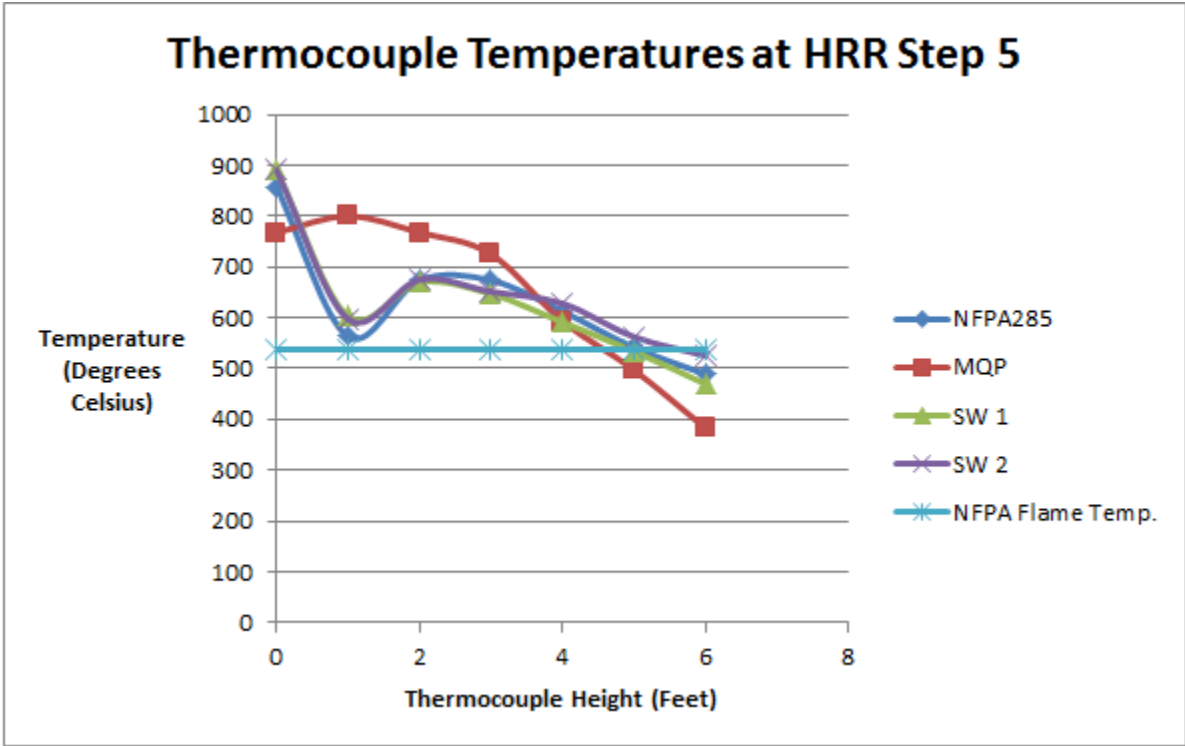
Figure 19: Thermocouple Temperatures at HRR Step 5
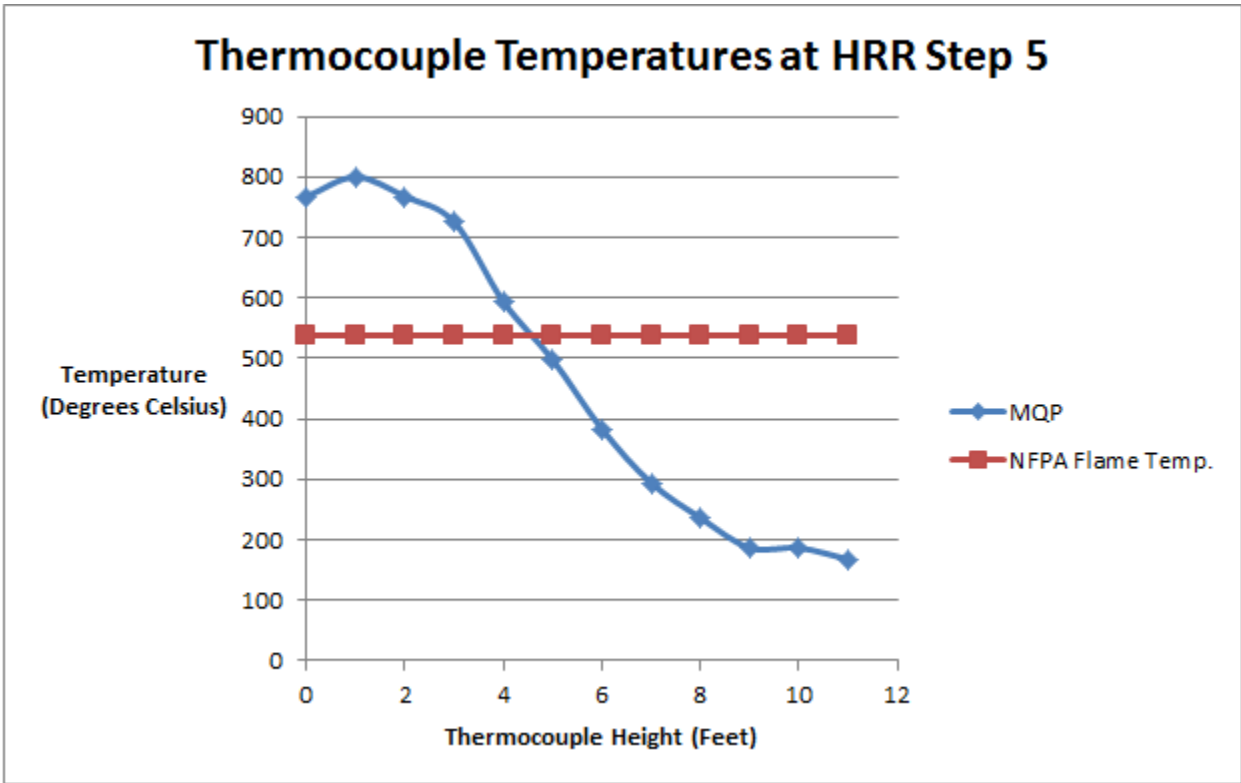
Figure 20: Thermocouple Temperatures at HRR Step 5 MQP and NFPA 285
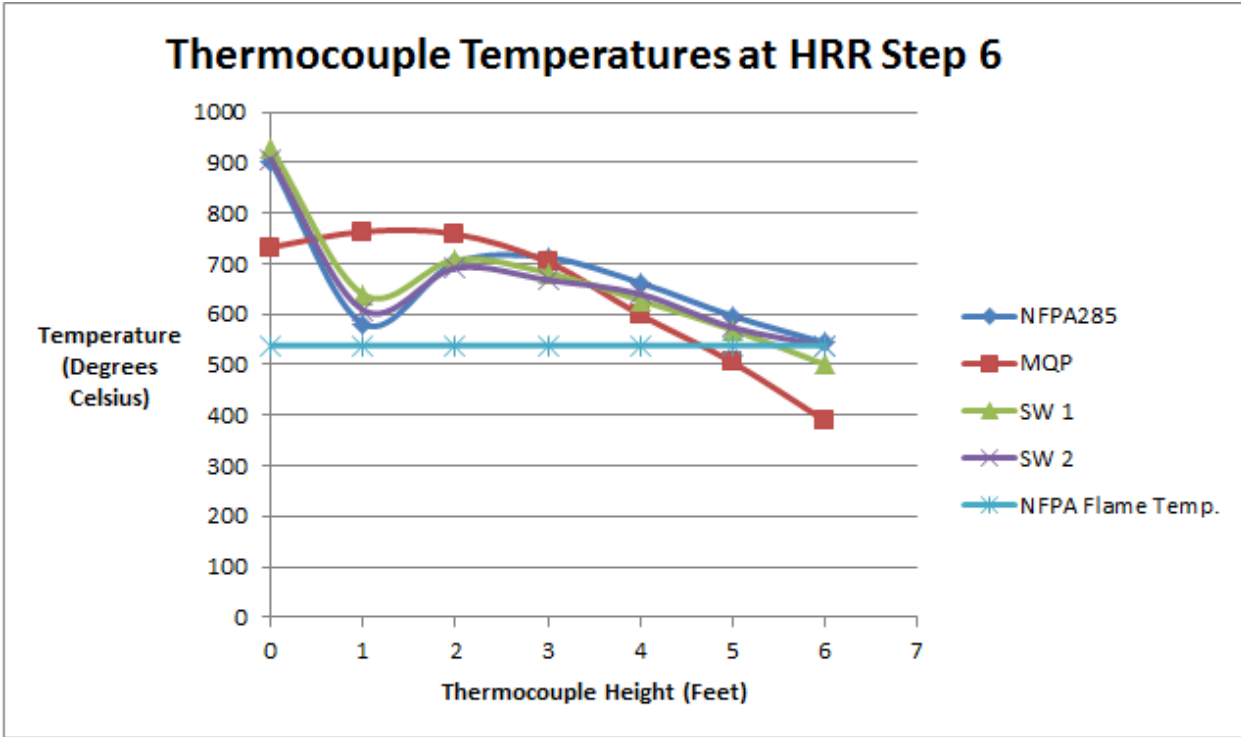
Figure 21: Thermocouple Temperatures at HRR Step 6
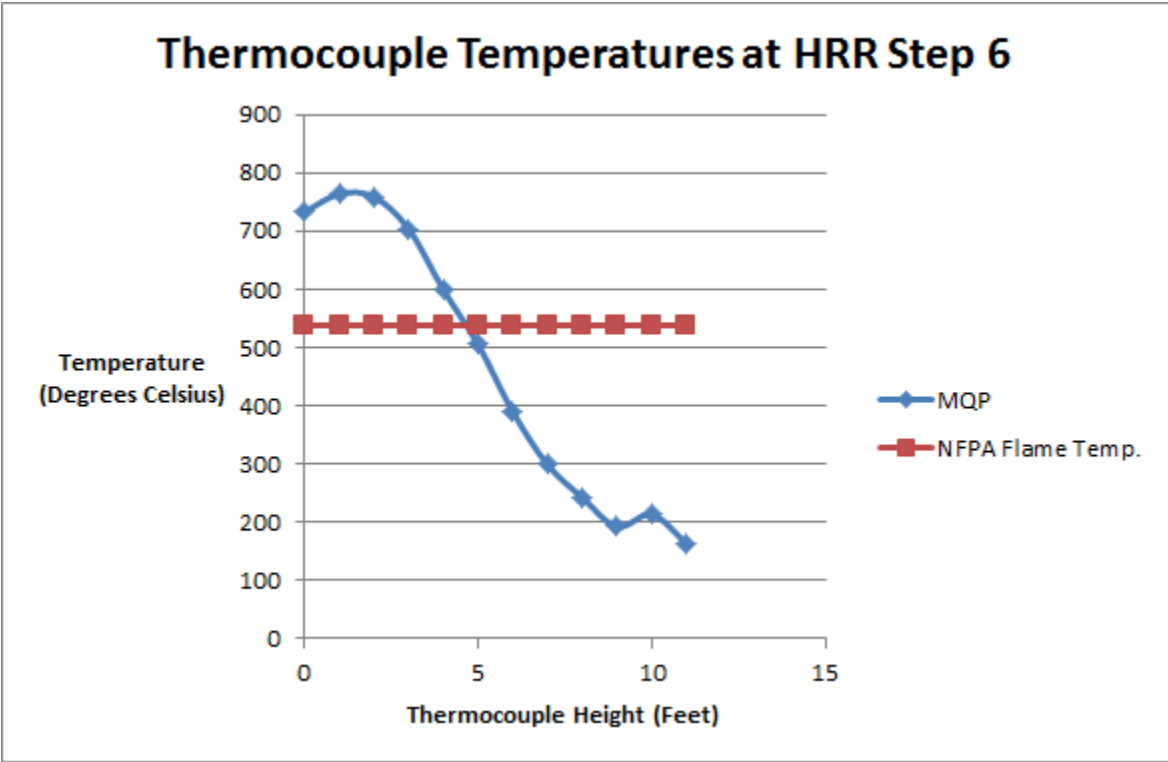
Figure 22: Thermocouple Temperatures at HRR Step 6 MQP and NFPA 285

The following table shows the average temperature data of the air cavities of the screening rig test and both Southwest tests.

Table 5: Air cavity temperature data

Last year's test data		Southwest 1		Southwest 2	
Time interval(min)	Average Temp(^{0}C)	Time interval(min)	Average Temp(^{0}C)	Time interval(min)	Average Temp(^{0}C)
0-5	26.5	0-5	32.2	0-5	43.3
5-10	38	5-10	36.7	5-10	90.6
10-15	44.2	10-15	43.3	10-15	128.1
15-20	55.1	15-20	48.9	15-20	165.6
20-25	64.7	20-25	57.2	20-25	193.3
25-30	67.7	25-30	71.1	25-30	212.8

Flame height comparison based on visual observations:

Table 6: Rig test flame heights and observations

Time (min:sec)	Flame Height (ft.)	Observations
0	About 9" at the edges and 3' in the middle	Beginning of burn test
00:24	About 1' at the edges and 3' in the middle	Charring is present at the 2' mark.
1:5	About 1' from the bottom of the wall at the edges and 3' in the middle	Charring is present at the 3' mark.
4:00	About 2' from the bottom of the wall at the edges and approaching 4' in the middle	Flame is present in first gap and charring is present past the 4' mark
5:03	Uniform flame plume with the flame reaching 5'	Flames are licking past the 5th thermocouple and charring is present to the 6'
15:31	Uniform flame plume with the flame reaching 6'	Charring is present at the 7' mark. There is sustained flames in the gap of the first two panels
20:35	Uniform flame plume at 6' with flame wisps reaching 7'	Charring is present at the 7.5' mark. There is sustained flames in the gap of the first two panels
30:14	Uniform flame plume at 6' with flame wisps reaching 7'	This is the end of the fire test

Table 7: Southwest August 9, 2012 flame heights and observations

Time (min:sec)	Flame height (ft.)	observations
0	No flame present	The top of the window starts at the 5' mark
7:45	No real flame height to speak of	The inner compartment is fully involved. There is the start of flames touching the top of the window
11:26	Flames are up to the 6' mark	Charring observed up to the 7' mark
15:20	Flames are up to the 6' mark	Charring observed up to the 9' mark
18:19	Flames on the sides are at the 6' mark and the flame at the centerline is at the 10' mark	Flames and charring are concentrated at the centerline
20	Flames are up to the 11' mark.	
21:16	Flames are up to the 11.5' mark.	Flames and charring pattern start wide at the bottom and get thinner as it travels up
23	Flames have receded to the 10' mark	
25:13	Flames have receded to the 9.5' mark	Flame size has reduced. A darker char pattern reaches up to 14'. Signs of less severe charring can be observed up to 16'

29:34	Flames have receded to the 9' mark	Flame size has reduced. A darker char pattern reaches up to 14'. Signs of less severe charring can be observed up to 16'
30	Flames have receded to the 9' mark	The test is ended after 30 min

Table 8: Southwest June 27, 2013 flame heights and observations

Time (min:sec)	Height (ft.)	Observations
0	No flames present	Start of test
5	No flames present on vertical surface	Burner is put into place
8:40	Flames are up to the 6' mark	There is barely any charring visible on the wall
15:51	Flames are up to the 7.5' mark	Charring is visible up to the 9' mark
16:27	Flames are up to 10' mark at the centerline and at the 6' mark on the sides	There is a distinct char pattern up to the 9' mark
20:32	Flames recede closer to the 9.5' mark	A char pattern in the approximate shape of an equilateral triangle with its point going up can be observed. The point is a bit above the 11' mark

29:26	Flames recede to the 8' mark	The char pattern is in a similar shape. It is wider at its edges than before and reaches the 12' mark

These tables were developed using a video of the screening rig test and from picture provided with both Southwest reports.

Appendix B: Instrumentation Calibration

In this project, thermocouple and thin skin calorimeter are two primary instruments that will be used for temperature measurement.

1.0 Thermal Couple

A thermocouple is created when two dissimilar metals touch and the contact point produces a small open-circuit voltage as a function of temperature. This thermoelectric voltage is known as Seebeck voltage.
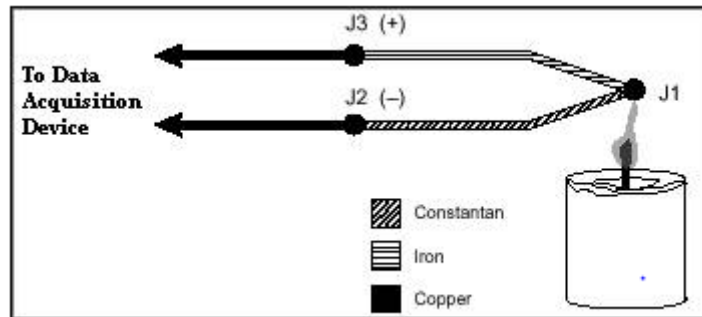
Figure 23: Diagram representing a thermocouple

The circuit contains three dissimilar metal junctions: J1, J2, and J3. This results in a Seebeck voltage between J3 and J2 that is proportional to the temperature difference between J1. Because copper wire is connected to both J2 and J3, there is no additional voltage contributed between the temperature difference of the J2/J3 junction and the point where the voltage is measured by the data acquisition

device. To determine the temperature at J1, you must know the temperatures of junctions J2 and J3. You can then use the measured voltage and the known temperature of the J2/J3 junction to infer the temperature at J1. Thermocouples require some form of temperature reference to compensate for the cold junctions. The most common method is to measure the temperature at the reference junction with a direct-reading temperature sensor and then apply this cold-junction temperature measurement to the voltage reading to determine the temperature measured by the thermocouple. By using the Thermocouple Law of Intermediate Metals and making some simple assumptions, you find that the measured voltage depends on the thermocouple type, thermocouple voltage, and the cold-junction temperature. The measured voltage is independent of the composition of the measurement leads and the cold junctions, J2 and J3.

Science behind thermocouples: If heat is applied at one end, the electrons at that end become more energetic. They absorb energy and move out of their normal energy states and into higher ones. Some will be liberated from their atoms entirely. These newly freed highly energetic electrons move toward the cool end of the wire. As these electrons speed down the wire, they transfer their energy to other atoms. As these electrons build up at the cool end of the wire, they experience an electrostatic repulsion. The not-so-energetic electrons at the cool end move toward the hot end of the wire, which is how charge neutrality is maintained in the conductor. As electrons move from the cold junction to the hot junction, these not-so-energetic electrons are able to move easier in one metal than the other. The electrons that are moving from the hot end to the cold end have already absorbed a lot of energy, and are free to move almost equally well in both wires. This is why an electric current is developed in the loop.

2.0 Thin Skin Calorimeter

The purpose of a thin skin calorimeter is to measure an incident heat flux. Incident heat flux is the sum of the incoming radiation and convection. This instrument is created by welding a thermocouple to the back of a thin metal plate. The thickness of the wire used is dependent on the thickness of the metal plate. The face of the plate is painted black to minimize radiation heat loss. Thin skin calorimeters can be calibrated under a known heat flux generated by a cone calorimeter.

Measurement on the heat transfer rate to a metal calorimeter of finite thickness is based on the assumption of one-dimensional heat flow. After an initial transient, the response of the calorimeter on the exposed face of the thin skin calorimeter is calculated by using a lumped parameter analysis:

$$q = \rho c_p \delta \frac{dT}{dt}$$

Where $\frac{dT}{dt}$ is rate of the temperature of the back is unexposed surface of the calorimeter.

ρ is density C_p is specific heat and δ is the thickness of the plate.

Energy balance within the thin skin calorimeter is an energy balance which can be simplified as

$$q_{storage} = q_{in} - q_{out}$$

Where q_{in} is the incident heat flux and q_{out} is the loss of heat from the plate to its surroundings. The loss can be summarized as

$$q_{out} = q_{conv} - q_{rad} - q_{cond}$$

Where qconv is the convective losses to the surrounding; qrad is the radiative losses to the surroundings and qcond is the conductive losses.

During a transfer of heat, heat loss should be take into account while calculating the flux. A thermic balance on a plate can be present as below, where □ is emissivity of the plate;

$$q_{incident} = \frac{q_{net} + q_{conv} + q_{rad} + q_{cond}}{\varepsilon}$$

With thermal condition influenced by convection, radiation and internal energy generation, energy stored in the plate of the thin skin calorimeter can by represented as

$$\rho C_p \delta \frac{dT}{dt} = \varepsilon q_i'' - \varepsilon \sigma (T_{PL}^4 - T_0^4) - h_{cov}(T_{PL} - T_\infty) - hcc(T_{PL} - T_0^i)$$

Where left hand side of the equation is the change of energy stored in the plate of the thin skin calorimeter. The first term on the right hand side is the radiative energy absorbed by the plate. The second term is the radiative energy emitted by the plate. The third term is the conductive heat loss. The last term is calculating the heat loss into the ceramic fiberboard which requires to use of a contact conductance factor (hcc).

For our project, we are assuming the plate is lumped sum and thermally thin which allows us to use Newtonian cooling and contact conductance to represent transfer coefficient. In order to calculate the contact resistance, an explicit finite difference method is used to perform this analysis. An explicit finite difference method uses values at a current time step to evaluate values at a future time step, which can be represent as following equation

$$\frac{\partial T}{\partial t} = \frac{T_n^{i+1} - T_n^i}{\Delta t}$$

(Where i represents time and n represents node.)

A boundary condition of initial node is also applied:

$$BC1: \; -K\frac{\partial T}{\partial t} = h_{cc}(T_{PL} - T_0)$$

Where T pl is the temperature of the plate and T0 is the temperature of the initial node 0.

The boundary condition of the final node is:

$$BC2: \; -K\frac{\partial T}{\partial t} = 0 \; \& \; T = Tn$$

Where Tn is the temperature of the final node,n. To simplify our solution, addition layer of insulation is added on the back face and the insulation is assumed to be perfect.

By using the explicit finite difference method, the two boundary condition can be rewriten as following two equations for calculating the initial and final nodes temperature.

$$\text{BC1}: T_n^{i+1} = 2FoBi\left(T_{PL} - T_n^i\right) - 2Fo\left(T_n^i - T_{n+1}^i\right) + T_n^i$$

$$\text{BC2}: T_n^{i+1} = 2Fo\left(T_{n-1}^i - BiT_\infty\right) - 2FoT_n^i - 2FoBi\,T_n^i + T_n^i$$

Where Fo is the fourier number, which is a dimensionless term that describe the ratio of the heat conduction rate to the rate of thermal energy storage in a solid.

$$\text{Fo} = \frac{\alpha \Delta t}{\Delta x^2}$$

Where Δt is time(s), Δx is thickness(m) and α is thermal diffusivity (m²/s) can be represent as

$$\alpha = \frac{k}{\rho Cp}$$

Where k is the thermal conductivity (kW/mK), ρ is the density (kg/m³) and Cp is specific heat (kJ/kgK).

Bi is athe dimesionless Biot number which can be determined by using equation below,

$$\text{Bi} = \frac{h_{cc}\Delta x}{k}$$

Finally for an interior node, the explicit finite difference solution is

$$\text{Interior}: T_n^{i+1} = Fo\left(T_{n+1}^i + T_{n-1}^i\right) + T_n^i - 2FoT_n^i$$

Additionally, because explicit finite difference method is not always stable, in order to achieve the correct value from each time step. A specific condition is needed to be followed;

$$\text{Fo} \leq \frac{1}{2}$$

$$\text{Fo}(1 + \text{Bi}) \leq \frac{1}{2}$$

Thin skin calorimeters measure the net heat flux experienced by a surface. By knowing the thin skin calorimeters' material properties, and properties of the environment we are able to calculate the convective, radiative, conductive affects. By knowing these values, the incident heat flux may be

measured. For this purpose, thin skin calorimeters will be placed on the surface of the cladding being tested. This will give us incident heat flux distribution with respect to location and time.

Step 1: Thin Skin Calorimeter Design

Based off past MQP team experiment and our previous experiment results, the team decide to revise the design of the thin skin calorimeter to improve its performance for this project.

The first layer of our thin skin calorimeter is a 2-inch-by-2-inch ASTI 301 stainless steel plate, which is spray painted black to minimize heat loss and absorb radiation. There are two metal wires are welded on the back of the plate and on the other side of these two wires are two type k thermocouples. This set up mimics the thermocouple concept where the plate acts as the third metal. The next two layer are 13mm thick substrates that are made of ceramic fiberboard. The last layer is a 16.6 mm thick gypsum wallboard.

Based on our B term experimental results, the team decide to create two different set up. The first set up we drill a hole in the center of the second layer and have the wire attached to the plate run through and out in between the two ceramic fiberboards. Have another thermocouple sitting in between two ceramic fiberboards and one in between ceramic fiberboard and gypsum wallboard.

To secure these layers and minimize the air gap within the setup, small ditches in between Ceramic Fiberboard and Gypsum Board (Drywall) are done to create space for placing thermocouple wire. We then use Ceramic fiberboard material to fulfill the hole on the side of thin skin calorimeter to minimized air gap and radiative heat transfer. Two metal screws are used to ensure the layers are tightly bounded.

Figure 24 provides a schematic of our first thin skin calorimeters set up.
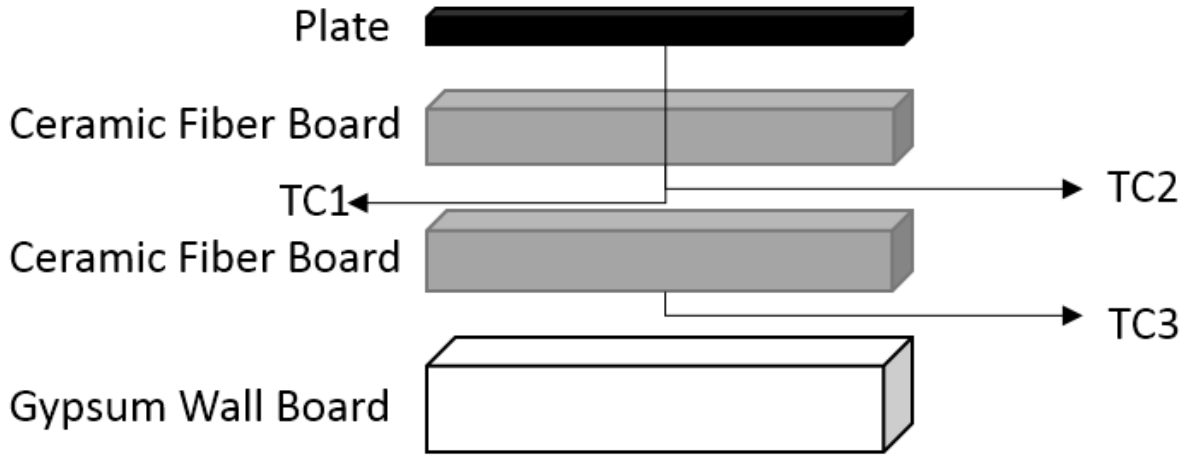
Figure 24: Thin Skin Calorimeter Design 1

The second set up for our thin skin calorimeter has "Thermocouple 1" only go through stainless steel plate to avoid drilling hole in the first ceramic fiberboard and prevent air gap. Figure 25 provides a schematic of our second thin skin calorimeters set up.
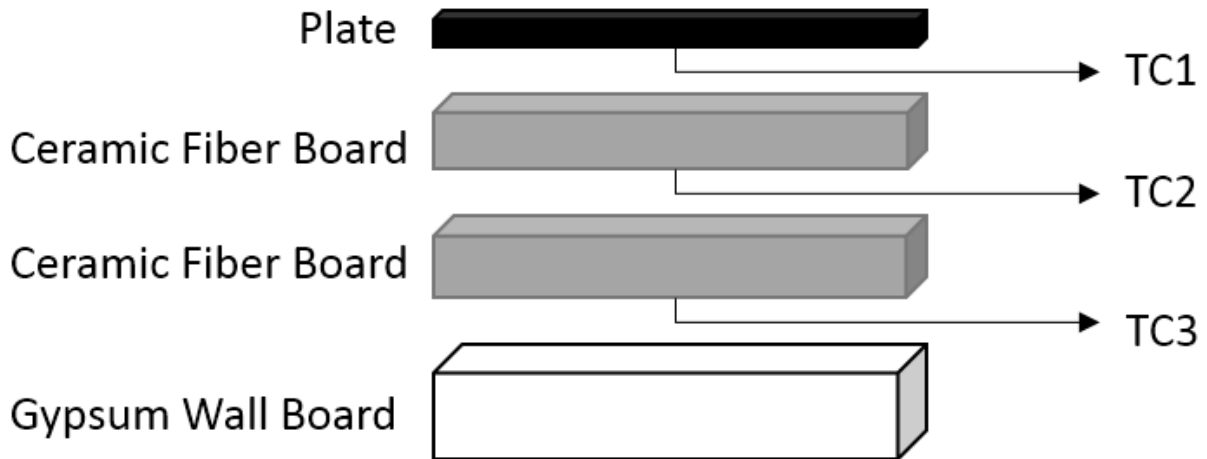
Figure 25: Thin Skin Calorimeter Design 2

Before the thin skin calorimeters are placed under the cone calorimeter, they are wrapped with two layers of insulation. The insulation is 4 inch thick Cerablanket. The following figure provide the insulation set-up.
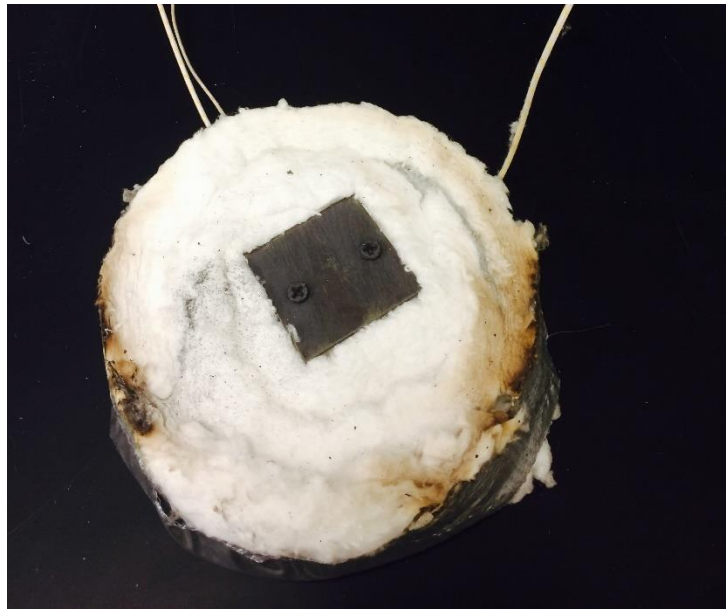
Figure 26: Thin Skin Calorimeter Insulation Set Up

Step 2: Finite Different Method Model

In order to better understand the thermal characteristics of thin skin calorimeter and better utilize the cone test data. A one dimensional finite difference model is created to determine the temperature distribution of the sample. Semi-infinite method is then utilized to verify the accuracy of the FDM model.

Finite Difference Method

With an assumption of twenty-six nodes that were distributed through the thin skin calorimeter. The first node locates at surface of the plate, the eighth node locates between the plate and ceramic fiberboard. The sixteenth node is at the interface between ceramic fiberboard and gypsum wall board.

Two different boundary conditions were used for the property estimation. The initial condition is simply using the thermocouple data from the surface of the plate.

The sample calculation of initial node is shown below:

$$\text{Change in Energy} = Convection\ out\ of\ Node - Conduction\ out\ of\ Node$$

$$\rho Cp \frac{\Delta x}{2} \frac{\left(T_n^{i+1} - T_n^i\right)}{dt} = hcc\left(T_{PL} - T_n^i\right) - k \frac{\left(T_n^i - T_{n+1}^i\right)}{dx}$$

$$T_n^{i+1} = \frac{2 \times hcc \times \Delta t}{\rho Cp\, \Delta x}\left(T_{PL} - T_n^i\right) - \frac{2 \times k\Delta t}{\rho Cp\, \Delta x^2}\left(T_n^i - T_{n+1}^i\right) + T_n^i$$

Because:

$$Fo = \frac{\alpha \Delta t}{\Delta x^2};\ \alpha = \frac{k}{\rho Cp}$$

$$Bi = \frac{h_{cc}\Delta x}{k}$$

$$FoBi = \frac{hcc\Delta t}{\rho Cp\, \Delta x}$$

Therefore

$$\text{Boundary Condition (BC) 1: } T_n^{i+1} = 2FoBi\left(T_{PL} - T_n^i\right) - 2Fo\left(T_n^i - T_{n+1}^i\right) + T_n^i$$

The equation for each interior node is derived below,

Interior:

$$q_{storage} = q_{in} - q_{out}$$

$$\rho Cp\delta \frac{\left(T_n^{i+1} - T_n^i\right)}{dt} = k \frac{\left(T_{n-1}^{i+1} - T_n^i\right)}{dx} - k \frac{\left(T_n^{i+1} - T_{n+1}^i\right)}{dt}$$

$$T_n^{i+1} = T_n^i + \frac{k\Delta t}{\rho Cp\Delta x^2}\left(T_{n+1}^i + T_{n-1}^i\right) - \frac{2k\Delta t}{\rho Cp\Delta x^2} T_n^i$$

$$Fo = \frac{\alpha \Delta t}{\Delta x^2};\ \alpha = \frac{k}{\rho Cp}$$

$$Fo = \frac{k\Delta t}{\rho Cp \times \Delta x^2}$$

$$T_n^{i+1} = Fo\left(T_{n+1}^i + T_{n-1}^i\right) + T_n^i - 2FoT_n^i$$

The second boundary condition for the back face of the thin skin calorimeter is shown below,

$$\text{Storage Energy} = Conduction\ out\ of\ Node - Convection\ out\ of\ Node$$

$$\rho Cp \frac{\Delta x}{2} \frac{(T_n^{i+1} - T_n^i)}{dt} = k \frac{T_{n-1}^i - T_n^i}{dx} - hcc(T_n^i - T_\infty)$$

$$T_n^{i+1} - T_n^i = \frac{2 \times k\Delta t}{\rho Cp\ \Delta x^2}(T_{n-1}^i - T_n^i) - \frac{2 \times hcc \times \Delta t}{\rho Cp\ \Delta x}(T_n^i - T_\infty)$$

Because

$$\text{FoBi} = \frac{hcc\Delta t}{\rho Cp\ \Delta x}$$

$$T_n^{i+1} - T_n^i = 2Fo(T_{n-1}^i - T_n^i) - 2FoBi\ (T_n^i - T_\infty)$$

$$\text{BC2}: T_n^{i+1} = 2Fo(T_{n-1}^i - BiT_\infty) - 2FoT_n^i - 2FoBi\ T_n^i + T_n^i$$

Semi- Infinite Method

In order to successfully conduct correct data analysis in a solid, it is important to ensure that the finite

different method is written correctly. Therefore, the team decide to use semi-infinite solid analysis to

verify the finite different method. The semi-infinite solid boundary condition assumes a constant incident

heat flux at the surface with convective and radiative heat losses. Carslaw and Jaeger define the following

equation, 1965 (Heat transfer Book)

$$\frac{T(x,t) - T_i}{T_\infty - T_i} = erfc\left(\frac{x}{2\sqrt{\alpha t}}\right) - \exp\left(\frac{h_{cc}x}{k} - \frac{h^2\alpha t}{k^2}\right) erfc\left(\frac{x}{2\sqrt{\alpha t}} + \frac{h_{cc}\sqrt{\alpha t}}{k}\right)$$

Detail Verification is explained in Appendix C2.

Step 3: Cone Test and Experiment Analysis

Cone Calorimeter

In order to calibrate our thin skin calorimeters to read an incident heat flux we need to use a cone calorimeter to supply a known incident heat flux. The cone is an upside down stainless steel dome with coils running in the inside of the dome. These coils heat up to a known temperature and release a known heat flux down toward the testing area. The cone uses a temperature controller in order to control the output temperature of the cone. For our experiments. The temperature settings are 25kW/m² (530 °C), 50 kW/m² (730 °C) and 75 kW/m² (840 °C).

Note 1—All dimensions are in millimetres.
Note 2—* Indicates a critical dimension.
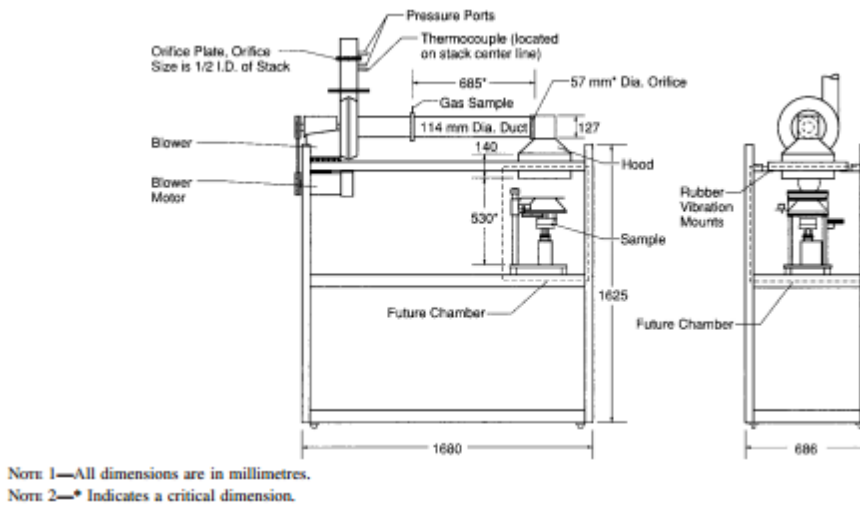
Figure 27: The cone side view

Note 1—All dimensions are in millimetres.
Note 2—* Indicates a critical dimension.
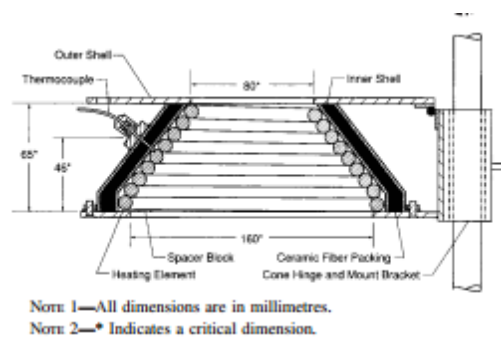
Figure 28: The cone cross sectional view
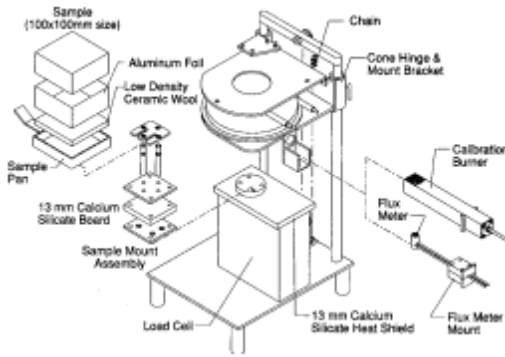
Figure 29: The cone top view

The cone calorimeter reads temperatures by attaching our thermocouples into the correct female adaptors, which located below the cone testing area. The temperature data in each one-second time interval is then computed through a developed program "Lab View". For our experiment, three thin skin calorimeters (assumed with same properties which is listed as the table below) were run under the cone for 10 minutes.

Table 9: Property of Thin Skin Calorimeter

Plate Properties	Values
Length (m)	0.05
Width (m)	0.05
Thickness (m)	0.044 (0.00146 for the plate)
Conductivity (kw/mK)	0.001
Density (kg/m^3)	80300
Specific Heat(kJ/kgK)	1
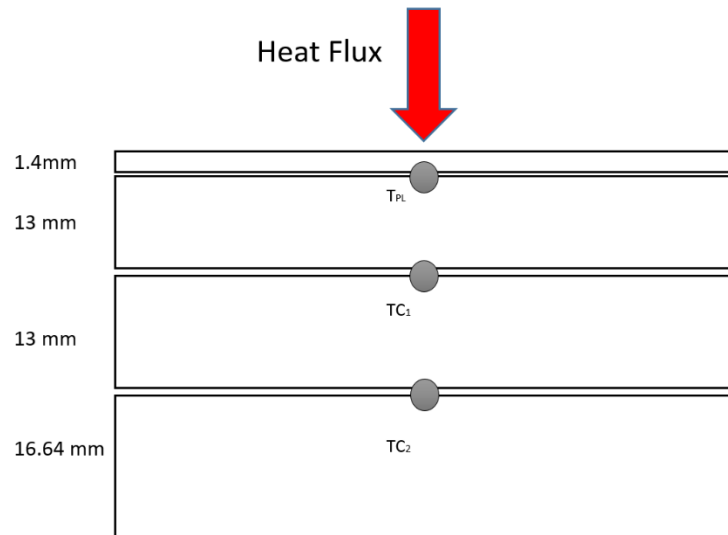
Figure 30: Thin Skin Calorimeter Sketch under Cone Test

Cone Experiment Results- Temperature Vs Time

In this section, the team studied the temperature distribution profile for all three boundary condition of three samples that has similar thermal and physical properties. The raw data was first analyzed by subtracting the initial temperature from each time step to maintain the starting temperature is at constant zero.

Boundary Condition 1

Heat Flux of 25kw/m²

25 kw/m² Plate

- 25kw/m2 Plate 1
- 25kw/m2 Plate 2
- 25kw/m2 Plate Average
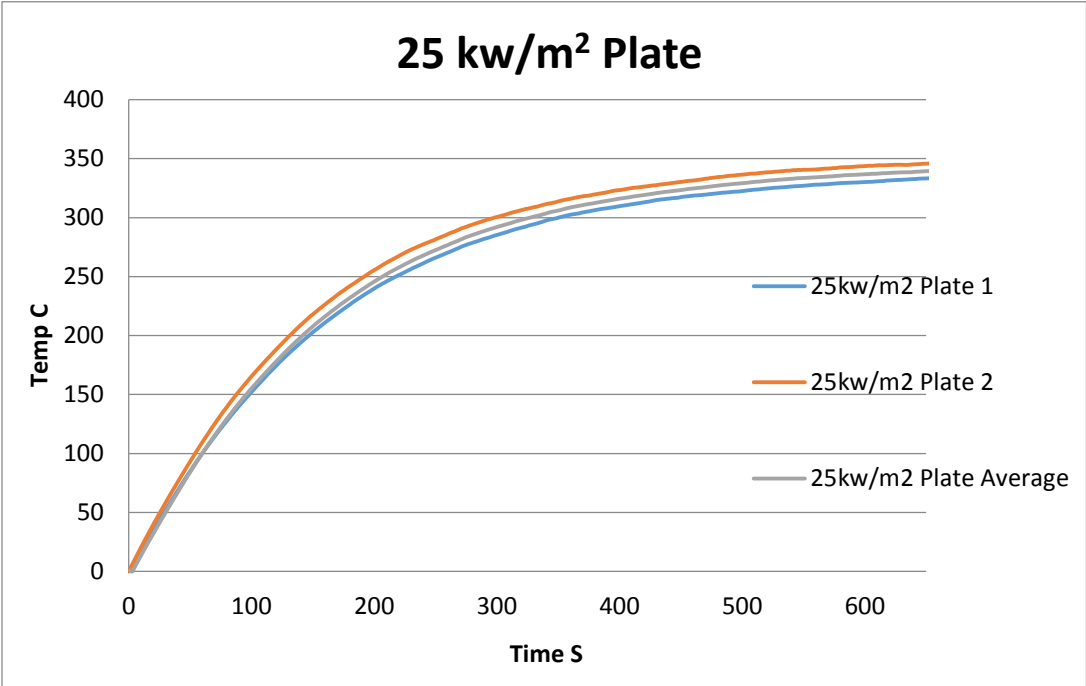
Figure 31: Heat Flux of 25kw/m2

50 kw/m² Plate
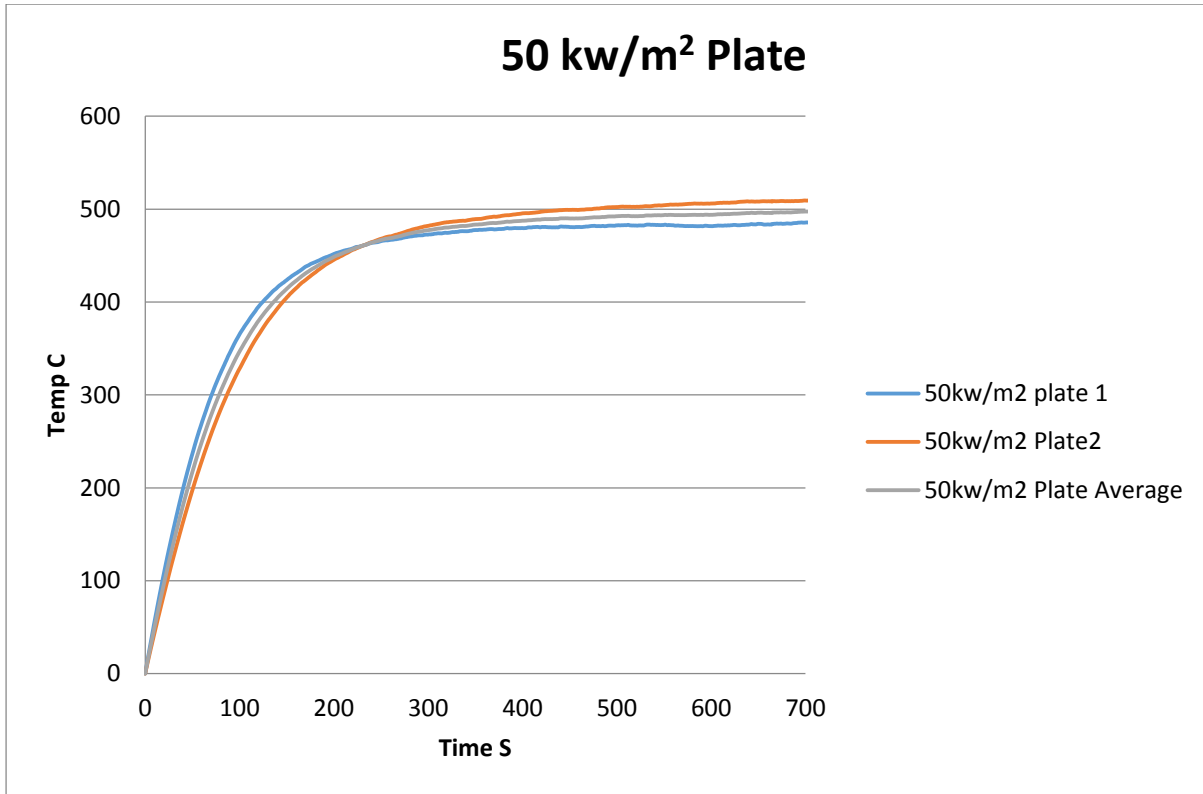
Figure 32: Heat Flux of 50kw/m2
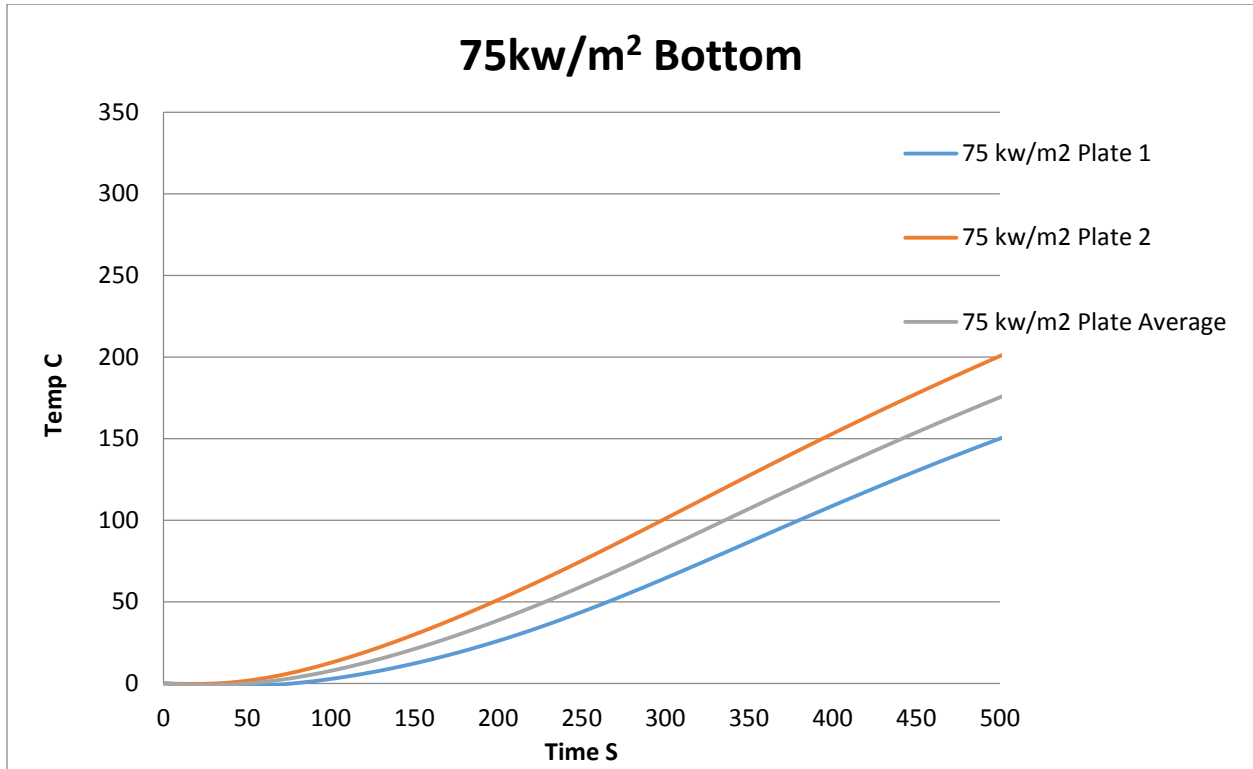
Figure 33: Heat Flux of 75 kw/m2

Interior Condition

Heat Flux of 25kw/m²

25kw/m² Middle
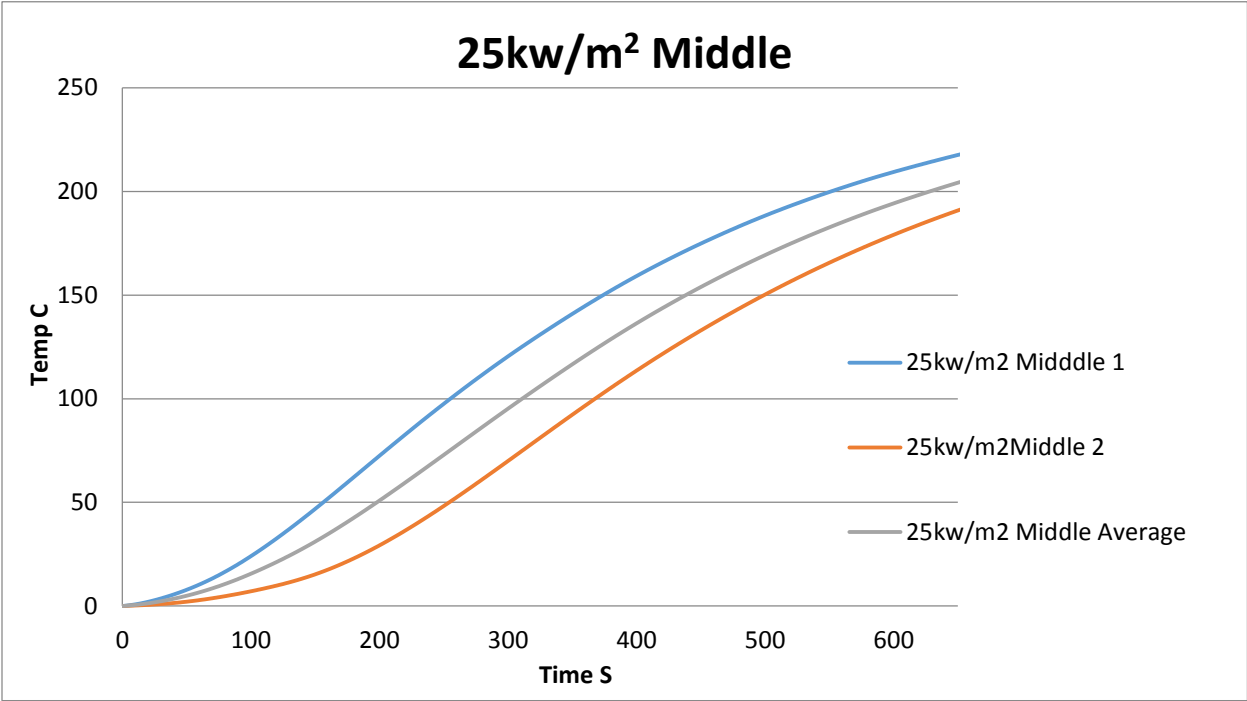
Figure 34: Heat Flux of 25kw/m2 interior condition

50kw/m² Middle
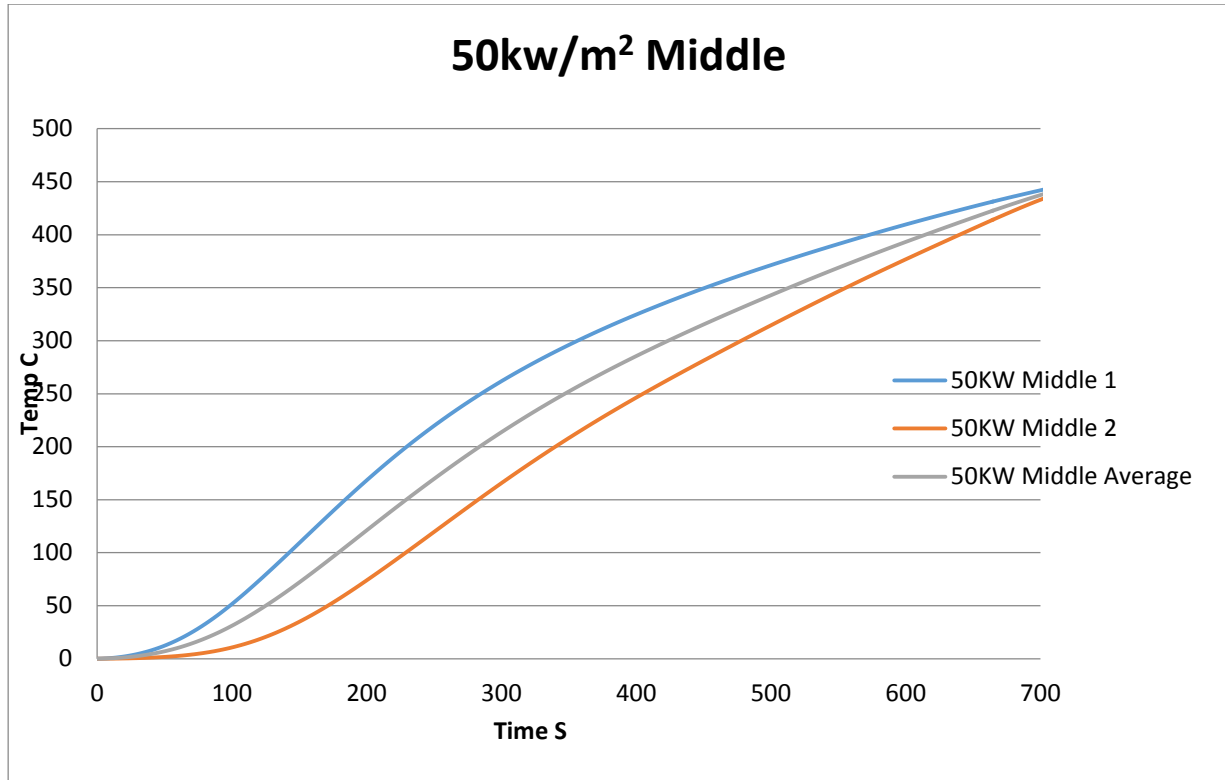
Figure 35: Heat Flux of 50kw/m2 interior condition

75 kw/m² Middle
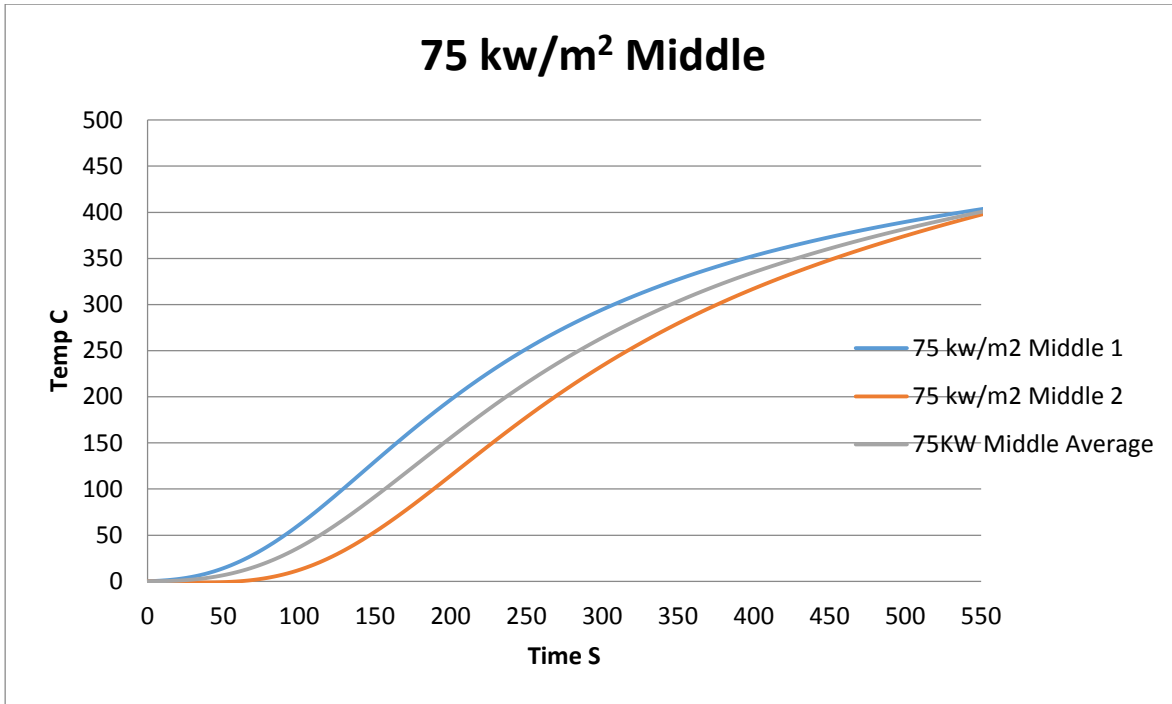
Figure 36: Heat Flux of 75kw/m2 interior condition

Boundary Condition 2

Heat Flux of 25kw/m²

25kw/m² Bottom
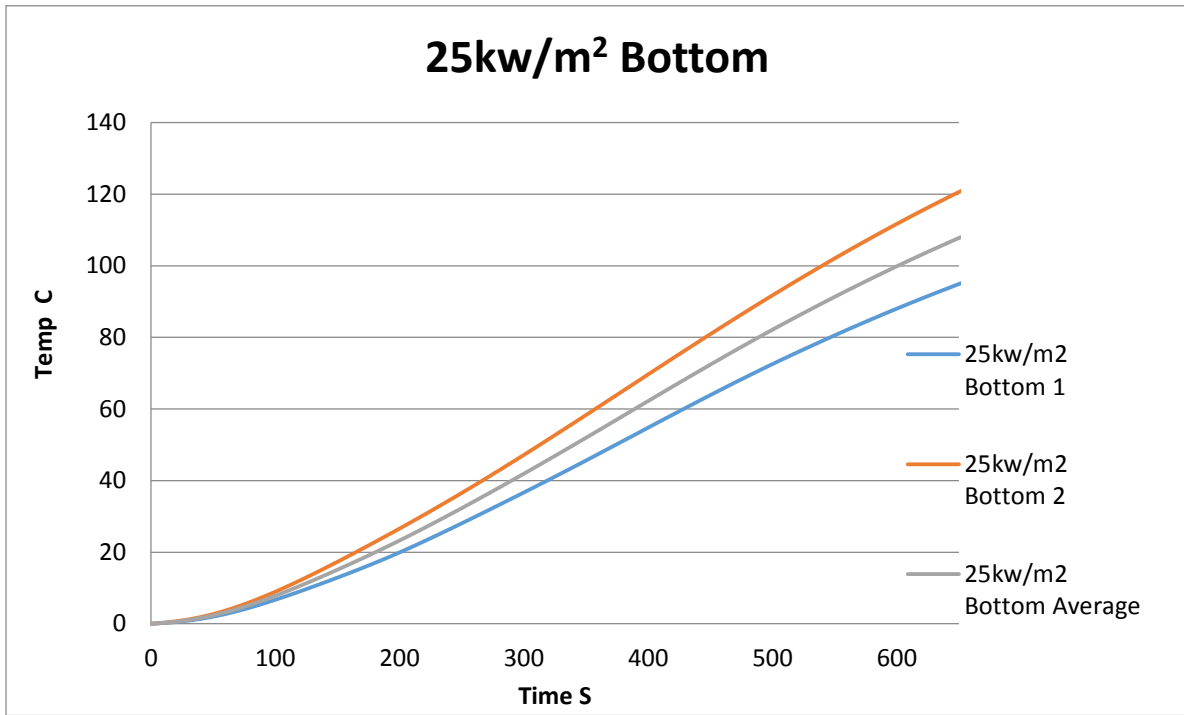
Figure 37: Heat Flux of 25kw/m2 boundary condition 2

Heat Flux of 50kw/m²
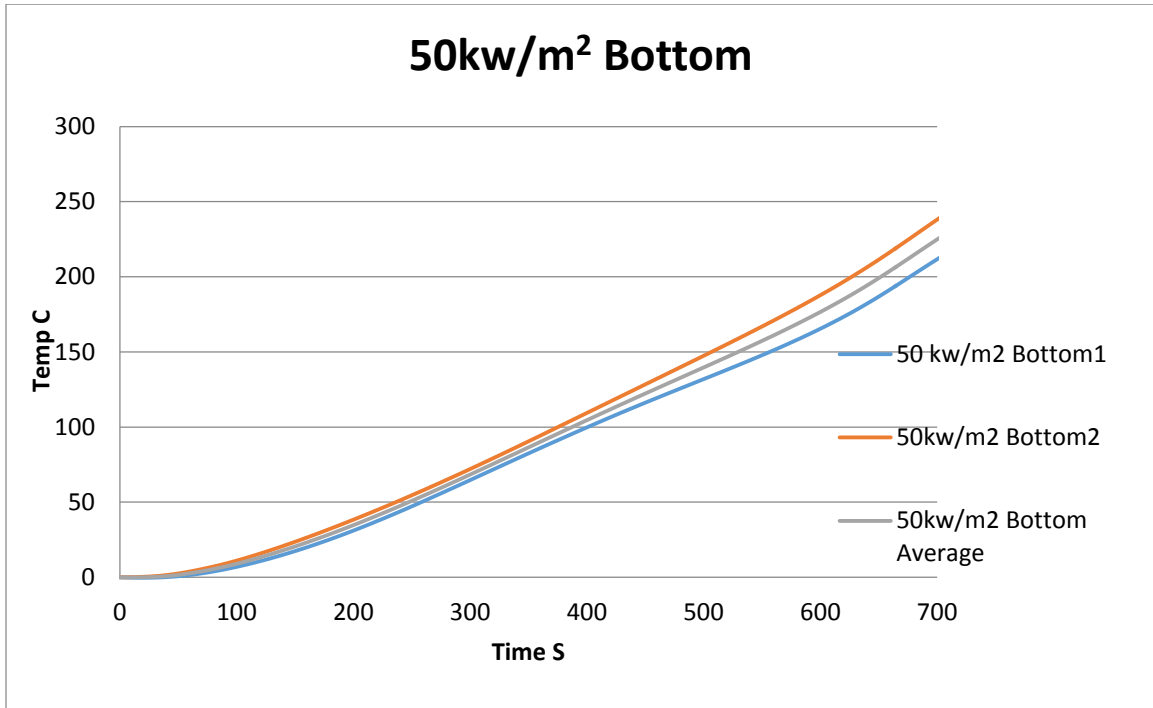
Figure 38: Heat Flux of 50kw/m2 boundary condition 2

Heat Flux of 75kw/m²
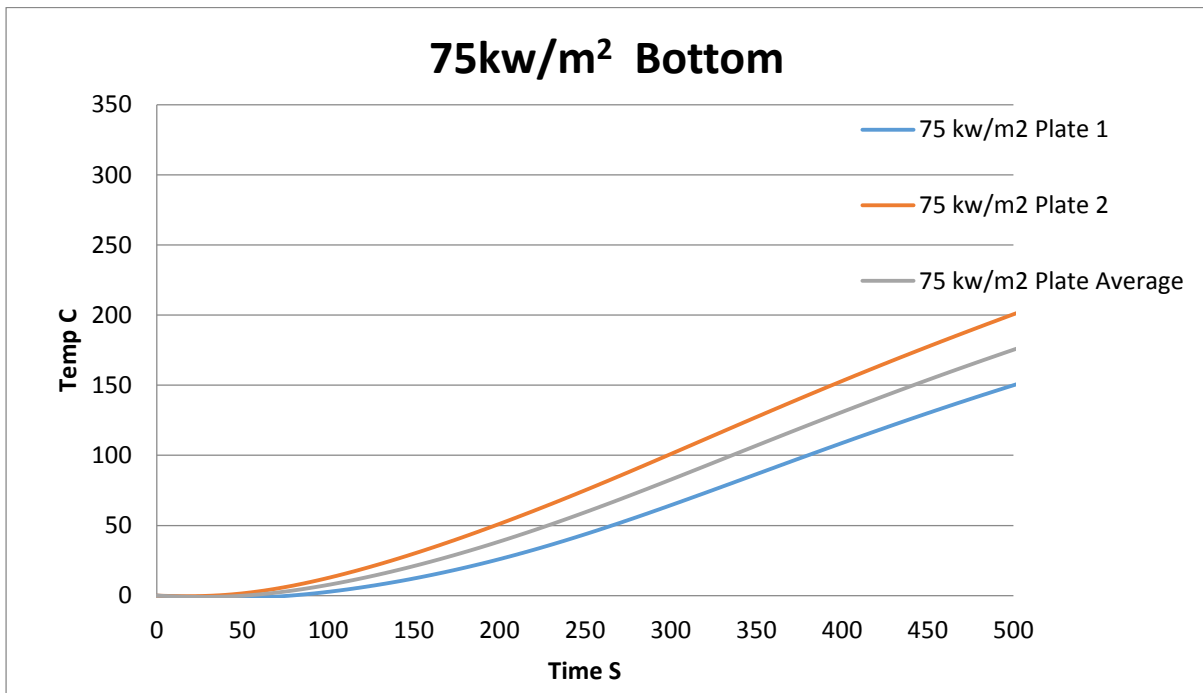
Figure 39: Heat Flux of 75kw/m2 boundary conditions 2

From our experimental data, all three boundary conditions appear to have similar trend and increment for each samples under different heat flux. In graphs above we discover that experimental error has cause temperature difference among samples by $\pm$ 50 °C, therefore the average of all trails were used to minimize the experimental error.

Overall Temperature Profile

Next, we studied the average temperature profiles of three thermal couples and we found all temperature profiles follow a similar trend under different heat flux.
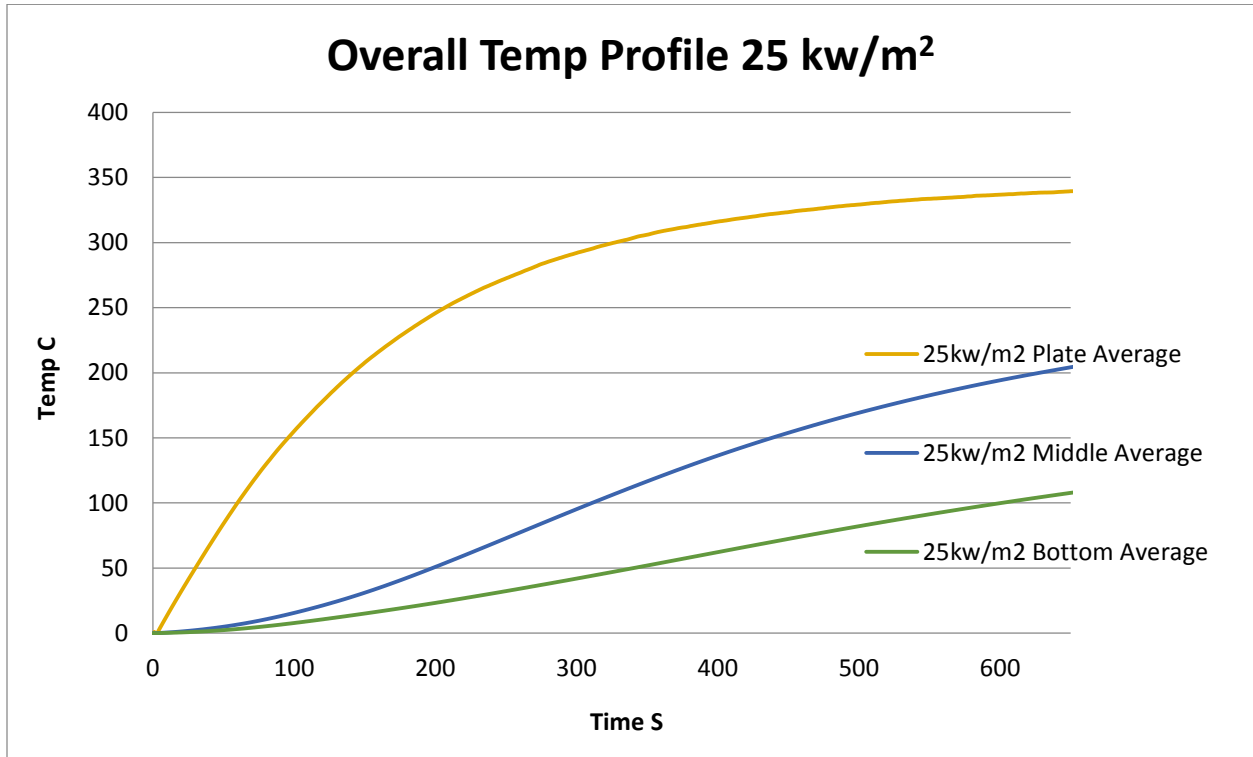
Figure 40: Overall Temp Profile 25 kw/m^2
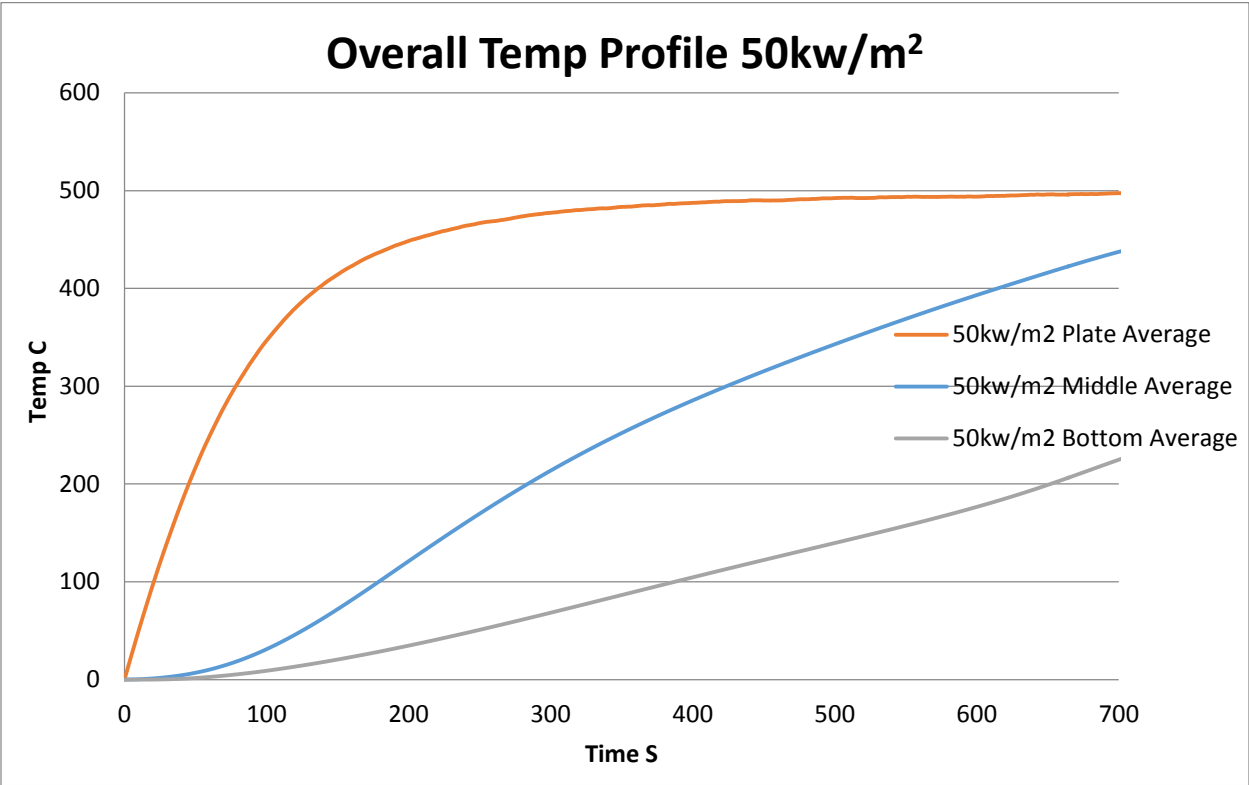
Figure 41: Overall Temp Profile 50 kw/m^2
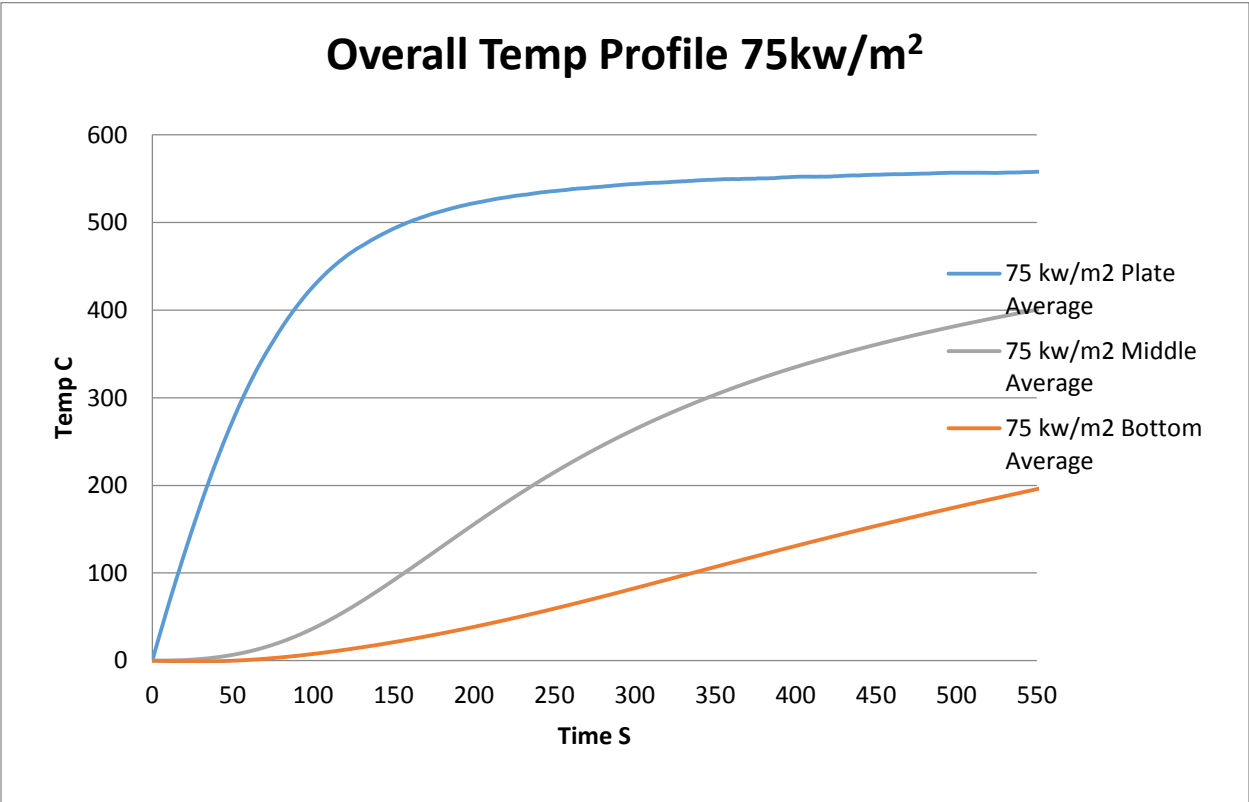
Figure 42: Overall Temp Profile 75 kw/m^2

66

Comparison Results Temperature vs Time

In this section, we will be comparing the plate, middle and bottom temperature distribution profiles under three different heat flux.

We will also study how temperature various with the depth of each thermocouple.

Plate Comparison
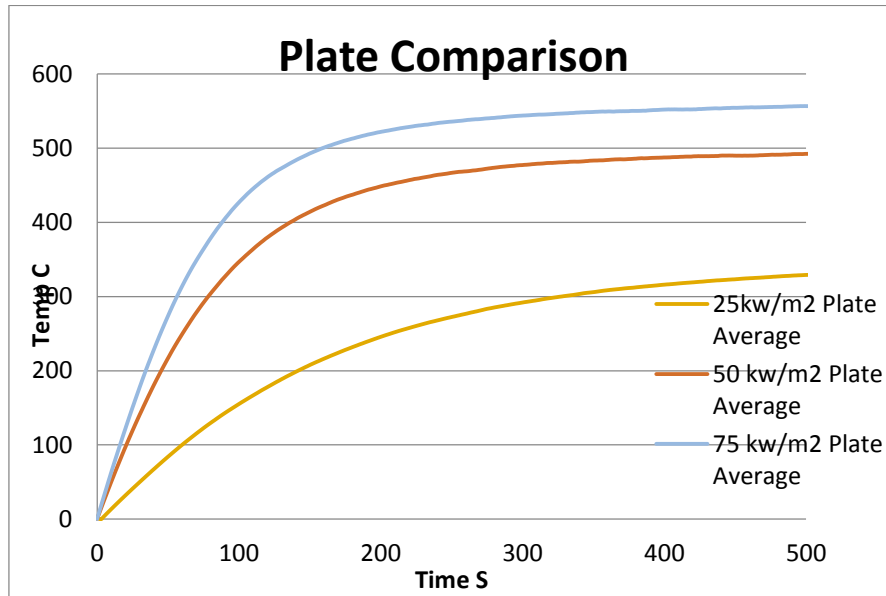
Figure 43: Plate Comparison

Figure 44: Middle Comparison

Figure 45: Bottom Comparison

From above experimental graphs, we observed that with an increasing heat flux we will result with a higher temperature trend. However,

Comparison Results Temperature vs Depth
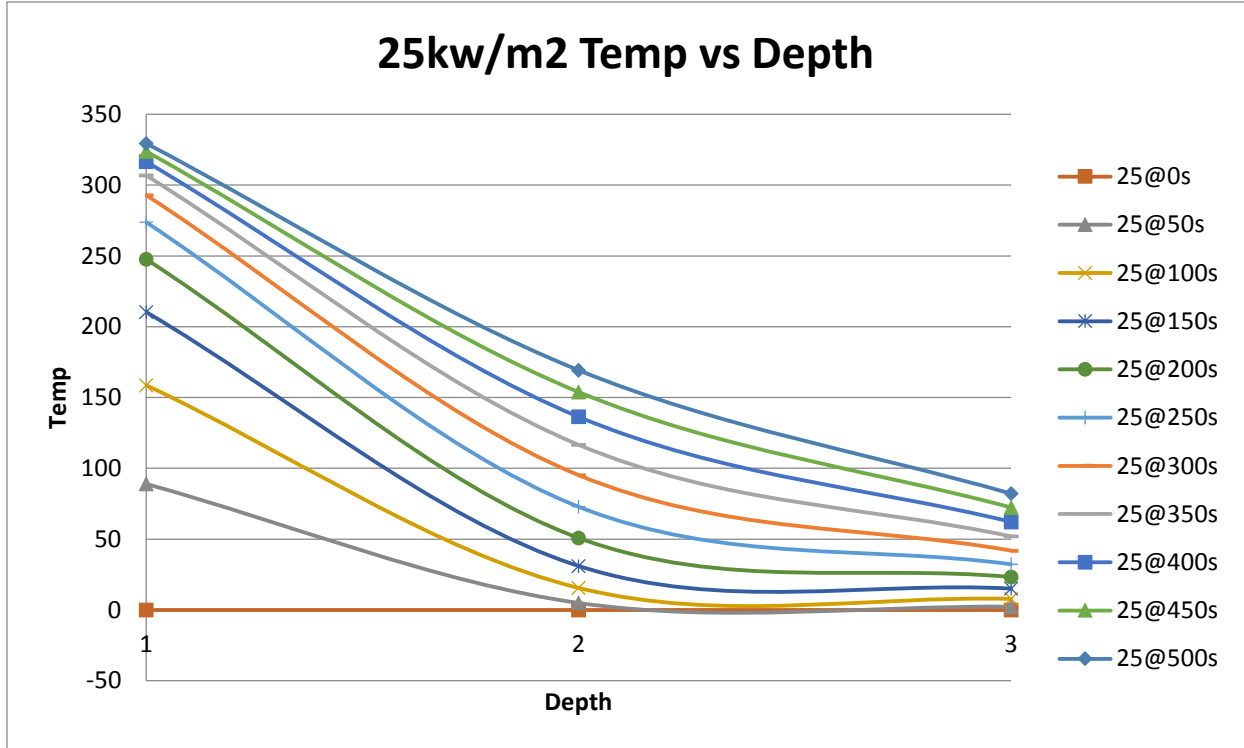
Heat Flux of 25kw/m²

Figure 46: Comparison Results Temperature vs Depth Heat Flux of 25kw/m2
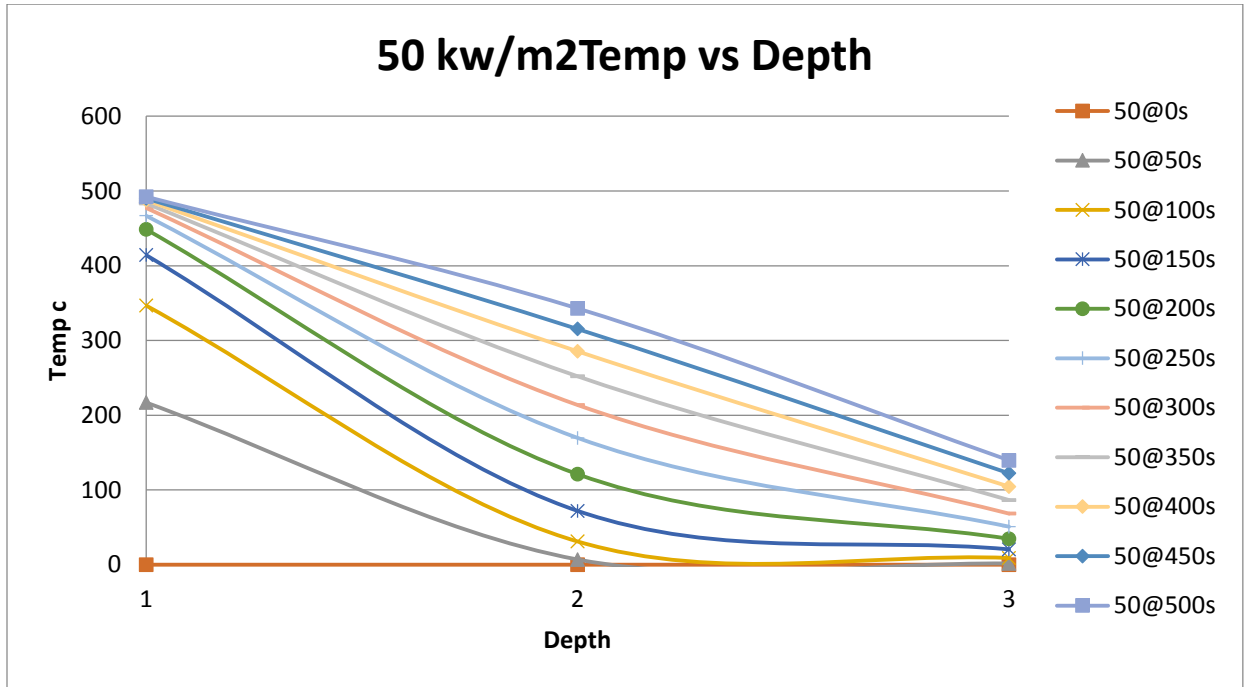
Figure 47: Comparison Results Temperature vs Depth Heat Flux of 50 kw/m2

Heat Flux of 75kw/m²
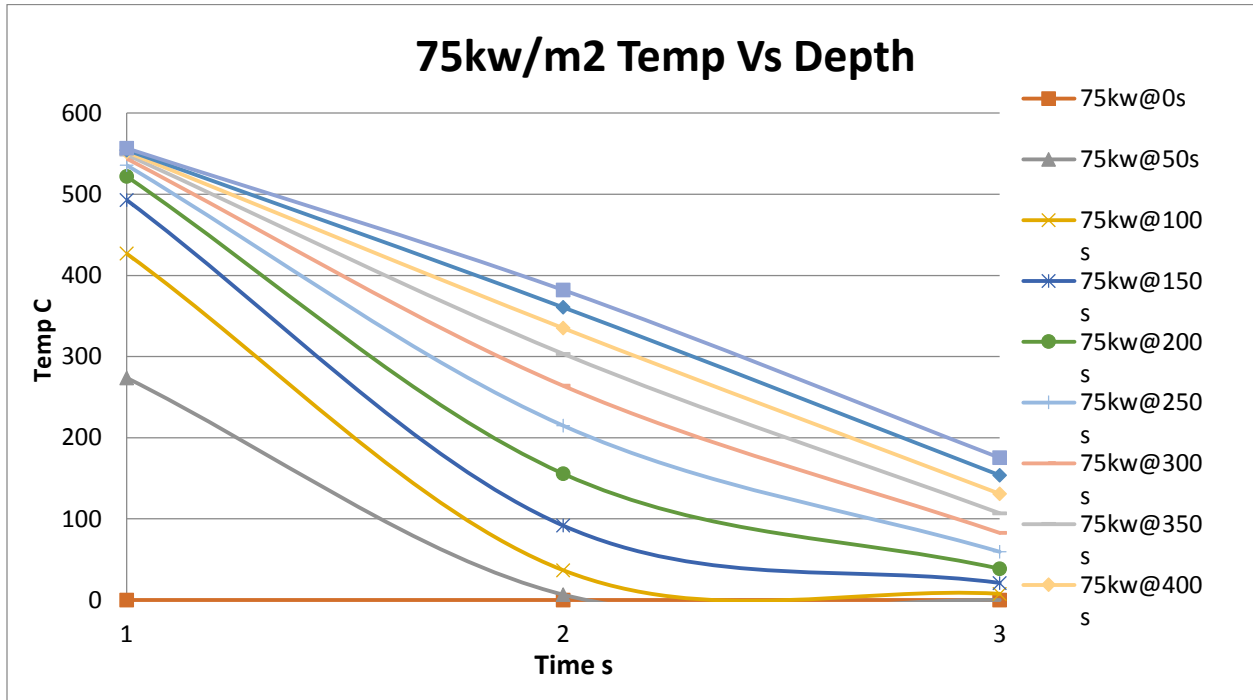
Figure 48: Comparison Results Temperature vs Depth Heat Flux of 75kw/m2

From all graph above, it is certain that temperature will decrease as the depth goes from plate to bottom

Step 4: Thin Skin Calibration

In order to calibrate our thin skin calorimeter (TSC) we will first need to develop a correct finite difference model. Once the correct model is determined, we will use experimental plate temperature data from cone test to evaluate contact conductance factor (hcc). Lastly, with known incident heat flux we will vary contact conductance and thermal properties parameters to better calibrate our model to match with our thin skin calorimeter.

For this project, we used 25kw/m², 50 kw/m²and 75 kw/m². The equations we use to calibrate our incident heat flux is:

$$\rho C p \delta \frac{dT_{PL}}{dt} = \varepsilon q_i'' - \varepsilon \sigma (T_{PL}^4 - T_0^4) - h_{cov} (T_{PL} - T_\infty) - hcc(T_{PL} - T_0^i)$$

Where Tpl is the temperature of the thin skin calorimeter, T_∞ is the ambient temperature, T_0 is the temperature of the first node using finite difference method and h_{cc} is the contact conductance between the thin skin plate and the ceramic fiberboard.

FDM & Semi-infinite Model Verification on Ceramic Fiber Board

In order to solve for temperatures changes within a solid, we will first need use finite difference method to simulate. When a finite difference analysis is used to solve for the temperatures in a solid it is important to ensure that the model is written correctly. For verification purpose, we then use semi-infinite analysis to ensure the accuracy of finite difference method and boundary conditions...

To comprise the sample, we assume 26 nodes and 25 mm of thickness for the finite difference model. Then use following thermal and material properties of ceramic fiberboard to calculate temperature for each node.

Table 10: Thermal and Material Properties of CFB

Tambient	700	k
k	0.002	kw/mk
CFB (ρ)	250	Kg/m3
Cp	1	J/gk
Hcc (Contact Conductance factor)	0.8	Kw/m2k
Dx	0.001	m

$$\alpha = \frac{k}{\rho Cp} = 0.0000008$$

$$\text{Fo} = \frac{\alpha \Delta t}{\Delta x^2} = 0.048$$

Additionally, because explicit finite difference method is not always stable, in order to achieve the correct value from each time step, fourier number need to follow condition below;

$$\text{Fo} \leq \frac{1}{2}$$

$$\text{Fo}(1 + \text{Bi}) \leq \frac{1}{2}$$

$$\text{Biot number 1} = \frac{h_{cc}\Delta x}{k} = 4$$

$$\text{Biot number 2} = \frac{h_{cc}\Delta x}{k} = 0$$

$$\text{Dt} = 0.06s$$

With given parameters, Newtonian equations of two boundary conditions and interior node were used to calculate the temperature changes over time.

Boundary Condition1:

$$T_n^{i+1} = 2FoBi\left(T_{PL} - T_n^i\right) - 2Fo\left(T_n^i - T_{n+1}^i\right) + T_n^i$$

Boundary Condition 2:

$$T_n^{i+1} = 2Fo\left(T_{n-1}^i - BiT_\infty\right) - 2FoT_n^i - 2FoBi\,T_n^i + T_n^i$$

Interior Node:

$$T_n^{i+1} = Fo\left(T_{n+1}^i + T_{n-1}^i\right) + T_n^i - 2FoT_n^i$$

Based on given condition, two boundary conditions are Node 1 &26 (Thermocouple 1 & Thermocouple 3) and the interior condition is Node 12. Sample calculations are included in Appendix C1. Detail calculation excel file can be found in Appendix C2.

Figure 49 and 50 show the comparison between finite difference and semi-infinite method.
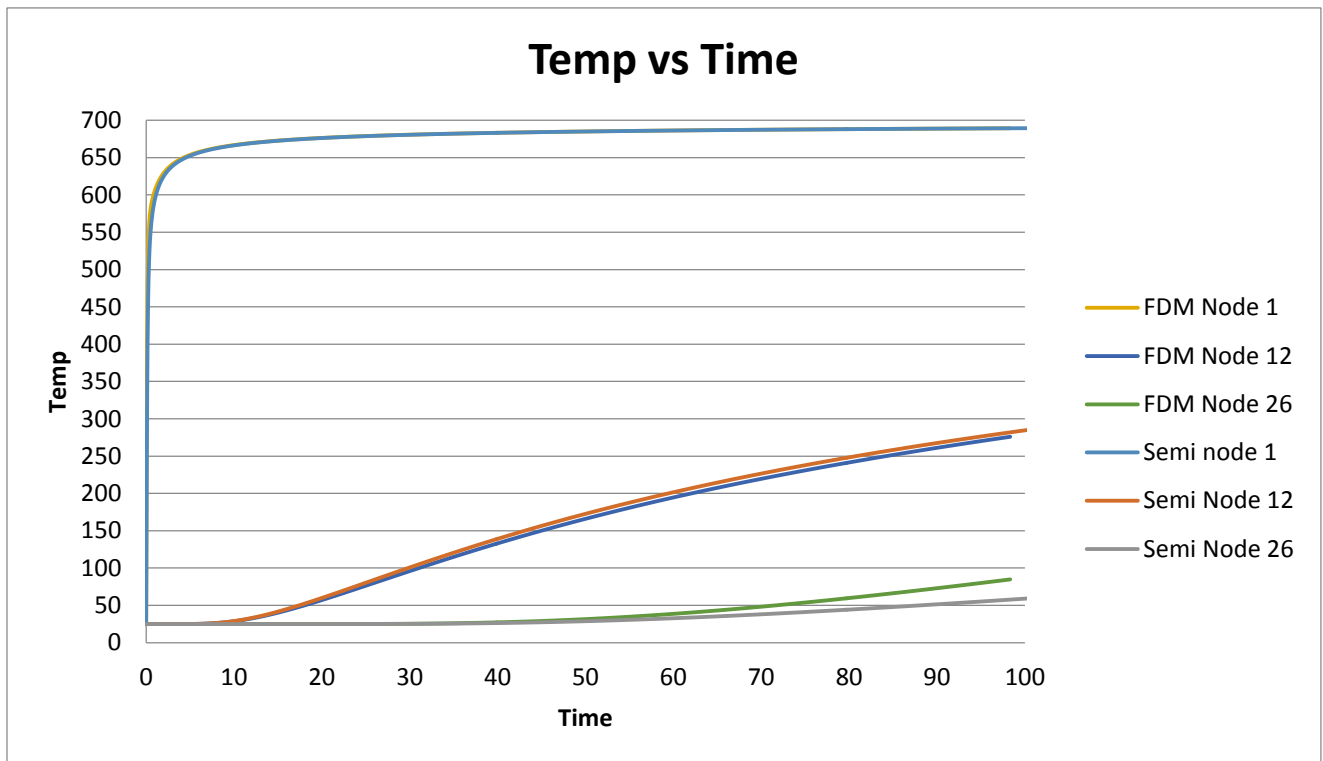
Figure 49: FDM & Semi-Infinite Temperature History Comparison
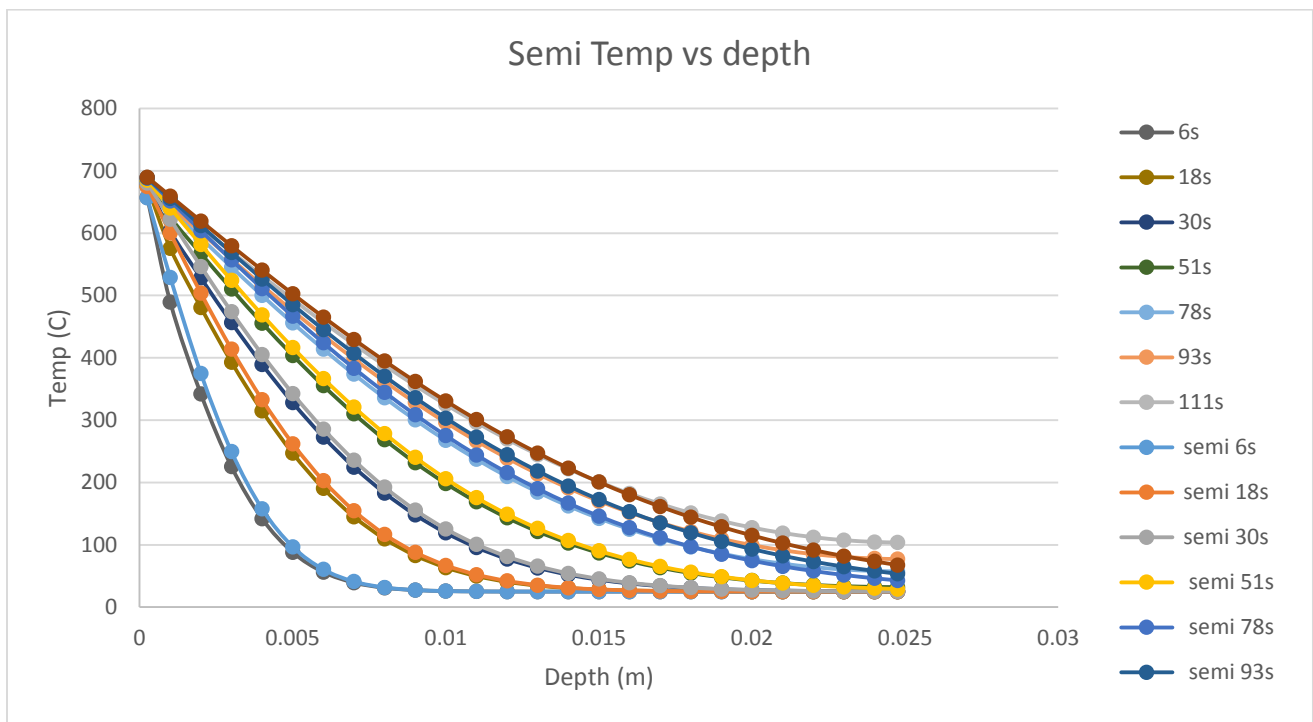
Figure 50: FDM & Semi-Infinite Temperature Profile Comparison

As the graphs show, the results for semi-infinite and finite difference methods are similar which concludes the finite difference boundary conditions are correctly derived and this method is correctly modeled.

Contact Conductance (hcc) verification

By assuming the plate is a lumped sum and thermally thin, this will allow us to include radiative, conductive and convective loss between the plate and the substrate into one heat transfer coefficient – contact conductance (hcc). By varying the contact conductance, we will be able further calibrate our thin skins.

Now the model for our thin skin calorimeters (TSC) has been created and we can use a cone calorimeter data to calibrate TSCs by using known thermal and physical properties of plate, ceramic fiberboard (CFB) and gypsum wall board (GWB).

Having experimental cone test data, we are able to evaluate contact conductance value when the comparison graph between the cone test and FDM of interior and back face temperature distribution are matching or close to each other. In this section, detail hcc verification process under different incident heat flux are included below.

Heat Flux of 25kw/m²

First, with given cone test plate results, polynomial 4th order equation is generated below.

Table 11: Temperature Debrief Data under Heat Flux of 25kw/m2

Time	Plate Average
0	0
1	1.961949408
2	3.919767795
3	5.862920103
4	7.792729086
5	9.710468233
.	.
.	.
.	.
.	.
.	.
648	339.4191705
649	339.4307485
650	339.4610757
651	339.531452
652	339.5905913
653	339.6309314

$$Y = (-3.2081 \times 10^{-9} \times x^4) + (6.5991 \times 10^{-6} \times x^3) - (0.005311 \times x^2) + (2.0684 \times x) - 1.4458$$

Next by using polynomial equation above, we are able to obtain a close matching plate temperature graph between finite difference analysis and cone test.

Figure 51: Plate Temperature Simulation with FDM Under 25kw/m2

By using plate temperature distribution as the heater for CFB and GWB and equations (1, 2 and 3) which can be found below, we will be able to calculate temperature of each node (between CFB and GWB).

$$BC1: T_n^{i+1} = 2FoBi(T_{PL} - T_n^i) - 2Fo(T_n^i - T_{n+1}^i) + T_n^i \ (\ 1 \ )$$

$$BC2: T_n^{i+1} = 2Fo(T_{n-1}^i - BiT_\infty) - 2FoT_n^i - 2FoBi \ T_n^i + T_n^i \ (\ 2 \ )$$

$$Interior: \ T_n^{i+1} = Fo(T_{n+1}^i + T_{n-1}^i) + T_n^i - 2FoT_n^i \ (\ 3 \ )$$

To determine a good estimation of hcc, we will compare the FDM simulation on thermal couple (TC) 2 and 3 with cone test of middle and bottom temperature profile using following condition and material properties of ceramic fiberboard (CFB) and gypsum wallboard (GWB).

Total Thickness	43	mm	dt	0.06	s	Total # of Nodes	44	
	Metal			CFB			Drywall/gypsum board	
hcc	/	kw/m2K	hcc	0.085	kw/M2k	hcc	0.025	kw/M2k
k	0.16	kw/mk	k	0.0002	kw/mk	k	0.00017	kw/mk
a	2.03822E-05		a	8.88889E-07		a	2.125E-07	
dx	0.001	m	dx	0.001	m	dx	0.001	m
Fo	1.222929936		Fo	0.053333333		Fo	0.01275	
Bi1	/		Bi1	0.425		Bi1	0.147058824	
rho	7850	kg/m3	rho	250	kg/m3	rho	800	kg/m3
cp	1	J/gk	cp	0.9	J/gk	cp	1	J/gk

This figure presents when hcc value is set equal to 0.085kw/m2k, will provide the closest comparison graphs between cone test and finite difference method for TC2 and TC3 temperature distribution over time under 25 kw/m2.
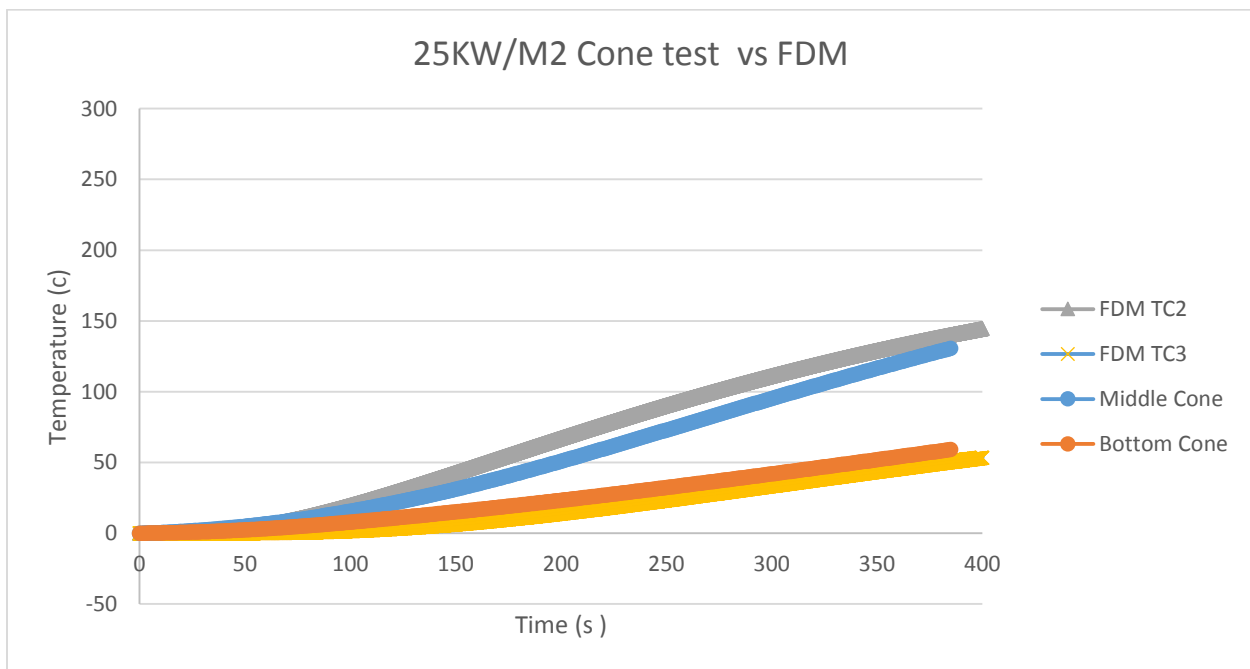
Figure 52: hcc verification under 25kw/m2

Heat Flux of 50kw/m^2

With given cone test plate results under 50 kw/m2 incident heat flux, a 4th order polynomial equation is generated below.

Time	Plate Average
0	0
1	5.198229383
2	10.37212566
3	15.50259618
4	20.56433744
5	25.58987096
.	.
.	.
.	.
.	.
.	.
648	495.8343408
649	495.9621448
650	496.1315698
651	339.531452
652	339.5905913
653	339.6309314

$$Y = (-1.1917 \times 10^{-8} \times x^4) + (2.2477 \times 10^{-5} \times x^3) - (0.015182 \times x^2) + (4.3798 \times x) - 26.1651$$

By using the equation above, a close match between FDM plate and cone test is generated.
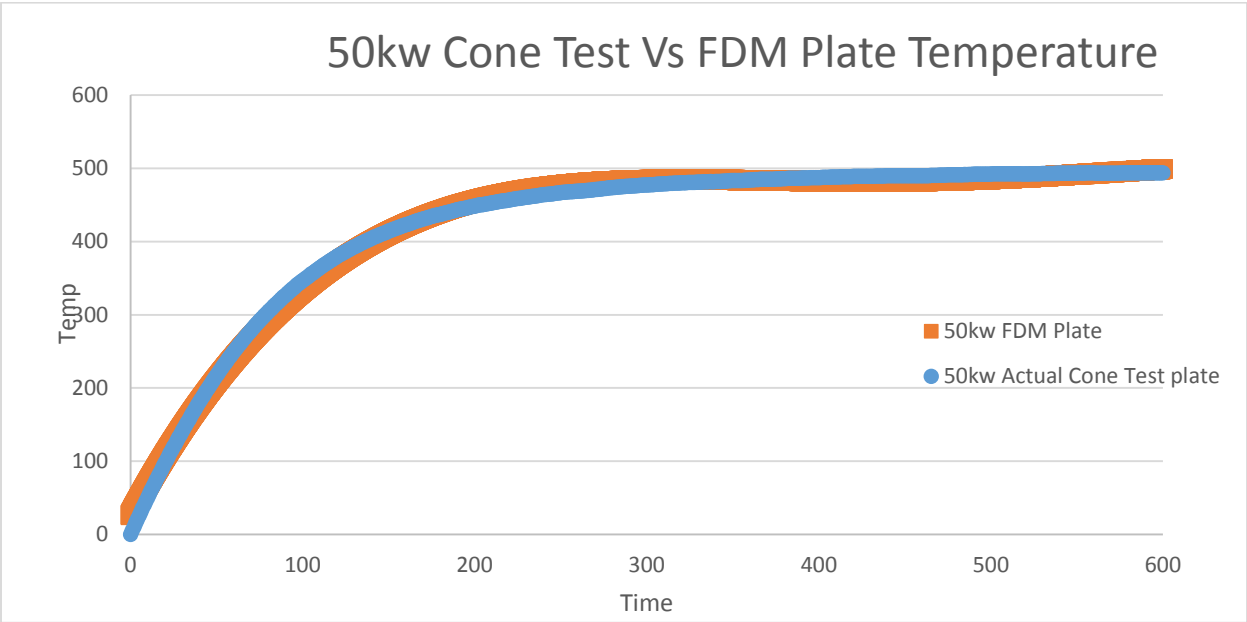
Figure 53: Plate Temperature Simulation with FDM Under 50kw/m2

By using plate temperature distribution as the heater for CFB and GWB and equations (1, 2 and 3), we will be able to calculate temperature of each node (between CFB and GWB).

In order to obtain a good estimation of hcc, we will compare the FDM simulation on thermal couple (TC) 2 and 3 with cone test of middle and bottom temperature profile using following condition and material properties of ceramic fiberboard (CFB) and gypsum wallboard (GWB).

Table 14: Thermal Properties of Plate, CFB and GWB for 50kw/m2.

Total Thickness	43	mm	dt	0.06	s	Total # of Nodes	44	
	Metal			CFB			Drywall/gypsum board	
hcc	/	kw/M2k	hcc	0.09	kw/M2k	hcc	0.01	kw/M2k
k	0.16	kw/mk	k	0.0002	kw/mk	k	0.00017	kw/mk
a	2.03822E-05		a	0.000001		a	2.125E-07	
dx	0.001	m	dx	0.001	m	dx	0.001	m
Fo	1.222929936		Fo	0.06		Fo	0.01275	
Bi1	/		Bi1	0.45		Bi1	0.058823529	
rho	7850	kg/m3	rho	250	kg/m3	rho	800	kg/m3
cp	1	J/gk	cp	0.8	J/gk	cp	1	J/gk

Figure 4 shows the closest comparison graphs between cone test and finite difference method for TC2 and TC3 temperature distribution over time under 50 kw/m2 when hcc value is set equal to 0.09 kw/m2k.
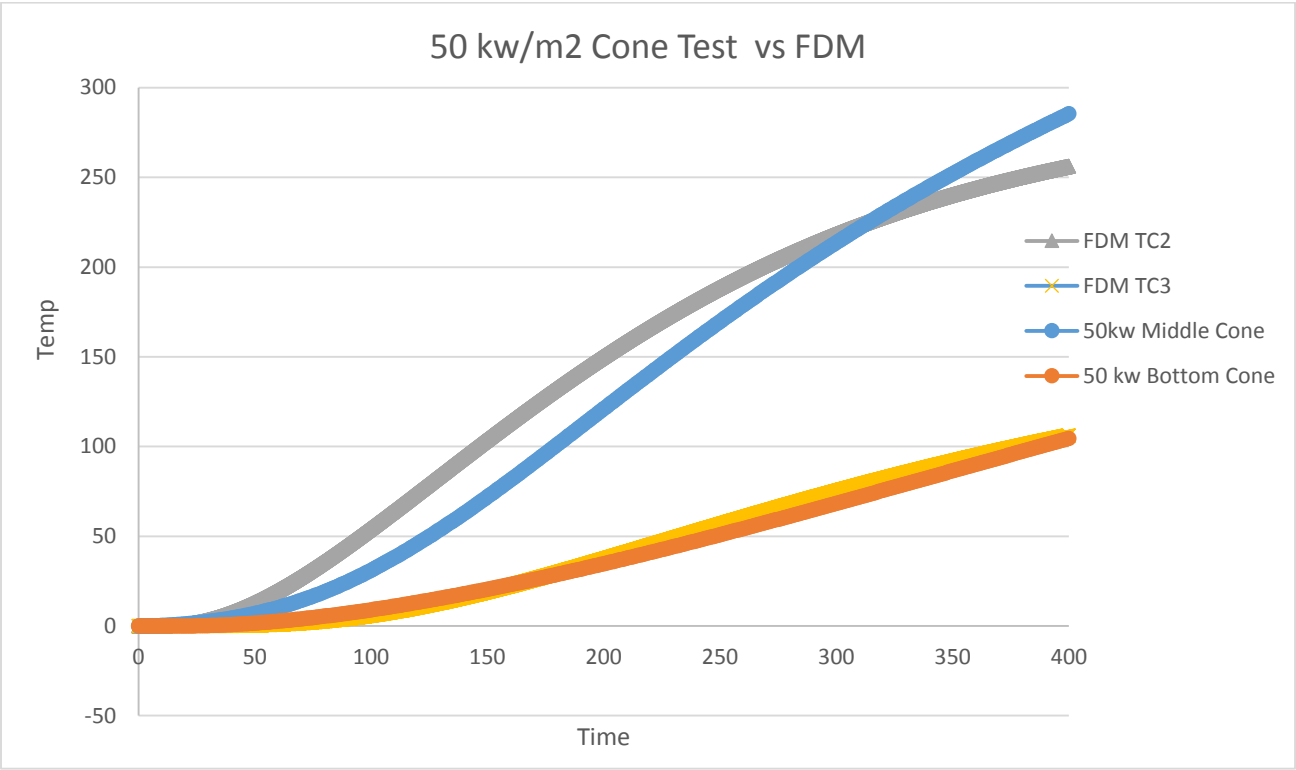
Figure 54: hcc verification under 50kw/m2

Heat Flux of 75kw/m^2

Under heat flux of 75kw/m2, we are able to generate a fourth order polynomial equation by using given cone test data.

Table 15: Temperature Debrief Data under Heat Flux of 50kw/m2

Time	Plate Average
0	0
1	6.510686291
2	12.95893351
3	19.39018428
4	25.6917769
5	32.03166916
.	.
.	.
.	.
.	.
.	.
535	557.0331748
536	557.0435373
537	557.0498674
538	557.1267336
539	557.1377062
540	557.1916333

$$Y = (-4.2869 \times 10^{-8} \times x^4) + (5.9644 \times 10^{-5} \times x^3) - (0.030038 \times x^2) + (6.5718 \times x) + 8.0043$$

By using polynomial equation above, a close match between FDM plate and cone test is shown below,

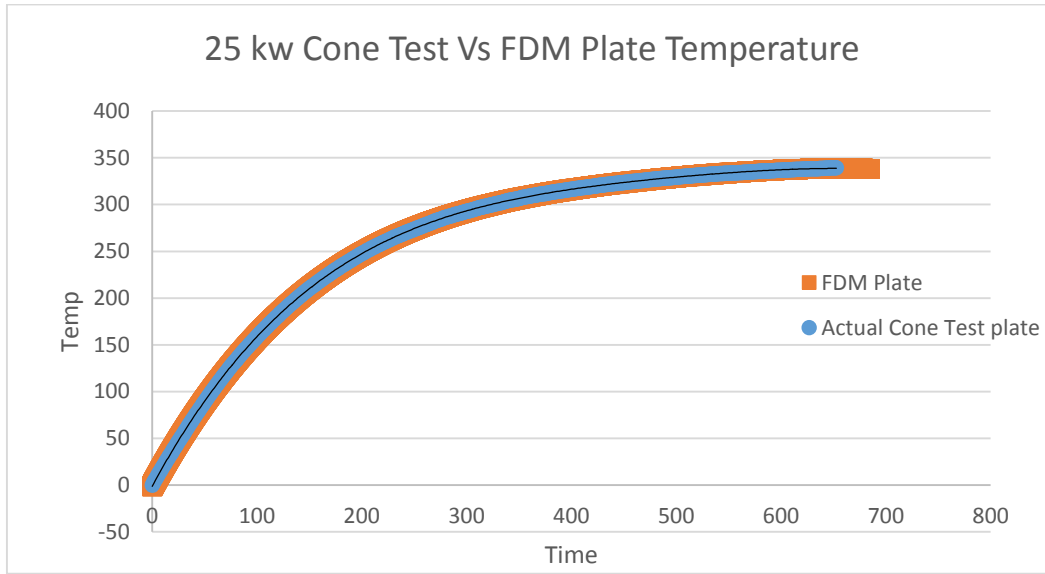## 75kw Cone Test vs FDM Plate Temperature
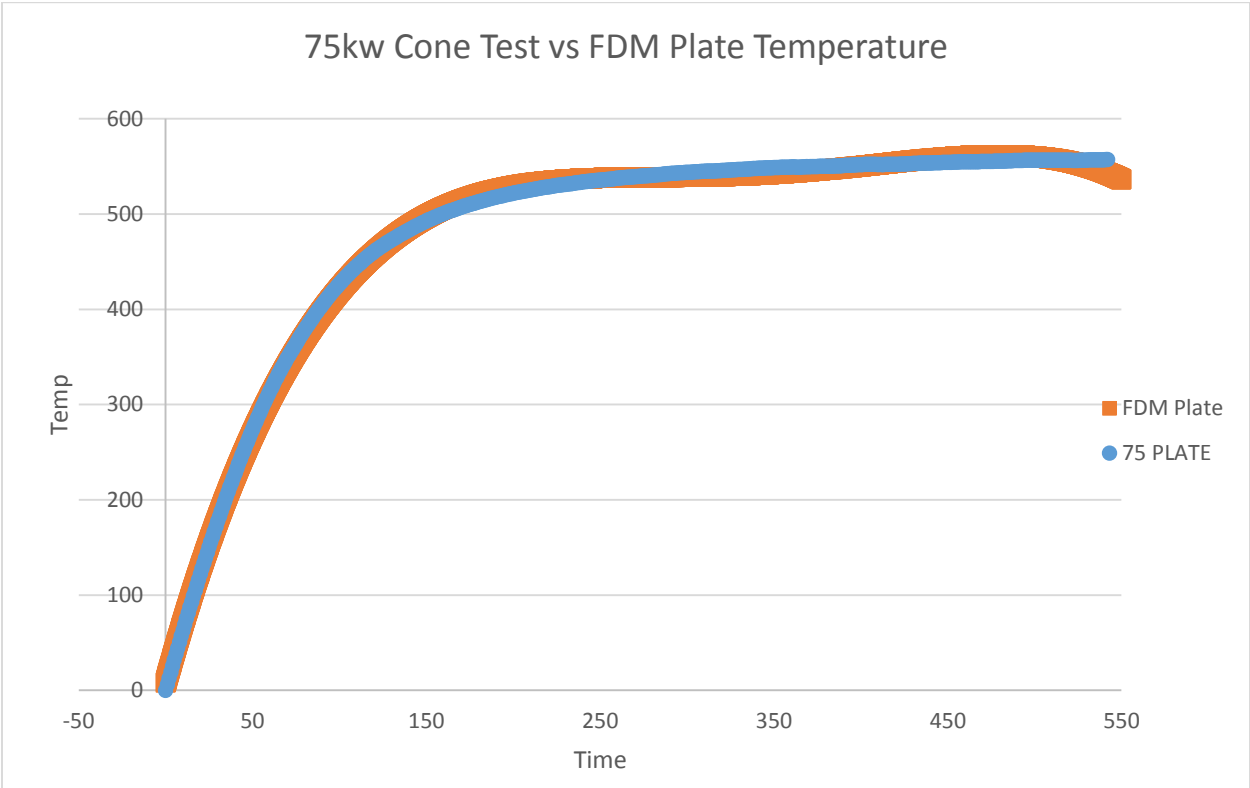
Figure 55: Plate Temperature Simulation with FDM Under 75kw/m2

By using plate temperature distribution as the heater for CFB and GWB and equations (1, 2 and 3), we will be able to calculate temperature of each node (between CFB and GWB).

In order to obtain a good estimation of hcc, we will compare the FDM simulation on thermal couple (TC) 2 and 3 with cone test of middle and bottom temperature profile using following condition and material properties of ceramic fiberboard (CFB) and gypsum wallboard (GWB).

Table 16: Thermal Properties of Plate, CFB and GWB for 75kw/m2.

Total Thickness	43	mm	dt	0.06	s	Total # of Nodes	44	
	Metal			CFB			Drywall/gypsum board	
hcc	/	kw/M2k	hcc	0.09	kw/M2k	hcc	0.01	kw/M2k
k	0.16	kw/mk	k	0.0002	kw/mk	k	0.00017	kw/mk
a	2.03822E-05		a	0.000001		a	2.125E-07	
dx	0.001	m	dx	0.001	m	dx	0.001	m
Fo	1.222929936		Fo	0.06		Fo	0.01275	
Bi1	/		Bi1	0.45		Bi1	0.058823529	
rho	7850	kg/m3	rho	250	kg/m3	rho	800	kg/m3
cp	1	J/gk	cp	0.8	J/gk	cp	1	J/gk

Figure 5 shows the closest comparison graphs between cone test and finite difference method for TC2 and TC3 temperature distribution over time under 50 kw/m2 when hcc value is set equal to 0.09 kw/m2k.
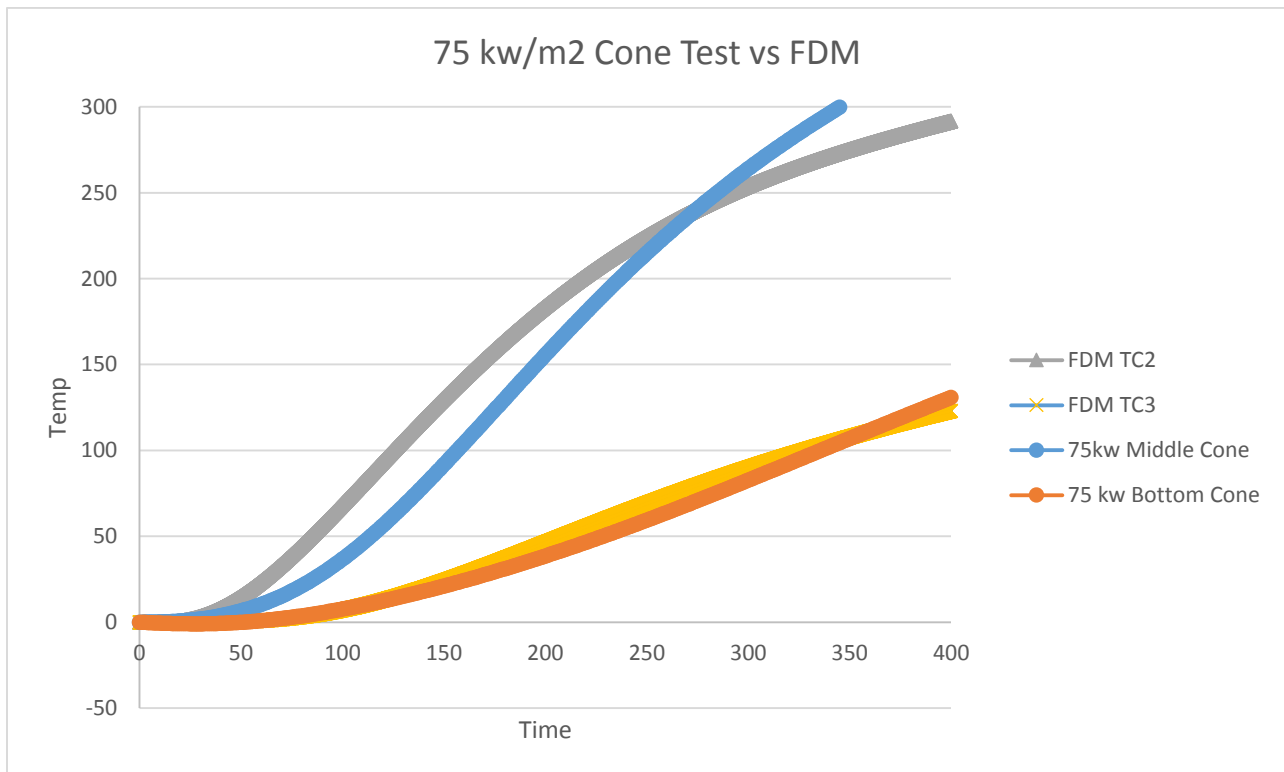
Figure 56: hcc verification under 75kw/m2

Calibration with Constant Contact Conductance

Now that with verified contact conductance and finite difference model, we can calibrate our thin skin calorimeter by having it to reproduce a known incident heat flux.

For our project, temperature setting of 530 °C gives a heat flux of 25 kW/m2, 730 °C gives a heat flux of 50 kW/m2 and 840 °C gives us a heat flux of 75 kW/m2.

With known govern equation below and following material properties, we are able to determine heat storage within each parameter.

Table 17: Material Properties for TS Calibration

T ambient	0	c
hcc of CFB	0.09	kw/M2k
dx	0.001	m
rho	7850	kg/m3
cp	0.8	J/Kg*K
stefan-boltzmann constant	5.67E-08	w/m2k4
Convection heat transfer coefficient	15	w/m2*k

Incident Heat Flux

$$\rho Cp\delta \frac{dT}{dt} = \varepsilon q_i'' - \varepsilon\sigma(T_{PL}^4 - T_0^4) - h_{cov}(T_{PL} - T_\infty) - hcc(T_{PL} - T_0^i)$$

Plate Temp Storage   Radiative Heat Loss   Convective Heat Loss   Heat Loss into CFB

Figures following show calibration for our thin skin under three incident heat flux.
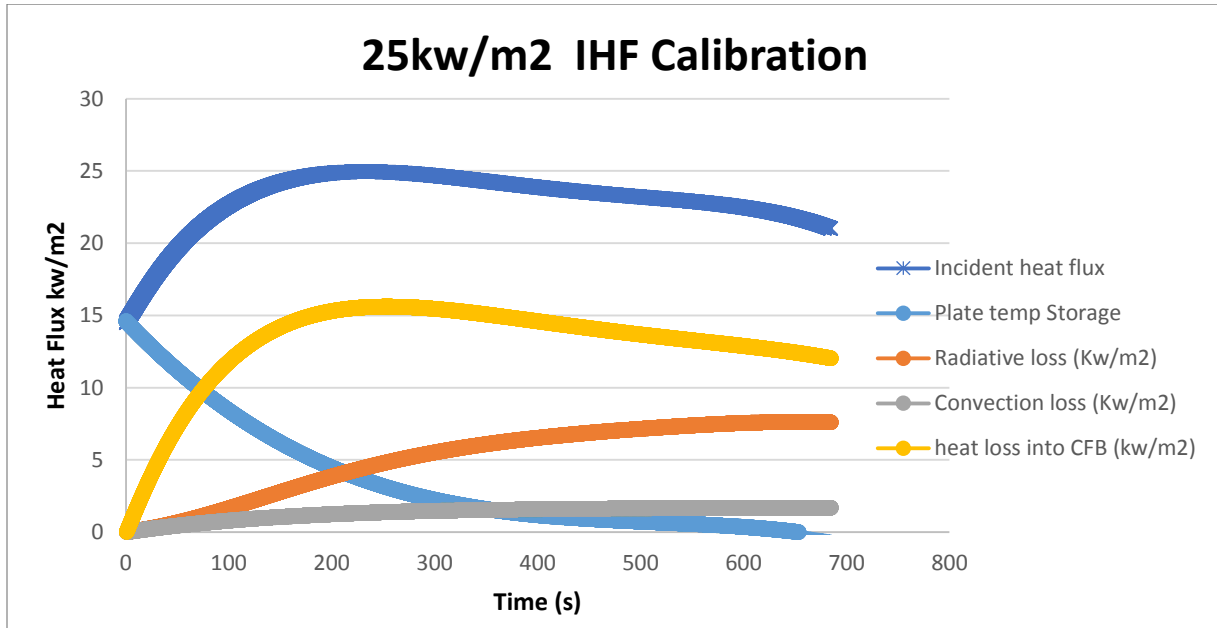
25kw/m2

Figure 57: Calibration of 25kw IHF

50kw/m2
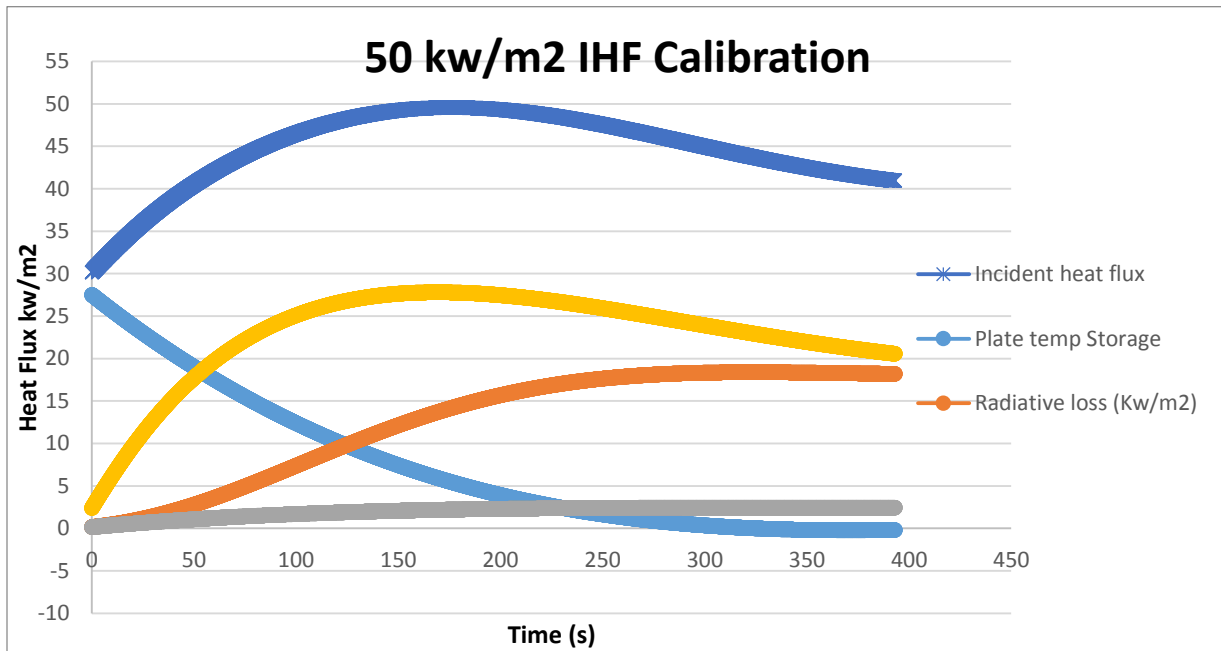
Figure 58: Calibration of 50kw IHF
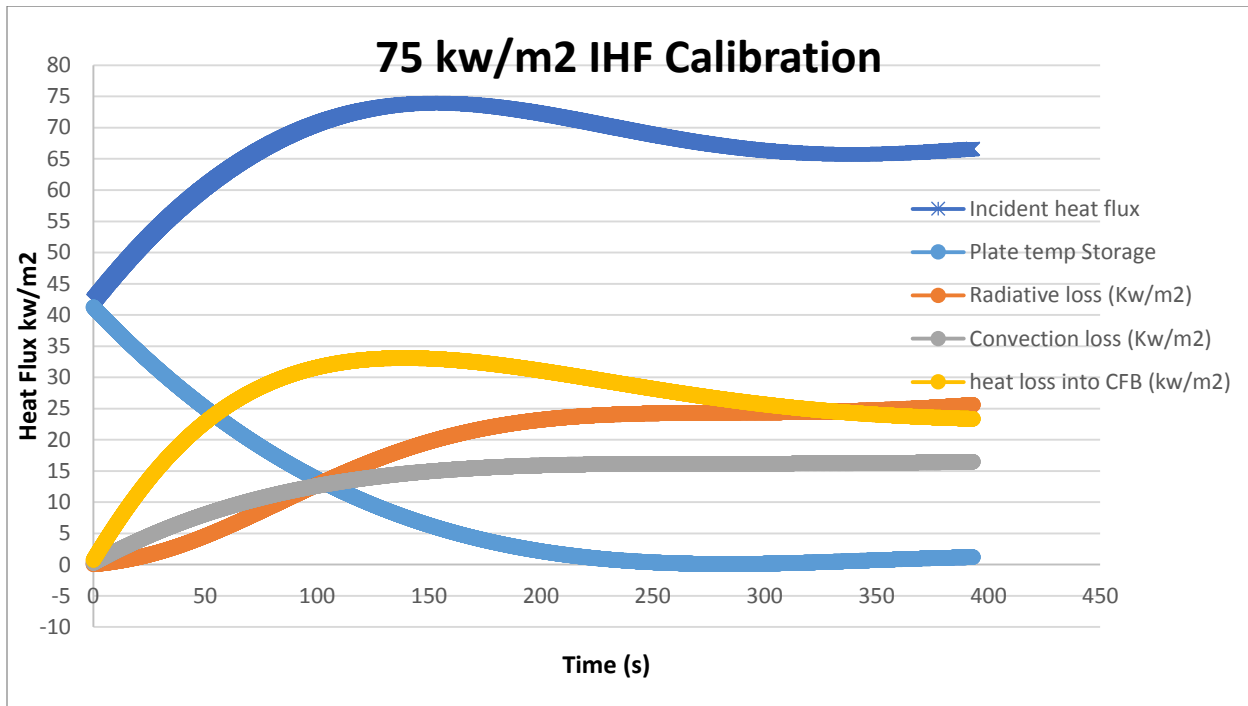
Figure 59: Calibration of 75kw IHF

Figures above show that the overall incident heat flux from FDM model contains some errors. The fluctuation of the heat loss into ceramic fiberboard affects the heat flux after 200s, which tells us to consider a better calibration in order to improve simulation on our thin skins. Another reason why there are errors occurred is delayed response from TCs and varying hcc value gives no significant change within the IHF calibration.

Calibration with Dynamic Contact Conductance

With the concern of if the calibration process from last section is a good representation for our project. In this section the team decide to study how radiation affect the calibration by dividing the contact conductance into two parts which can be represents as

$$hcc\ dynamic = h\ radiation + h\ conduction$$

After determine dynamic hcc values, we will then compare the incident heat flux calibration with the previous calibration process (constant hcc) to determine if radiation can improve the calibration process results.

To study the effects of radiation, we will first use the cone experimental data and temperature from each node using FDM. We will then use the following equation to determine a sequence of dynamic h radiation.

$$hradiation = \sigma\ (T_{PL}^2 + T_{CFB}^2)(T_{PL} + T_{CFB})$$

Where σ is Stefan-bolzmann constant, T_{PL} is plate temperature from cone test. T_{CFB} is temperature of node one which locates between plate and ceramic fiberboard.

With known thermal conductivity of air is 0.04w/mk, we then use h radiation sequence to backtrack thickness of air gap between plate and CFB when the h cond gives the closest trend of known incident heat flux.

$$h_{cond} = \frac{thermal\ conductivity\ of\ air}{thickness\ of\ air\ gap}$$

Sample Calculation for Incident Heat Flux of 25kw/m2k is shown below,

Given condition

k	0.0002	kw/mk
a	8.88889E-07	
dx	0.001	m
Fo	0.053333333	
rho	250	kg/m3
Stefan Boltzmann Constant	5.67E-08	W/m2k4
cp	0.9	J/gk

$$hradiation = \sigma \ (T_{PL}^2 + T_{CFB}^2)(T_{PL} + T_{CFB})$$

$$Bi = \frac{hcc * dx}{k}$$

All temperature value for radiative calculation is in K.

$$T \ (K) = T(°C) + 273 + T_{\infty}$$

h radiation is then calculated at listed below

Table 19: Calibration values

#	Delta T (s)	Time	h conduction of air gap(w/m2k)	h radiation (W/M2K)	stefan-boltzmann constant (w/m2k4)	hcc (kw/m2k)	bi	Radiative Plate Temp (K)	Radiative Node1 Temp (K)
0	0.06	0	66.006601	0.00000000000000	5.67E-08	0.0000000000000000	0	296.5542000000000	298
1	0.06	0.06	66.006601	5.95840453418392	5.67E-08	0.0719650051942499	0.0004	296.6782848818250	298
2	0.06	0.12	66.006601	5.96212801895729	5.67E-08	0.0719687286790233	0.0004	296.8023315330030	298
3	0.06	0.18	66.006601	5.96585283040265	5.67E-08	0.0719724534904687	0.0004	296.9263399620830	298
4	0.06	0.24	66.006601	5.96957891297120	5.67E-08	0.0719761795730372	0.0004	297.0503101776150	298
5	0.06	0.3	66.006601	5.97330622046950	5.67E-08	0.0719799068805355	0.0004	297.1742421881500	298
6	0.06	0.36	66.006601	5.97703471434137	5.67E-08	0.0719836353744074	0.0004	297.2981360022340	298
7	0.06	0.42	66.006601	5.98076436227672	5.67E-08	0.0719873650223427	0.0004	297.4219916284140	298
8	0.06	0.48	66.006601	5.98449513708338	5.67E-08	0.0719910957971494	0.0004	297.5458090752370	298
9	0.06	0.54	66.006601	5.98822701577132	5.67E-08	0.0719948276758373	0.0004	297.6695883512480	298
10	0.06	0.6	66.006601	5.99195997880816	5.67E-08	0.0719985606388742	0.0004	297.7933294649900	298

The closest trend line that we are able to get under 25kw/m2 incident heat flux is when

$$hcond = 0.066\,\frac{kw}{m2k}\,; thickness\ of\ air\ gap = 0.0006061\ m$$

The comparison graph between two calibration processes are shown below.
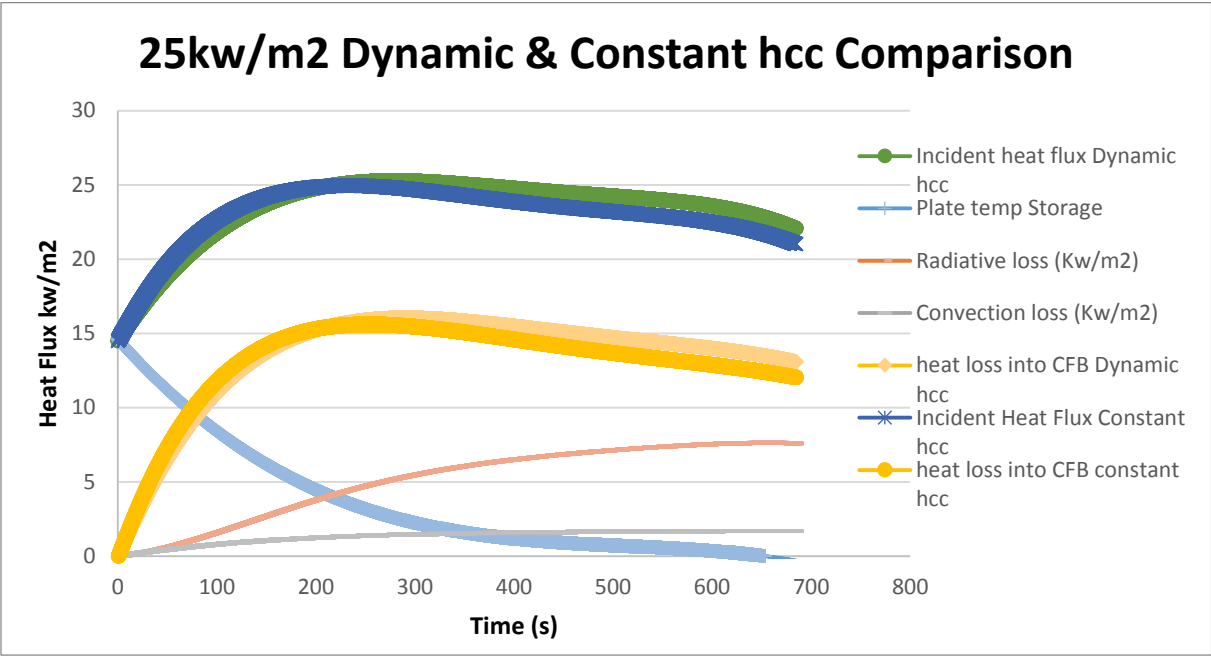
Figure 60: 25 kw/m^2 Dynamic & Constant hcc Comparison

 With similar approach we are able to

The closest trend line that we are able to get under 50kw/m2 incident heat flux is when

$$hcond = 0.06 \frac{kw}{m2k}; thickness\ of\ air\ gap = 0.000667\ m$$

The comparison graph between two calibration processes are shown below.

50 kw/m2 Dynamic & Constant hcc Comparision

Y-axis: Heat Flux kw/m2

X-axis: Time (s)

Legend:
- Dynamic Temp Storage
- Dynamic Radiative Loss
- Dynamic Convection loss
- dynamic Heat loss into CFB(KW/M2)
- dynamic hcc Incident heat flux
- Constant hcc Incident heat flux
- Radiative loss (Kw/m2)
- heat loss into CFB (kw/m2)
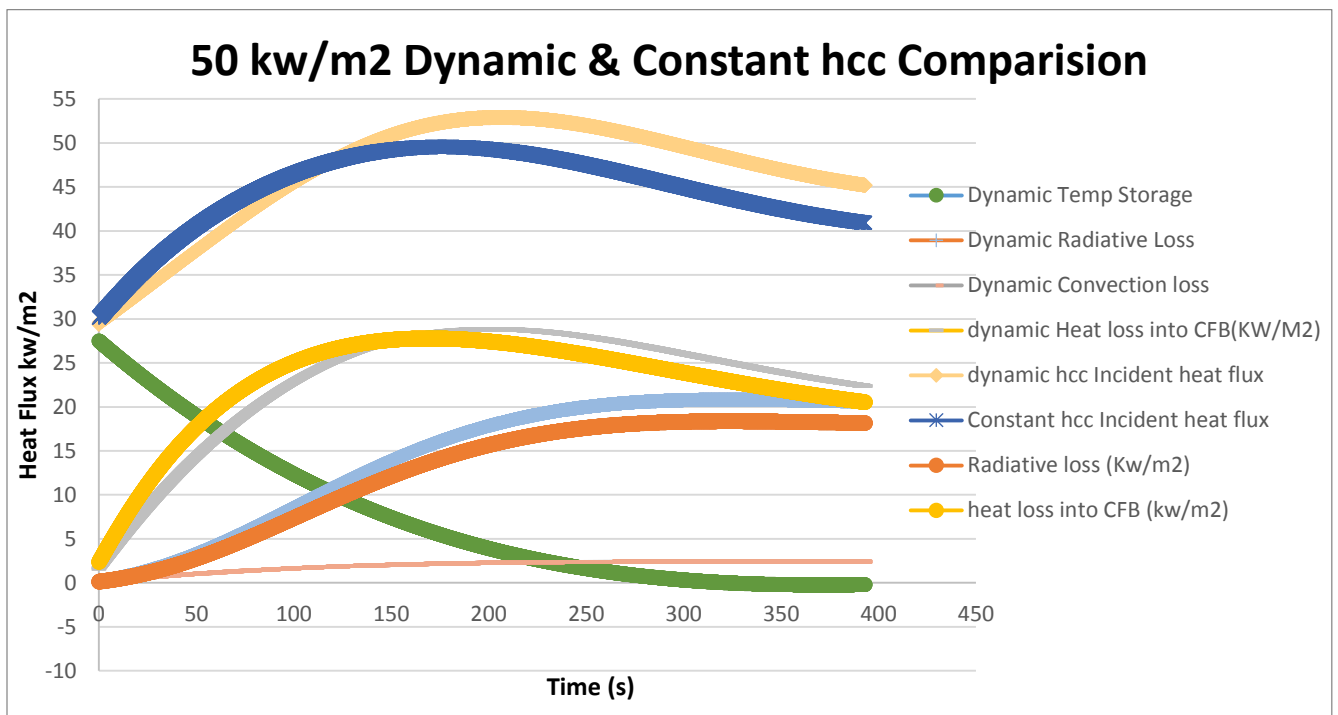
Figure 61: 50 kw/m^2 Dynamic & Constant hcc Comparison

The closest trend line that we are able to get under 50kw/m2 incident heat flux is when

$$hcond = 0.066 \frac{kw}{m2k}; thickness\ of\ air\ gap = 0.000606061\ m$$

The comparison graph between two calibration processes are shown below.
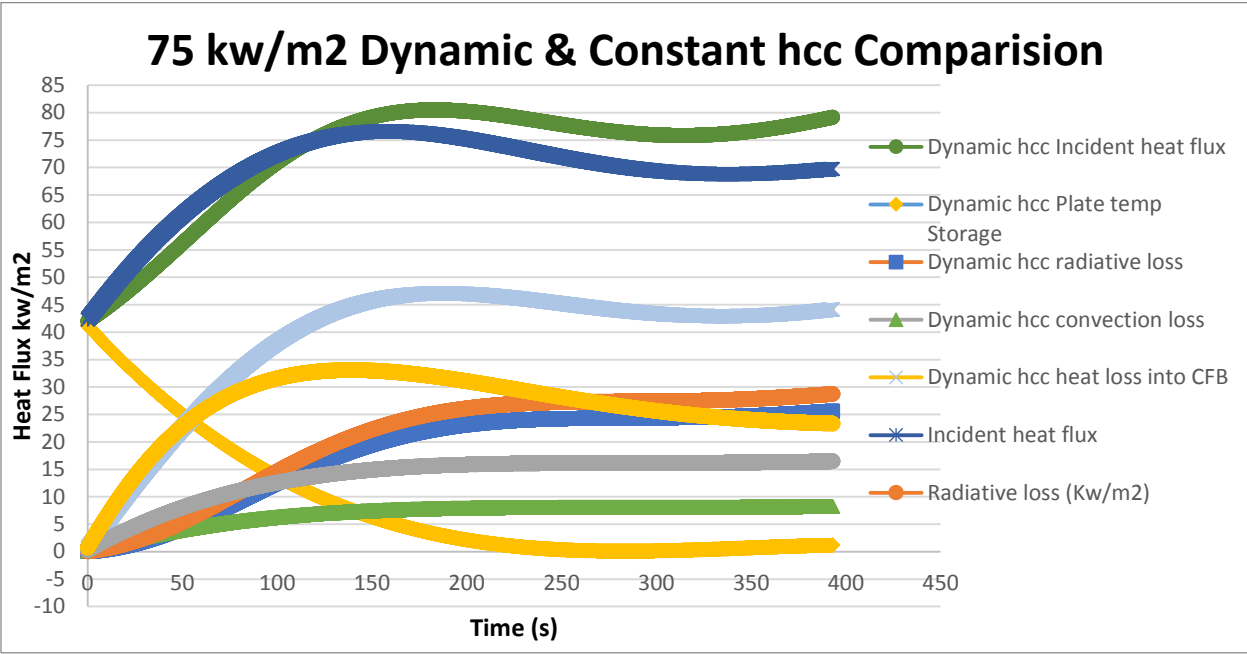
Figure 62: 75 kw/m^2 Dynamic & Constant hcc Comparison

Through figures above, we discover that radiation has some minor effects to our model. However, these minor changes do not improve the delayed response time nor as the fluctuation phenomenon. Two calibration process provides error of ±10kw/m2. Since the fluctuation of the heat loss into ceramic fiberboard only affects the heat flux after 200s and for our project we will be working on time base of minutes (10-40min), we can state that this dynamic hcc simulation is a good model for our project.

Detailed calibration calculation for dynamic hcc is listed in appendix C5.

Appendix C

Appendix C1: Finite Difference Method Boundary Condition Sample Calculation

Following calculation shows, how temperature of each node at different location is determined.

Node 1 (BC1)

$$T_\infty = 700\ k;\ \ T_n^i = Node\ 1\ at\ Time\ 0s = 25\ k;$$

$$T_{n+1}^i = Node\ 2\ at\ Time\ 0s = 25\ k;\ Fo = 0.048;\ Bi = 4$$

$$T_n^{i+1} = 2FoBi\big(T_\infty - T_n^i\big) - 2Fo\big(T_n^i - T_{n+1}^i\big) + T_n^i\ (1)$$

$$= 2 \times 0.048 \times 4(T_\infty - 25) - 2 \times 0.048(25 - 25) + 25 = 284.2\ k$$

Node 26 (BC2)

$$T_{n-1}^i = Node\ 25\ at\ Time\ 0s = 25k\ ;\ \ T_n^i = Node\ 26\ at\ Time\ 0s = 25\ k;\ Bi = 0$$

$$T_n^{i+1} = 2Fo\big(T_{n-1}^i - BiT_\infty\big) - 2FoT_n^i - 2FoBi\ T_n^i + T_n^i\ (2)$$

$$= 2 \times 0.048(25 - 0 \times 25) - 2 \times 0.048 \times 25 - 2 \times 0.048 \times 0 \times 25 + 25 = 25$$

Node 12 (Interior)

$$T_{n+1}^i = Node\ 13\ at\ Time\ 0s = 25\ k;\ T_{n-1}^i = Node\ 11\ at\ Time\ 0s = 25k\ ;$$

$$T_n^i = Node\ 12\ at\ Time\ 0s = 25\ k;$$

$$T_n^{i+1} = Fo\big(T_{n+1}^i + T_{n-1}^i\big) + T_n^i - 2FoT_n^i\ (3)$$

$$= 0.048 \times (25 + 25) + 25 - 2 \times 0.048 \times 25 = 25$$

Appendix C2: Finite Difference Method and Semi-Infinite Method Verification

Finite Difference

With given condition

X:Thickness of Plate (m)	0.025
Ti: Initial Temperature (C)	25
Dx: Distance between each node (m)	0.001
K: Thermal Conductivity (kw/mK)	0.016
Cp: Specific Heat of the plate (kJ/kgK)	1
T∞:Ambient Temperature (C)	30
Hcc: Contact Conductance (kw/m² K)	0.1
ρ:Density (kg/m³)	7850

Table 20: Finite difference method given conditions

Thermal diffusivity is calculated by using

$$\alpha = \frac{k}{\rho C p}$$

$$\alpha = \frac{0.016\text{kw/mk}}{7850\text{kg/m3} \times 1\text{kJ/kgK}} = 2.038 \times 10^{-6}$$

In order to achieve the stable condition;

$$\text{Fo} \leq \frac{1}{2} \quad ; \text{Fo} = \frac{\alpha \Delta t}{\Delta x^2}$$

With Dx of 0.001m

$$\text{Dt} = \frac{0.5 * 0.001\text{m}^2}{2.038 \times 10^{-6}} = 0.2 \ s$$

fourier number is calculated as a fixed value:

$$\text{Fo} = \frac{2.038 \times 10^{-6} \times 0.2s}{0.001m^2} = 0.4076$$

Biot Number is calculated under different node

$$\text{Bi} = \frac{h_{cc}\Delta x}{k}$$

$$\text{Node 1: Bi} = \frac{\frac{0.1kw}{m^2} * 0.001m}{0.016kw/mk} = 0.00625$$

Node 26 Condition 1: (same hcc value): Bi =0.00625

Node 26 Condition2: (with hcc=0): Bi=0

Semi-Infinite Difference Method

With given condition

Table 21: Semi-infinite difference method given conditions

X:Thickness of Plate (m)	0.025
Ti: Initial Temperature (C)	25
Dx: Distance between each node (m)	0.001
K: Thermal Conductivity (kw/mK)	0.016
Cp: Specific Heat of the plate (kJ/kgK)	1
T∞:Ambient Temperature (C)	30
Hcc: Contact Conductance (kw/m² K)	0.1
ρ:Density (kg/m³)	7850

Thermal diffusivity is calculated by using

$$\alpha = \frac{k}{\rho Cp}$$

$$\alpha = \frac{0.016 \text{kw/mk}}{7850 \text{kg/m3} \times 1 \text{kJ/kgK}} = 2.038 \times 10^{-6}$$

In order to achieve the stable condition;

$$\text{Fo} \leq \frac{1}{2} \quad ; \ \text{Fo} = \frac{\alpha \Delta t}{\Delta x^2}$$

With Dx of 0.001m

$$\text{Dt} = \frac{0.5 * 0.001 \text{m}^2}{2.038 \times 10^{-6}} = 0.2 \ s$$

fourier number is calculated as a fixed value:

$$\text{Fo} = \frac{2.038 \times 10^{-6} \times 0.2s}{0.001m^2} = 0.4076$$

Biot Number is calculated under different node

$$\text{Bi} = \frac{h_{cc}\Delta x}{k}$$

$$\text{Node 1: Bi} = \frac{\frac{0.1kw}{m^2} * 0.001m}{0.016kw/mk} = 0.00625$$

Node 26 Condition 1: (same hcc value): Bi =0.00625

Node 26 Condition2: (with hcc=0): Bi=0

$$\frac{T(x,t) - T_i}{T_\infty - T_i} = erfc\left(\frac{x}{2\sqrt{\alpha t}}\right) - \exp\left(\frac{h_{cc}x}{k} - \frac{h^2\alpha t}{k^2}\right)erfc\left(\frac{x}{2\sqrt{\alpha t}} + \frac{h_{cc}\sqrt{\alpha t}}{k}\right) (1.2)$$

Node 1:

$$\frac{T(x,t) - 25°C}{30°C - 25°C} = erfc\left(\frac{0.00025m}{2\sqrt{2.038 \times 10^{-6} \times 0.2s}}\right)$$

$$- \exp\left(\frac{0.1\text{kw/m2 K} \times 0.00025m}{0.016kw/mk}\right.$$

$$\left.- \frac{0.1\text{kw/m2 K}^2 \times 2.038 \times 10^{-6} \times 0.2s}{0.016kw/mk^2}\right)erfc(\frac{0.00025m}{2\sqrt{2.038 \times 10^{-6} \times 0.2s}}$$

$$+ \frac{0.1\text{kw/m2 K} \times \sqrt{2.038 \times 10^{-6} \times 0.2s}}{0.016kw/mk^2})$$

$$T(x,t) = 25.0156$$

Node 2-26 is then be calculated with same equation but with changing thickness and time, detail calculation results can be found from the following table;

Verification Excel file is included on USB submission.

Table 22: Semi-Infinite Difference Method Calculation Results (Node 1-26)

#	Delta T (s)	Time	Node 1	Node 2	Node 3	Node 4	Node 5	Node 6	Node 7	Node 8	Node 9	Node 10	Node 11	Node 12	Node 13	Node 14	Node 15	Node 16	Node 17	Node 18	Node 19	Node 20	Node 21	Node 22	Node 23	Node 24	Node 25	Node 26

Appendix C3: Contact Conductance Verification

In this section, verification excel file can be found on USB submission.

Appendix C4: Constant hcc Calibration Calculation

In this section, detail calibration excel file can be found on USB submission.

Appendix C5: Dynamic hcc Calibration Calculation

In this section, detail calibration excel file can be found on USB submission.

Appendix D: Back face Temperature

Material Properties

The rig was built with two aluminum alloys, 6061- T6 and 6061-T6516, which have a melting point of 650C; 923K which is lower than the upper temperatures the intermediate scale rig will be subjected to (upwards of 800C; 1073K) during fire tests. Insulation is therefore necessary to limit the temperatures the intermediate scale rig will be exposed to during fire tests.

While the melting temperature of the aluminum is 650C; 923K, its material properties are affected at significantly lower temperatures. The previous MQP completed in April, 2015 by Sean Gills, Nicholas Houghton, David Scott, and Joseph Weiler researched the temperature at which long term thermal effects would take place on the intermediate scale rig. It was determined as a recommendation that the temperature be limited to 2/3 of the temperature of aging during manufacturing. Since aging occurs approximately at 180C; 453K the limiting temperature threshold was determined to be 120C; 393K. The MQP group determined this by investigating the losses to the yield strength, and tensile strength, and increase in strain with elevated temperatures. Also investigated was the temperatures at which the aluminum is heated, formed, and aged during manufacturing since the aluminum the rig is composed of is treated.

The MQP team also considered the temperature at which the aluminum would cause harm with human interaction. A study by Ungar and Stroud at the NASA/Johnson Space Center determined that any temperature of aluminum below 45C; 318K would be below the threshold of pain for human touch. It would be ideal to keep the temperature of the back of the aluminum below 45C; 318K, using insulation. Another consideration we will be taking into account because of the setup of our practice wall, is the dehydration of sheetrock, or gypsum board. Since the practice wall is composed of a front face of sheetrock for the first practice test, and then insulation, followed by the sheetrock for the second practice test. We would like to ensure that the second panel of sheetrock will be in sufficient condition for a second practice test, and be able to support a safe temperature at the back face. From several studies on gypsum by Mehaffey et al, Gerlich et al, McIntosh et al, gypsum board has been determined to contain approximately 21% water by weight. When gypsum boards are heated to temperatures above 80C; 353K,

the chemically bound water dissociates from its crystal lattice and evaporates. This process, known as "dehydration" of gypsum, and takes place at temperatures between ~80 C and ~250 C (353K-523K). A study by Benichou in 2001 found that the mass loss of gypsum wallboard remains nearly unchanged up to 100C; 373K. Between 100 C and 160 C (373K-433K) the mass loss under four hours of exposure is approximately 15 percent, as moisture is lost.

Cerablanket; ceramic fiber blanket insulation, and sheetrock; or gypsum board, are to be used to insulate the rig, and as a means to mount instrumentation. Cerablanket is utilized due to its low thermal conductivity, accessibility, and previous reliability in WPI's fire laboratory. The back face of the practice wall to which the gypsum wallboards and cerablanket is mounted is a 0.8" sheet of plywood. Also, for wall stability a standard wood frame is also used in discrete locations. The following table illustrates the practice wall materials and thicknesses. From left to right, the front face to the back face respectively. The total thickness is 0.13462m.

Table 23: Practice Wall Material Thickness

Sheetrock	Cerablanket	Sheetrock	Plywood	Wood frame (in discrete locations)
0.5"	1 ¾"	0.5"	0.8"	1 ¾"
0.0127m	0.04445m	0.0127m	0.02032m	0.04445m

The material properties of these substances are outlined in the following table.

Table 24: Practice Wall Material Thermal Properties

	Notation	Thermal Conductivity (W/mK) k	Density (kg/m³) rho	Specific Heat (J/kgK) Cp	Thermal Diffusivity (m²/s) a=k/rhoCp
Sheetrock	a, c	0.17	481	1300	2.718695E-7
Cera blanket	b	0.04	96.1	670	6.212434E-7
Plywood	d	0.13	545	1215	1.963227E-7
Wood	e	0.11	561	1400	1.400560E-7

Sources: Engineering Toolbox, Manufacturers' Websites

Temperature Diffusion Time

By using semi-infinite 1D conduction analysis with exposure to a hot gas temperature, to determine the time for the temperature gradient to reach the wall, the thermal diffusivity over the material thickness is considered a constant average.

The constant thermal diffusivity, determined with relation to the thickness of each layer is calculated, for example:

$$a_T = \frac{(a_a t_a) + (a_b t_b) + (a_c t_c) + (a_d t_d)}{t_T}$$

$$where: a = thermal\ diffusivity, and\ t = thickness$$

$$\frac{a_T}{=}\frac{(2*2.71865E-7)*0.0127+(6.212434E-7)*0.04445+(1.963227E-7)*0.02032+(1.40056E-7)*0.04445}{(2*0.0127+0.04445+0.02032+0.04445)}$$

$a_T = 3.32129E - 7\ m^2/s$ There is not a practiced method to modeling multiple layers with a singular average thermal diffusivity term, however this method is justified intuitively by taking into account the thickness ratio of each material. All thermal diffusivity terms are in the range of 1.4E-7 m2/s to 6.2E-7 m2/s so the resulting 3.3E-7 m2/s will produce representative results, as this range is reasonable.

Thermal conductivity is added in series with respect to the length.

$$k_T = \frac{t_T}{\left(\frac{t_a}{k_a}\right) + \left(\frac{t_b}{k_b}\right) + \left(\frac{t_c}{k_c}\right) + \left(\frac{t_d}{k_d}\right) + \left(\frac{t_e}{k_e}\right)}$$

$$where: k = \frac{t}{R}, and\ R = \frac{t}{k}$$

$$R_T = R_a + R_b + R_c + R_d + R_e$$

$$k_t = 0.073924\ W/mK$$

Back Face of Wood Frame

Semi-infinite behavior may be assumed if the thickness of the overall insulating body is greater than or equal to 4 times the square root of the overall thermal diffusivity multiplied by the time. (Drysdale, 2011)

$$\Delta x \geq 4\sqrt{(at)}$$

Using this equation the time at which the heat reaches the back face of our wall may be determined.

$$0.13462m \geq 4\sqrt{(3.32129E - 7\frac{m^2}{s} * t)}$$

$$t = 3410.3\ seconds, or\ 56.84\ minutes$$

In addition, by using semi-infinite behavior, the time at which the back face sees a temperature rise on the order of 15% may be determined by the following equation.

$$\Delta x \geq 2\sqrt{(at)}$$

$$0.13462m \geq 2\sqrt{(3.32129E - 7\frac{m^2}{s} * t)}$$

$$t = 13641.19 \; seconds, or \; 227.35 \; minutes$$

Since the duration of the test we will be completing is providing exposure to the burner flame for 30 minutes, and then incorporates a cool down phase, the back face temperature of the wall through these layers due to 1D conduction should not be within the range of damage to the rig (40C; 313K).

Back Face of Plywood

Let us now consider the semi-infinite conduction model to the back face of the plywood, since the wood frame is only in discrete locations.

The new constant thermal diffusivity value becomes,

$$a = \frac{3.84857E - 8}{0.09017} = 4.26813E - 7\frac{m^2}{s}$$

The new thickness not considering the wood framing becomes 0.09017m. Using the semi-infinite analysis:

$$\Delta x \geq 4\sqrt{(at)}$$

$$0.09017m \geq 4\sqrt{(4.26813E - 7\frac{m^2}{s} * t)}$$

$$t = 1190.6 \; seconds, or \; 19.84 \; minutes$$

This time is not ideal, since it is within our testing range, however this plywood wall will not be in direct contact with the rig, since the framing will leave an air gap. The time to 15% temperature rise at the back face of the plywood is determined:

$$\Delta x \geq 2\sqrt{(at)}$$

$$0.09017m \geq 2\sqrt{(4.26813E - 7\frac{m^2}{s} * t)}$$

$$t = 4762.4 \; seconds, or \; 79.37 \; minutes$$

These calculations indicate that by the commencement of the 30-minute testing period, the heat will have

reached the back face, however the temperature rise on the back face will be less than 15%. Based off of

NFPA 285 calibration the approximate front face temperature for the 30 minutes of testing will be

considered 700C; 973.15. A 15% temperature rise to the back face would indicate

$$T_{15\%} = 700 * 0.15 = 105C; \ 378K$$

Therefore this temperature rise calculation will be a good measure of the point of dehydration to the

sheetrock (within the range of 80C-250C). However further analysis is required to insure the safe human

pain threshold temperature of the aluminum is not reached (40C; 313K).

Back Face of Cerablanket

Since the degradation of the second gypsum sheetrock is a concern, a semi-infinite analysis will be taken

at the back face of the cerablanket, at the front face of the second gypsum board. At this location, the

thermal diffusivity term is calculated to be, a= 5.43605E-7 m²/s. The thickness of the front layer of

gypsum, and layer of cerablanket, t= 0.05715m.

$$\Delta x \geq 4\sqrt{(at)}$$

$$0.05715m \geq 4\sqrt{\left(5.43605E - 7\frac{m^2}{s} * t\right)}$$

$$t = 375.52 \ seconds, or \ 6.26 \ minutes$$

This time is not ideal, since it is within our testing range, additional thickness of cerablanket may be

required to keep the second layer of gypsum sheetrock from dehydrating to a critical state. The time to

15% temperature rise at the back face of the cerablanket, and front face of the second layer of gypsum

sheetrock is determined:

$$\Delta x \geq 2\sqrt{(at)}$$

$$0.05715m \geq 2\sqrt{\left(5.43605E - 7\frac{m^2}{s} * t\right)}$$

$$t = 1502.08 \ seconds, or \ 25.05 \ minutes$$

Since this temperature rise is seen within the 30-minute test exposure, we can assume that with this

design there will be degradation of the second layer of sheetrock.

Temperature Diffusion Time Results

The results from all three conditions are summarized in the following Table.

Table 25: Thermal Diffusion Time at Depth Results

	Effective Thermal Diffusivity (m²/s) a	Effective Thermal Conductivity (W/mK) k	Thickness (m)	Time for thermal penetration to back face (mins)	Time for 15% Temperature Rise (mins)
Back face of Wood frame	3.32129E-7	0.073924	0.13462	56.84	227.35
Back face of Plywood	4.26813E-7	0.063636	0.09017	19.84	79.37
Back face of Cera blanket	5.43605E-7	0.048189	0.05715	6.26	25.05
Back face of additional layer of Cera blanket	5.7757E-7	0.044228	0.1016	18.62	74.5

The results for temperature diffusion with respect to time indicate that within the 30 minutes of testing,

there is temperature diffusion to the back face of the plywood, but on the order of less than a 15% rise.

The plywood is not in direct contact with the aluminum rig, so there is not a significant concern for the

durability of the aluminum with regards to temperature ware. There is however, a concern for the

dehydration of the second layer of the gypsum sheetrock which was designated for a second practice test.

The 15% temperature rise is reached by the front face of the second layer of gypsum sheetrock.

The temperature of the gas in each gas flow phase at each centerline height is known from the NFPA 285

design test, the Southwest Institute study, and a previous MQP study is mentioned in the comparison

chapter. Since the temperature gradient, and diffusion calculations were based on the temperature of the

front face of the practice wall at the material, and not the gas temperature of the fire, convective loss must

be taken into consideration before using the temperature gradient analysis to determine back face

temperatures.

We will be using a max heat flux of 40kW/m², and a max temperature at the lower height of the rig, in the

last five-minute phase of 700C. For a temperature gradient to be on the order of 15%, the back face

temperature would be 105C. Therefore, if the max temperature of 700C was seen throughout the 30 minute span, the temperature at the front face of the second layer of gypsum would reach 105C at the 25.05minute mark. Since the temperature is not a constant maximum value, this temperature would be reached after the 25 minutes.

By using a temperature average over the 30-minute test period, this would give a lower bound of the temperature at the second layer of gypsum board to provide context for the problem. An average value of the gas is on the order of 600C. This would indicate at 25 minutes the temperature at the second layer gypsum reaching 90C. Since the dehydration process begins for the sheetrock at temperature of 80C, this is more reasonable, however the exposure may still support dehydration.

Additional Layer of Cerablanket Analysis

Working backwards, we can determine the thickness of the cerablanket given that ideally there is not a 15% temperature rise at the back face of the cerablanket/front face of the gypsum sheetrock until 30-minutes into the test. Therefore:

$$t = 30min = 1800sec$$

$$\Delta x = 0.05715m + \text{added thickness}$$

$$a = \frac{((5.43605E - 7m2/s)0.05715m + (6.212434E - 7m2/s) * \text{added thickness})}{\Delta x}$$

Using the equation for 15% temperature rise:

$$\Delta x \geq 2\sqrt{(at)}$$

$$0.05715m + \text{added thickness}$$
$$\geq 2\sqrt{(((5.43605E - 7\frac{m^2}{s})0.05715m + (6.212434E - 7\frac{m^2}{s}) * \text{added thickness})t/\Delta x)}$$

$$0.05715m + b \geq 2\sqrt{(((3.1067E - 8\frac{m^3}{s}) + (6.212434E - 7\frac{m^2}{s}) * b)t/0.05715m + b)}$$

If one more layer of cerablanket were added, the added thickness (b) would be 0.04445m.

$$0.1016m \geq 2\sqrt{(5.7757E - 7\frac{m^2}{s} * t)}$$

The time to 15% temperature rise at the back of the second layer of gypsum would be,

$$t = 4468 \sec or\ 74.5 mins$$

With initial temperature rise,

$$0.1016m \geq 4\sqrt{\left(5.7757E - 7\frac{m^2}{s} * t\right)}$$

$$t = 1117.02 \sec or\ 18.62 mins$$

Therefore, it is recommended that an additional layer of cerablanket be added to the practice wall to protect the second layer of gypsum sheetrock; to ensure that the board is in good condition and not significantly dehydrated, and so that it may be used in a second practice test. With the one layer composition, there will be dehydration of the gypsum sheetrock.

Temperature Calculations

Using analysis of measured gas temperature, heat transfer coefficient and heat flux, an idea of the temperature profile over time may be generated to indicate the duration of critical exposure. The gas temperature and heat transfer coefficient of reference are determined from previous MQP, NFPA 285, and Kreysler tests. The magnitude of the parameters under consideration are reported in the following table.

Table 26: Time-Step Gas Temperature and Heat Transfer Coefficient from Prior Testing

Time step (mins)	Gas Temperature (C)	hc (W/m2K)
0-5	300	27
5-10	500	31
10-15	590	32
15-20	615	35
20-25	650	37
25-30	700	40

It is important to consider these may not be the most extreme conditions, as there is variance.

Finite Difference Method

The finite difference method is used to determine the temperature at depth within the solid. This approach is used to model both the incident heat flux boundary condition, and the convective heating from the gas temperature boundary. These results may be compared with the semi-infinite solution.

Interior Nodal Equation:

General 1D heat conduction

$$\frac{dT}{dx} = \propto \frac{d^2T}{dx^2}$$

$$\propto = thermal\ diffusivity$$

$$dx = spacial\ node$$

$$dt = time\ node$$

FDM

$$f_{i+1} = f_i + f'_i dx + \frac{f''_i}{2!} dx^2 + \ldots \frac{f_i^n}{n!} dx^n$$

$$f_{i-1} = f_i - f'_i dx + \frac{f''_i}{2!} dx^2 - \ldots \frac{f_i^n}{n!} dx^n$$

The sum of the two above equations:

$$f''_i = \frac{f_{i+1} - 2f_i + f_{i-1}}{dx^2} + 0(dx^2) \approx \frac{f_{i+1} - 2f_i + f_{i-1}}{dx^2}$$

Applied to temperature

$$\frac{T^{i+1}_m - T^i_m}{dt} = \propto \frac{T^i_{m-1} - 2T^i_m + T^i_{m+1}}{dx^2}$$

$$T^{i+1}_m = \propto \frac{dt}{dx^2}\left(T^i_{m-1} - 2T^i_m + T^i_{m+1}\right) + T^i_m$$

$$T^{i+1}_m = \propto \frac{dt}{dx^2}\left(T^i_{m-1} + T^i_{m+1}\right) + (1 - 2 \propto \frac{dt}{dx^2})T^i_m$$

$$Fo = \propto \frac{dt}{dx^2}$$

Interior Nodal Equation:

$$T^{i+1}_m = Fo(T^i_{m-1} + T^i_{m+1}) + (1 - 2Fo)T^i_m$$

Incident heat flux boundary

Front Face Boundary Condition:

$$\dot{q}''_{net} = -k\frac{dT}{dx} = \dot{q}''_{inc} - h\left(T_{x,t} - T_\infty\right)$$

For purposes of consistency

$$T_{x,t} = T^i_m$$

By Taylor series expansion

$$f_{i+1} - f_{i-1} \Rightarrow f'_i = \frac{f_{i+1} - f_i}{2dx}$$

Applied to temperature gradient

$$\frac{dT}{dx} = \frac{T^i_{m+1} - T^i_{m-1}}{2dx}$$

$$\dot{q}''_{net} = -k\frac{T^i_{m+1} - T^i_{m-1}}{2dx} = \dot{q}''_{inc} - h(T^i_m - T_\infty)$$

Solve for T^i_{m-1}

$$T^i_{m+1} - T^i_{m-1} = (\frac{-2dx}{k})[\dot{q}''_{inc} - h(T^i_m - T_\infty)$$

$$-T^i_{m-1} = -T^i_{m+1} + (\frac{-2dx}{k})[\dot{q}''_{inc} - h(T^i_m - T_\infty)$$

$$T^i_{m-1} = T^i_{m+1} + \left(\frac{2dx}{k}\right)[\dot{q}''_{inc} - h(T^i_m - T_\infty)]$$

$$T^i_{m-1} = T^i_{m+1} + \left(\frac{2dx}{k}\right)\dot{q}''_{inc} - \left(\frac{2dx}{k}\right)h(T^i_m - T_\infty)$$

$$T^i_{m-1} = T^i_{m+1} + \left(\frac{2dx}{k}\right)\dot{q}''_{inc} - \left(\frac{2dx}{k}\right)hT^i_m + \left(\frac{2dx}{k}\right)hT_\infty$$

$$Bi = \frac{dxh}{k}$$

$$T^i_{m-1} = T^i_{m+1} + \left(\frac{2dx}{k}\right)\dot{q}''_{inc} - 2BiT^i_m + 2BiT_\infty$$

Insert this into the interior nodal equation

$$T^{i+1}_m = Fo([T^i_{m+1} + \left(\frac{2dx}{k}\right)\dot{q}''_{inc} - 2BiT^i_m + 2BiT_\infty] + T^i_{m+1}) + (1 - 2Fo)T^i_m$$

$$T^{i+1}_m = FoT^i_{m+1} + Fo\left(\frac{2dx}{k}\right)\dot{q}''_{inc} - 2FoBiT^i_m + 2FoBiT_\infty + FoT^i_{m+1} + (1 - 2Fo)T^i_m$$

$$T^{i+1}_m = FoT^i_{m+1} + Fo\left(\frac{2dx}{k}\right)\dot{q}''_{inc} - 2FoBiT^i_m + 2FoBiT_\infty + FoT^i_{m+1} + T^i_m - 2FoT^i_m$$

$$T^{i+1}_m = 2FoT^i_{m+1} + 2Fo\left(\frac{dx}{k}\right)\dot{q}''_{inc} - 2FoBiT^i_m + 2FoBiT_\infty + T^i_m - 2FoT^i_m$$

$$T^{i+1}_m = 2Fo\left(\frac{dx}{k}\right)\dot{q}''_{inc} + 2FoBiT_\infty + 2FoT^i_{m+1} + T^i_m(1 - 2Fo - 2FoBi)$$

To back face of plywood, with: 1 layer of cera blanket
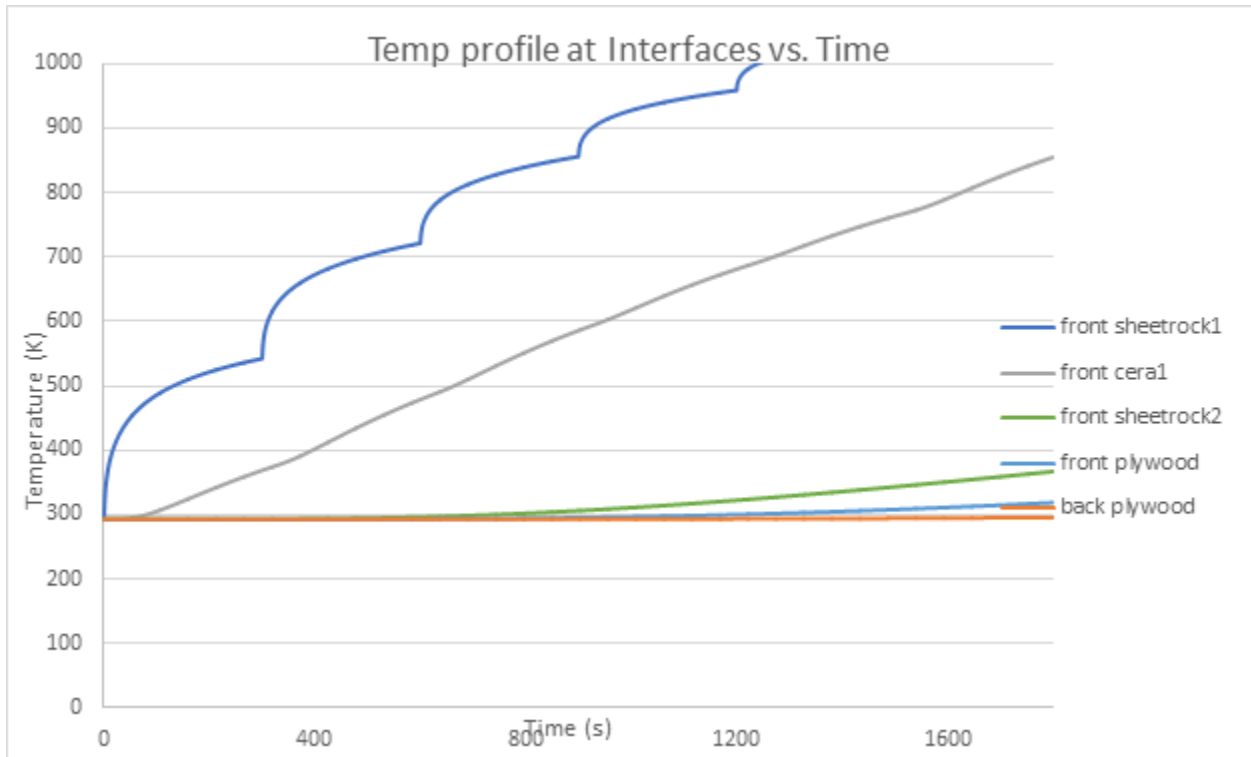
Figure 63: Temp profile at interfaces vs. time

Figure 64: Temperature profiles at 5min intervals

With two layers of cerablanket:
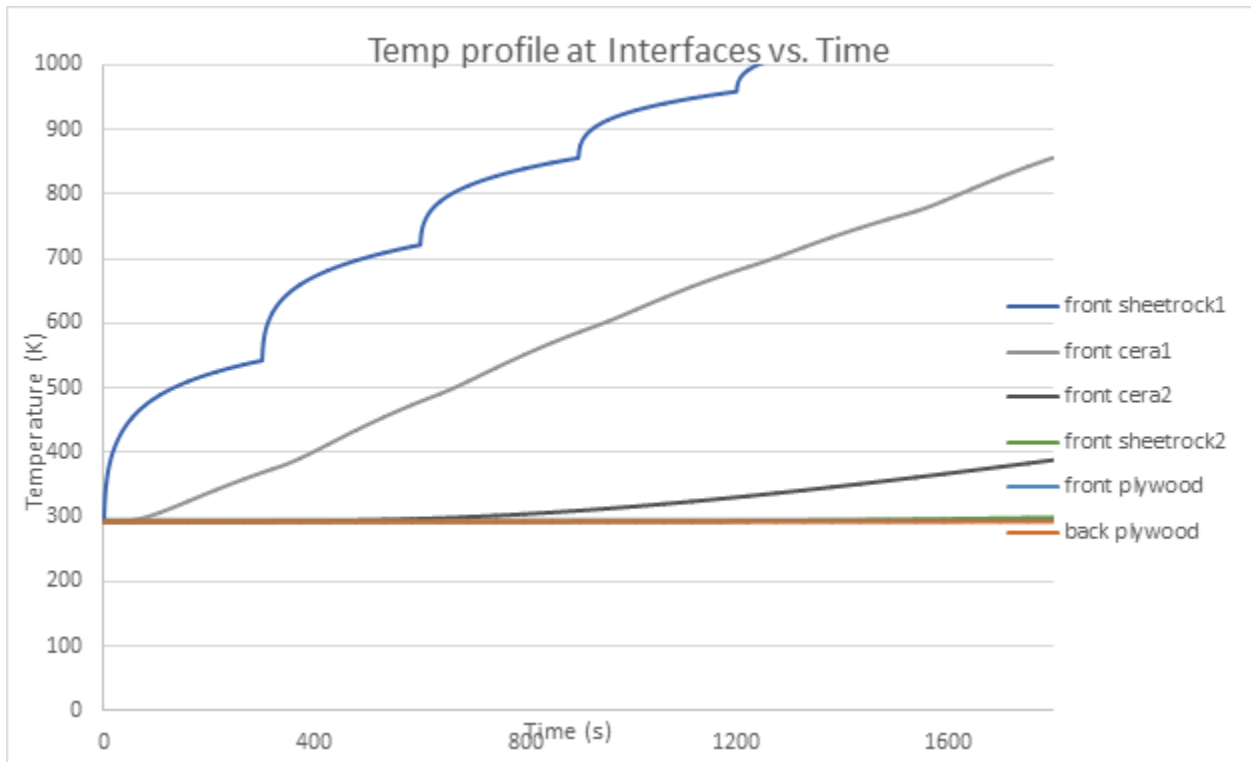
Figure 65: Temp profile at interfaces vs. Time
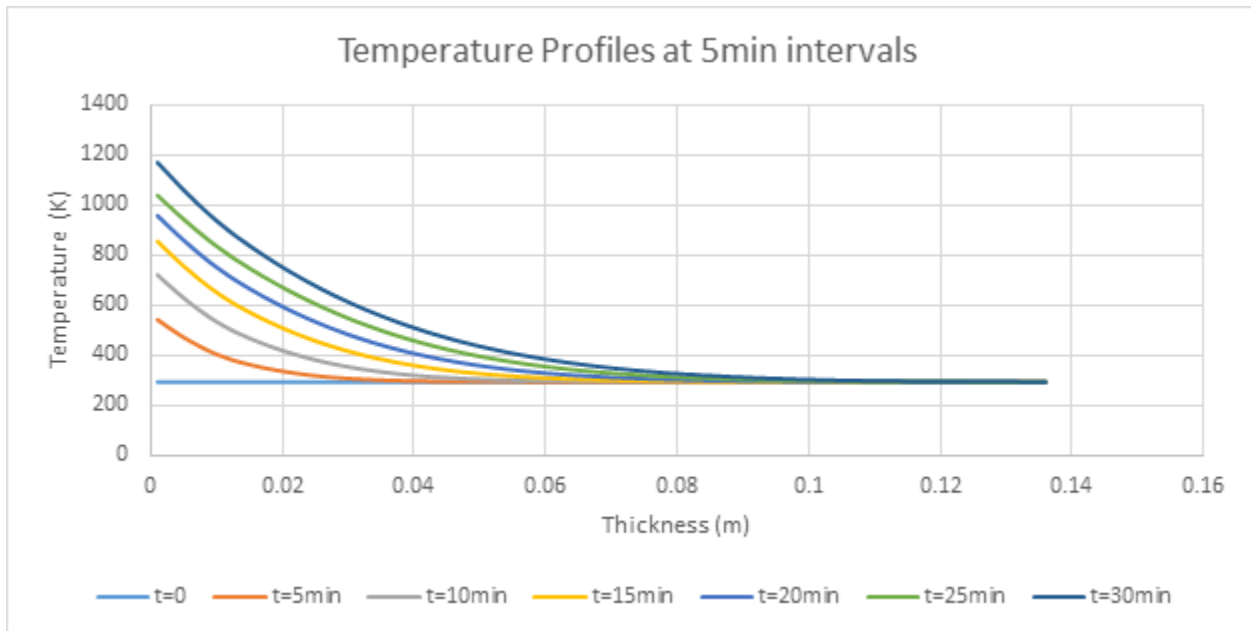
Figure 66: Temperature profiles at 5min intervals

Convective heating by gas temperature boundary

Front Face Boundary Condition:

$$\dot{q}''_{net} = -k\frac{dT}{dx} = h\left(T_g - T_{x,t}\right)$$

For purposes of consistency

$$T_{x,t} = T^i{}_m$$

By Taylor series expansion

$$f_{i+1} - f_{i-1} \Rightarrow f'_i = \frac{f_{i+1} - f_i}{2dx}$$

Applied to temperature gradient

$$\frac{dT}{dx} = \frac{T^i{}_{m+1} - T^i{}_{m-1}}{2dx}$$

$$\dot{q}''_{net} = -k\frac{T^i{}_{m+1} - T^i{}_{m-1}}{2dx} = h(T_g - T_m)$$

Solve for $T^i{}_{m-1}$

$$T^i{}_{m-1} = T^i{}_{m+1} + (\frac{2dxh}{k})(T_g - T^i{}_m)$$

$$Bi = \frac{dxh}{k}$$

$$T^i{}_{m-1} = T^i{}_{m+1} + (2Bi)(T_g - T^i{}_m)$$

Insert this into the interior nodal equation

$$T^{i+1}{}_m = Fo(T^i{}_{m+1} + 2Bi(T_g - T^i{}_m) + T^i{}_{m+1}) + (1 - 2Fo)T^i{}_m$$

$$T^{i+1}{}_m = 2BiFoT_g + 2FoT^i{}_{m+1} + T^i{}_m(1 - 2Fo - 2BiFo)$$

To back face of plywood, with: 1 layer of cerablanket
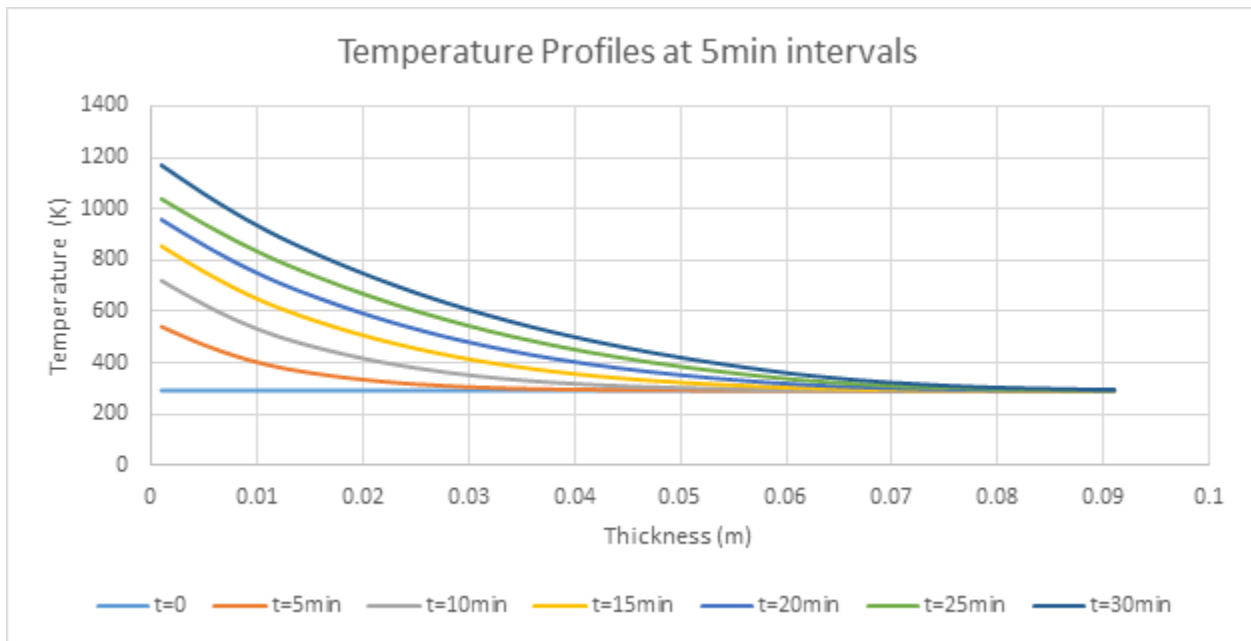
Figure 67: Temp profile at interfaces vs. time 1 layer of Cerablanket

Figure 68: Temperature profiles at 5min intervals with 1 layer of cerablanket

With 2 layers of cerablanket:

Figure 69: Temperature profiles at 5min intervals with 2 layers of cerablanket

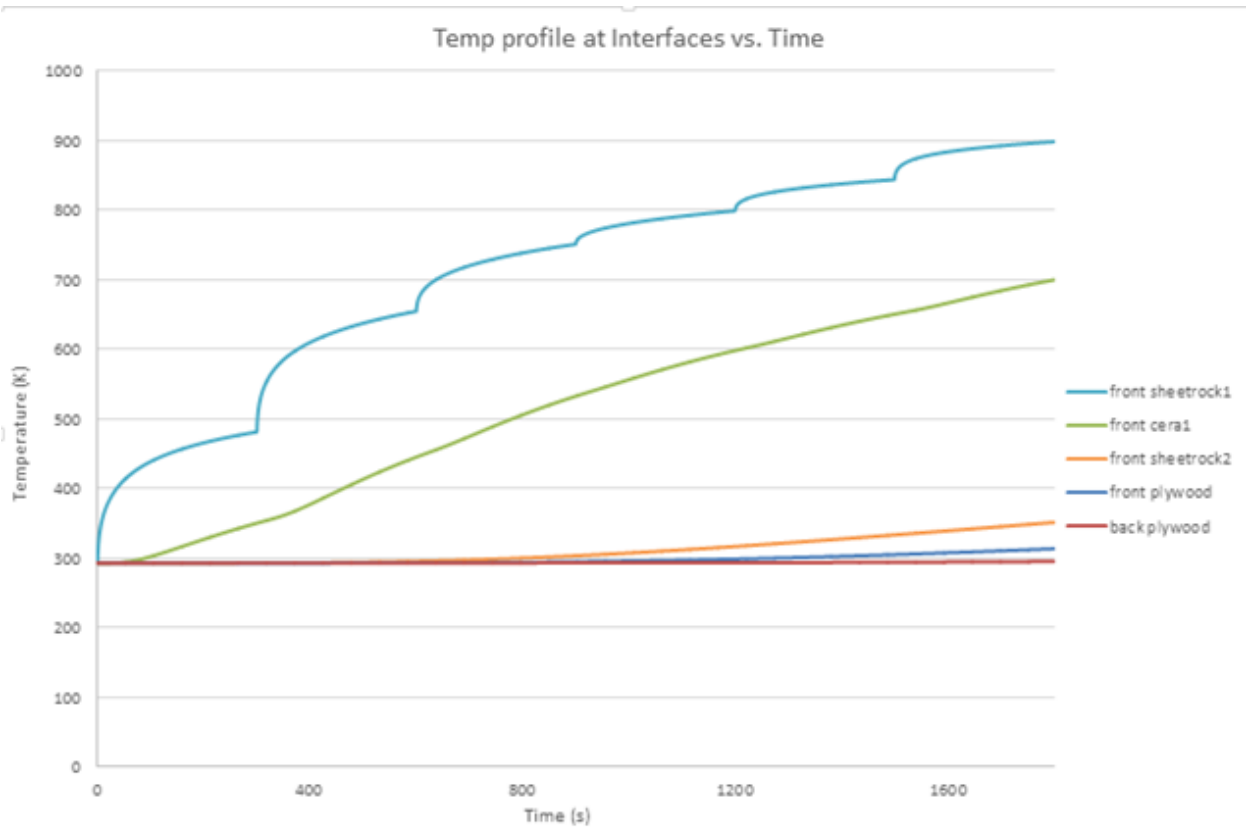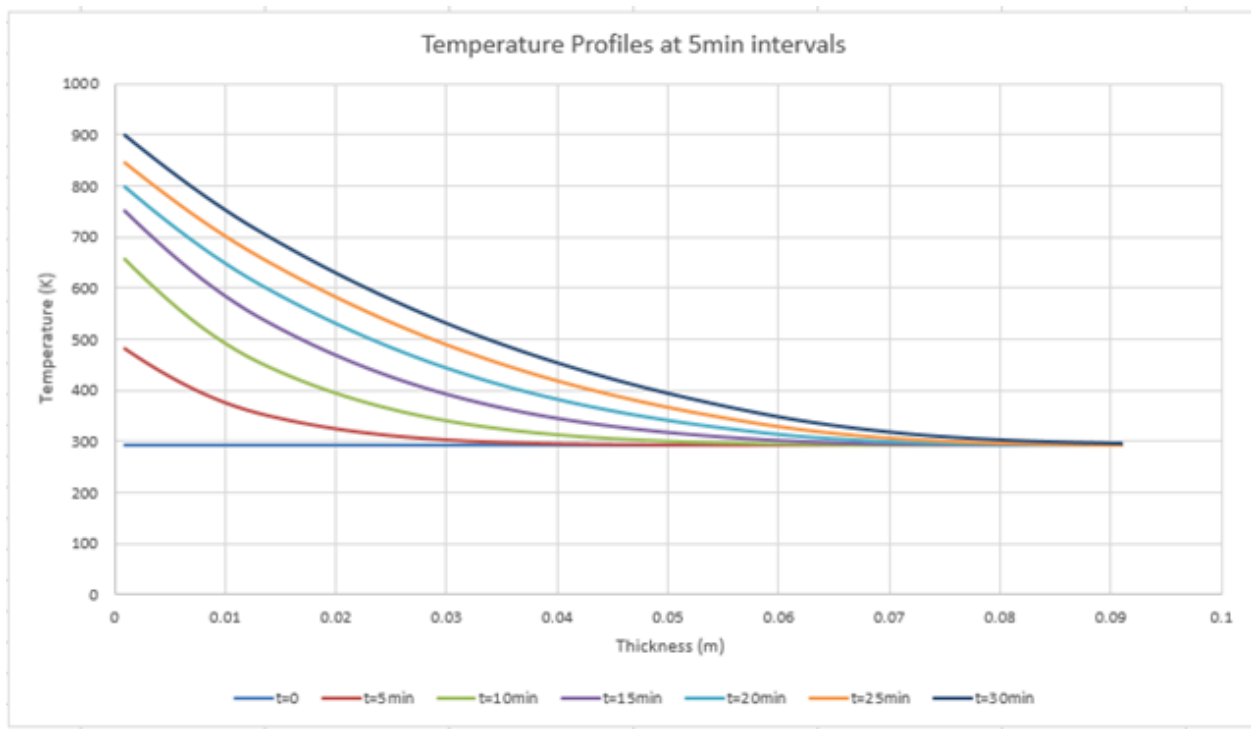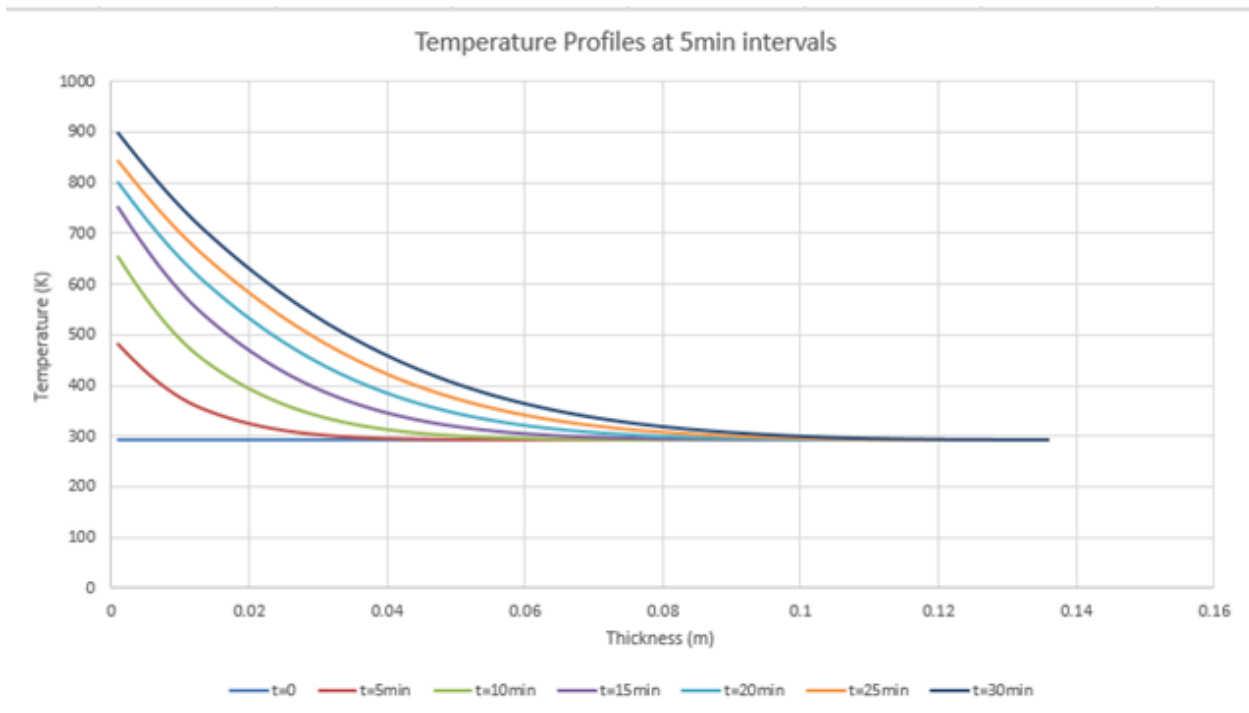*Figure 70: Temperature profiles at 5min intervals with 2 layers of cerablanket*

Appendix E: Mobile Base Calculation

Clamp Force of the Platform Top

The following equation was used to determine the force needed for the rig to shear the top layer of the platform when pushed...

$FClamp = T/ (DBolt*\mu)*N$

Where: T = Torque applied to the bolt/screw (assumed 200 Lbin. Of torque used to secure each screw with drill)

DBolt = Diameter of the bottom of the bolt/screw (Measured to be 0.25 inches)

μ = friction coefficient of the wood with the bolt/screw = 0.2

N = number of fasteners in the face of the wood, which for our platform is 12 screws

So

$FClamp = (200 Lbin.)/ (0.25in.*0.2)*(12 screws)$

$FClamp = 48,000 LBS$

A monumental and unrealistic force of 48,000 pounds would be required to shear the top of the platform.

Rolling Friction of the Rig

Next we determined the push force required to get the rig and platform assembly on the assumed four wheels...

We use the following equation...

$F = f*W/R*N$

Where f = friction coefficient of the hard rubber wheels on the concrete floor, it was found to be 0.02

W = weight of the rig, 806.6 Lbs.

R = radius of each wheel, 3.5 inches (since we will use 7 inch wheels)

N = number of wheels, 4

We solve accordingly...

$F = (0.02)*(806.6 Lbs. /3.5 in.)*(4 wheels)$

$F = 18.4 Lbs.$

18.4 pounds of force will be required to move the rig and platform on all four wheels simultaneously.

Sliding Force

The following calculations were done as a means of determining the force required to slide the rig on the platform. It was done in concurrence with the rolling friction calculation above.

$F = \mu s*w$

Where: µs = static friction coefficient between the rig and the platform, which was found to be a minimum of 0.2 (aluminum and dry wood)

W = weight of the rig, 806.6 pounds

So F = (0.2)*(806.6)

F = 161.3 Lbs.

161 pounds of push force is required to slide the rig over the platform, which is much greater (almost by a factor of 10) than the force required to move the four wheels of the platform.

Center of Gravity for the Rig and Platform Assembly

The following calculations were taken to determine the 3-dimensional (x, y, z) center of gravity for the rig and platform. Note that the dimensions were as follows: x from the left of the rig to the right, y from the front of the rig to the back of the rig, and z from the bottom of the rig to the top of the rig...

Figure: Symmetry of the rig frame in the x-direction

First of all, we assumed that the assembly is perfectly symmetric in the x-dimension, and therefore placed the center of gravity at an x-coordinate that coincided with that assumption. Therefore C_x = 28.5 inches

Next we determined the y-coordinate of the center of gravity, which is split up by weight in the following picture...

Figure: Drawing that features the weight segments of the rig in the y-direction

From the figure above, we have three segments of the rig that have different weights

First we have the two sidewalls and part of the bottom of the side rails, assuming the vast majority of the weight is in the sidewalls, we solve for the weight of the first segment...

C_{1y} = (44/52)*(373.14 Lbs.) = 315.7 Lbs.

The second segment of the rig contains the back wall, the vertical piece of the side rails and a part of the side walls as well, the following equation was used to determine the weight of this segment, assuming that 1/3rd of the weight of the side rails is concentrated in this segment...

C_{2y} = (8/52)*(373.14Lbs) + (137.34 Lbs.)+ (1/3)*(296.12 Lbs.) = 293.5 Lbs.

The third segment contains only the remaining piece of the side rails. Its weight equation is as follows...

C_{3y} = (2/3)*(296.12 Lbs.) = 197.4 Lbs.

Now we can solve for the y-coordinate of the center of gravity for the assembly, including the platform in the calculation...

C_y = (50/856.6)*(36.5 in.) + (315.7/856.6)*(22in.) + (293.5/856.6)*(48) + (197.4/856.6)*(62.5)

C_y = 41.1 inches

For the center of gravity in the z-direction, we use a similar method with the y-direction, except now we have two segments instead of three

Figure: Drawing that features the weight segments of the rig in the z-direction.

The first (bottom) segment is made up of the bottom of the side rails along with the bottom portion of the side walls, and the back wall (also $C_{1y} + C_{2y} = 609.2$ Lbs.)

We first solve for C_{1z} using the following...

$C_{1z} = (2/3)*(296.12 \text{ Lbs.}) + (18/96)*(609.2 \text{ Lbs.}) = 311.6$ Lbs.

We now solve for segment 2, which is made of the sum of the first two y-direction segments only...

$C_{2z} = (78/96)*(609.2 \text{ Lbs.}) = 495$ Lbs.

We now solve for the center of gravity, including the platform...

$C_z = (50/856.6)*(2 \text{ in.}) + (311.6/856.6)*(13 \text{ in.}) + (495/856.6)*(56 \text{ in.})$

$C_z = 37.2$ inches

We have a final center of gravity of (28.5, 41.1, 37.2)

Bending Stress

We now look to the maximum bending stress to occur to the platform's supporting members, and see if it exceeds the wood's rupture modulus of 5,100 PSI (for Southern Pine, Engineering Toolbox)

$\sigma = (3*W*L) / (2*w*d2)$, Where

W = Weight of load = 2400 Lbs. based on the ratings of the wheels

L = Maximum length of the supporting member = 72 inches

w = width of the supporting member = 2 inches

d = depth/height of the supporting member = 6 inches

We solve for σ,

$\sigma = (3*2400 \text{ Lbs.}*72 \text{ inches})/ (2*2 \text{ inches}*(6 \text{ inches}) 2)$

$\sigma = 3600$ PSI

The maximum bending stress of the assembly is 1500 PSI less than the wood's rupture modulus of 5,100 PSI.

Tipping Force/Moment

The following calculations were to determine the force required to tip the rig if the platform were to hit a bolt or some other obstruction on the floor

Without considering velocity, we use the following equilibrium equation to determine the push force necessary to tip a stopped rig over...

$T_w = T_C$

$W*C_x = F*$height of push

So essentially, we determine which force will cause the push torque or T_C, to be greater than the torque generated by the rig upon the front wheel

We first have our givens...

W = 856.6 Lbs.

Cx = 28.5 in.

We then solve for F, using a push height of 80 inches which was used as a "worst case" scenario.

F = (W*Cx)/h = (856.6 LBS*28.5 in.)/80 in.

F = 305.0 Lbs.

A minimum static force of 305 Lbs. would need to be exerted to tip the rig over, when stopped.

These preliminary calculations were done to make sure that while moving the rig on this platform, we would not be in any risk of breaking the platform or tipping over the rig, which would be a very unpleasant situation for us.

Appendix F: Burner Design

Based on the MQP completed in 2015 by Blake Cornachini, Matt Foley, Scott Knight, and Tom Ritchey, "Calibration of an Intermediate Scale Fire Test for Exterior Wall Assemblies: Source Fire," our burner settings were determined. By utilizing the 2D plume theory, adapting heat transfer principles, and running fire models, the source fire simulates the thermal insult of NFPA 285. The NFPA 285 test involves the base of our practice wall placed directly above a window. The rig accommodates for this with side channels that are used to match the vertical gas flow exhausting from the NFPA 285 window. In the NFPA 285 test there are two burners, one in the room, and one at the window.

In order to accurately compare the fire of NFPA 285 and that of the designed burner, it was necessary to characterize NFPA 285 in terms of the plume which the test specimen is exposed to. This characterization comes primarily from the calibration provided within NFPA 285 as well as existing work completed by Czarnowski et al.

NFPA 285 provides external plume centerline temperature data for one to six feet above the top of the window frame, and heat flux data for two to four feet above the window frame. Utilizing the existing 2D and spill plume theory, Czarnowski et al. determined that the flow resulting from the dual burner arrangement of NFPA 285 could be considered nominally a 2D Spill Plume. Next it was necessary to characterize the plume of an NFPA 285 calibration in terms of the modes of heat transfer between the resultant plume and the wall specimen. To do this fundamental radiation and convection heat transfer equations were utilized, along with data from the calibration procedure. Utilizing the calibration heat flux values from NFPA 285, the total heat flux to the three locations along the centerline of the wall was known.

$$q''_{total} = q''_{conv} + q''_{rad}$$

The heat flux due to radiation was calculated by determining the emissivity of methane, from data in NFPA 285.

$$q''_{rad} = \varepsilon \sigma T^4$$

By knowing this value, the convective heat transfer coefficient of the plume was determined.

$$h_c = \frac{(T_{plume} - T_\infty)}{q''_{conv}}$$

Since the NFPA 285 test can be characterized as a 2D plume, this means that the smoke plume created is only considered to exist in two directions, height and width, and it is assumed to be infinitely long in the third direction. For this reason, a line burner was chosen as the type of burner for this project. A line burner is a cylindrical pipe with a straight slot cut out along its length. A mesh screen lines the slot to diffuse the gas as it exits the burner, where it is ignited to create a non-premixed flame. The burner was designed for this project to resemble the window burner from NFPA 285 as closely as possible. For this reason, the pipe diameter and slot thickness were maintained from NFPA 285, while the slot length needed to be scaled down from 48 inches to fit in the intermediate rig assembly. This resulted in a final slot size of 0.5 inches by 28 inches. The main two inch pipe is fed on both sides by symmetric one inch diameter steel piping to ensure even gas flow.

Figure 71: Line Burner Assembly

In the previous MQP Rig Assembly, the test wall was balanced on the burner box as shown in the following figure, so the burner was placed under the burner box. The same results may be achieved by supporting the line burner in front of the test specimen, and inserting the gas line from the front of the assembly.
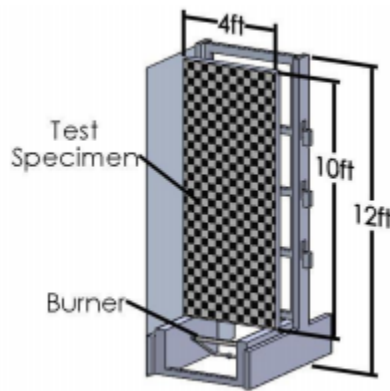
Figure 72: Line Burner Placement

The previous MQP group performed practice tests on a temporary test specimen with the burner at different heights and distances from the bottom of the test specimen in an effort to best simulate the window opening. The optimum placement of the line burner was determined to be 9 inches below the bottom of the test specimen, and 1 ¾ inches horizontally in front of the test specimen, and centered along the length of the slot.

Although NFPA 285 uses natural gas, propane gas was used for testing because it has a higher soot yield and is more readily available in the WPI Fire Protection Laboratory. A higher soot production is beneficial to this project because it increases the radiative heat flux produced by the burner. This is necessary because the combined plume created by the room and window burners in NFPA 285 carries more convective heat flux than can be produced by the single burner designed for this project. For this reason, radiative heat flux produced by soot can be used to supplement some of the missing heat flux.

A comparison table between methane and propane supports this decision

Table 27: Methane and Propane Comparison Table

Property	Methane	Propane
Chemical Formula	CH4	C3H8
Density (kg/m^3)	.668	1.882
Heat of Combustion (kJ/g)	50.00	46.45
Soot Yield (g/g)	0.000	0.024
Flame Temp (K)	1446	1554
Soot Volume Fraction	4.49E-6	7.09E-6
Total Calculated Emissivity	0.112	0.188

The MQP group which focused on the burner scaled the HRR from NFPA 285, and their practice tests by using the width of the window for NFPA 285 (1.98m), and the length of the line burner for their tests (0.71m). After scaling the NFPA 285 heat release rates from the window and room burners, they were converted to flow rates by using the heat of combustion and density of propane, and added together.

These heat flows were then tested, and the temperature and heat flux results were compared to expected values. The temperature profiles of all the burns, were scaled by the height above the burner divided by the heat release rate per unit width to the 2 /3 power, following the precedent set by Yuan & Cox. The profiles were compared to the theoretical temperature rise as correlated by Yuan &Cox. The data from the burns collapsed well about the correlation with some notable variation.

By leveraging the existing 2D plume theory, the team was able to fit a correlation to the results by imposing the physical constraints of the three flame regions, continuous, intermittent and plume upon the data. The correlation was fit using an average error minimization technique. The form of Yuan & Cox's equation was replicated, keeping the exponential constants the same and

varying the coefficient B. This correlation adjusts the existing theory based upon a burner in the open to a line burner against a vertical face.

The heat flux profiles were then compared, and a similar method was employed to create a correlation for heat flux by separating the three flaming regions, continuous, intermittent, and plume, with an adjusted B value.

The group concluded that 2D plume theory with three flaming regions aligned all data collected with expected NFPA 285 comparison results. Also the line burner against a wall required adjustment in calculations.

Based on their test, comparisons, and analysis, the MQP group developed a set of recommended burner flow rates for the 6, five minute steps to match NFPA 285 testing.

Table 28: Burner Flow Rates (CFM)

NFPA 285 (min)	Burner (CFM)
0 to 5	4.7
5 to 10	6
10 to 15	7.5
15 to 20	12
20 to 25	13.6
25 to 30	15

All considerations were taken at the 3 foot height from the base of the test specimen. This was done due to the mass of hot gases exiting the burn compartment of NFPA 285, the measurements closer to the window frame are reported as lower than those farther up. Fire plume theory states that the centerline temperature measurements should be at a maximum closest to the origin of the fire and decrease in magnitude as you ascend vertically up the plume. The reason for the divergence of NFPA 285 from the theory is what the group has defined as "Exit Effects". This is

due to the momentum of the compartment exhaust separating the thermal boundary layer away from the wall horizontally, before it eventually attaches to the wall further up the face.

When considered as an absolute average, the burner was able to reproduce temperatures and heat fluxes by the MQP group to within 19% and 23% of NFPA 285 respectively. When you discount the points deemed "Exit Effects" this accuracy improves to 14% and 13%. Finally, in the initial time step of NFPA 285 only the room burner is ignited. This profile is highly difficult to replicate with a single line burner, and when removed from the data set the accuracy of the results improves further to 11% for each. These results were based off a test specimen with the same face as the practice wall we will be analyzing, therefore we do not foresee any large deviations, and can expect to obtain similar temperature and heat flux values.

Appendix G: Standard Operating Procedure

Pre Test

Since our goal is to run fire tests that can successfully mimic a full-scale NFPA 285 test, it is important to follow the same test operating procedure as of that outlined by NFPA 285. The following steps shall take place after the transport of the rig to under the hood. They coincide with 2012 NFPA 285, 8.1.1 through 8.1.5.

1. The thermocouples and thin skin calorimeter(s) on the test wall shall be checked to ensure that they are properly working. This can be achieved by checking the data acquisition for a temperature signal along with the successful calibration of the thin skin calorimeter.

2. The burner shall be turned on and burned to a small extent before final positioning. That way we can ensure a vertical flame direction up the wall during the test.

3. The final positioning of the burner shall be so that its horizontal centerline is approximately 9 inches from the bottom surface of the wall and the vertical centerline is approximately 2 inches from the wall assembly in accordance with 2012 NFPA 285 4.4.9 through 4.4.12, and past MQP test results.

4. Take note of the ambient conditions in the test lab, including the temperature, relative humidity, and airflow (if possible).

5. Videotape the rig assembly noting all instrumentation placement, wall materials, and processes being utilized, note any variations made from previous assemblies. Include a timer in the screen of the video for the observer to use as reference. Continue to video tape until 5 minutes post-test.

These steps shall be followed in order to ensure a properly run fire test.

Test

After the Pre Test Procedure is complete, the Testing Procedure will be as follows

1. Continue to video tape until 5 minutes post-test. While testing, note on the video

   recording when the time step changes, and any observations: including heat experienced,

   flame behavior, smoke behavior, material condition, and any other notable observations.

2. Since our burner has capabilities for programmable gas flow rates, we will be using this

   feature to increase the heat release rate each five minutes.

Table 29: Burner Flow Rate by Time Step

Time Step (min)	Burner Flow Rate (CFM)
0-5	4.7
5-10	6
10-15	7.5
15-20	12
20-25	13.6
25-30	15

2. Ensure the area surrounding the rig is safely cleared, turn on the gas, and ignite the

   burner.

3. After the burner is ignited, we will ensure that all instruments are still in working order,

   in position, and reading reasonable values.

4. For each 5 minute time step we will be recording the burn pattern, but also making

   qualitative remarks, and recording all of them, and recording a video or taking pictures

5. After each 5-minute time step the gas flow rate is increased. The calibration of the burner

   before the test will provide the desired flow rates to provide equitable results to NFPA

   285 4.4.13 and 7.1.11

6. The gas is provided for 30 minutes. After 30 minutes the gas is turned off

7. Any residual burning on the test specimen shall not be extinguished until not less than 10 minutes after the gas is turned off

Post Test

Upon the completion of the test, the following measures shall be taken...

1. Continue video until 5 minutes post-test, then video may be turned off. After the 30 minutes to allow the rig to cool down, a video should be taken of the inspection of the rig and its condition.

2. The rig shall be left under the hood for no less than 30 minutes to cool off for further analysis.

3. The data from the test shall be saved.

4. The top layer of sheetrock and the layer of cerablanket shall be taken off of the wall and observed for damage.

5. Pictures or video will be taken of Post Test conditions